



HAL
open science

Combined Analysis: structure-texture-microstructure-phase-stresses-reflectivity determination by x-ray and neutron scattering

Daniel Chateigner

► **To cite this version:**

Daniel Chateigner. Combined Analysis: structure-texture-microstructure-phase-stresses-reflectivity determination by x-ray and neutron scattering. DEA. 2010, pp.496. cel-00109040v2

HAL Id: cel-00109040

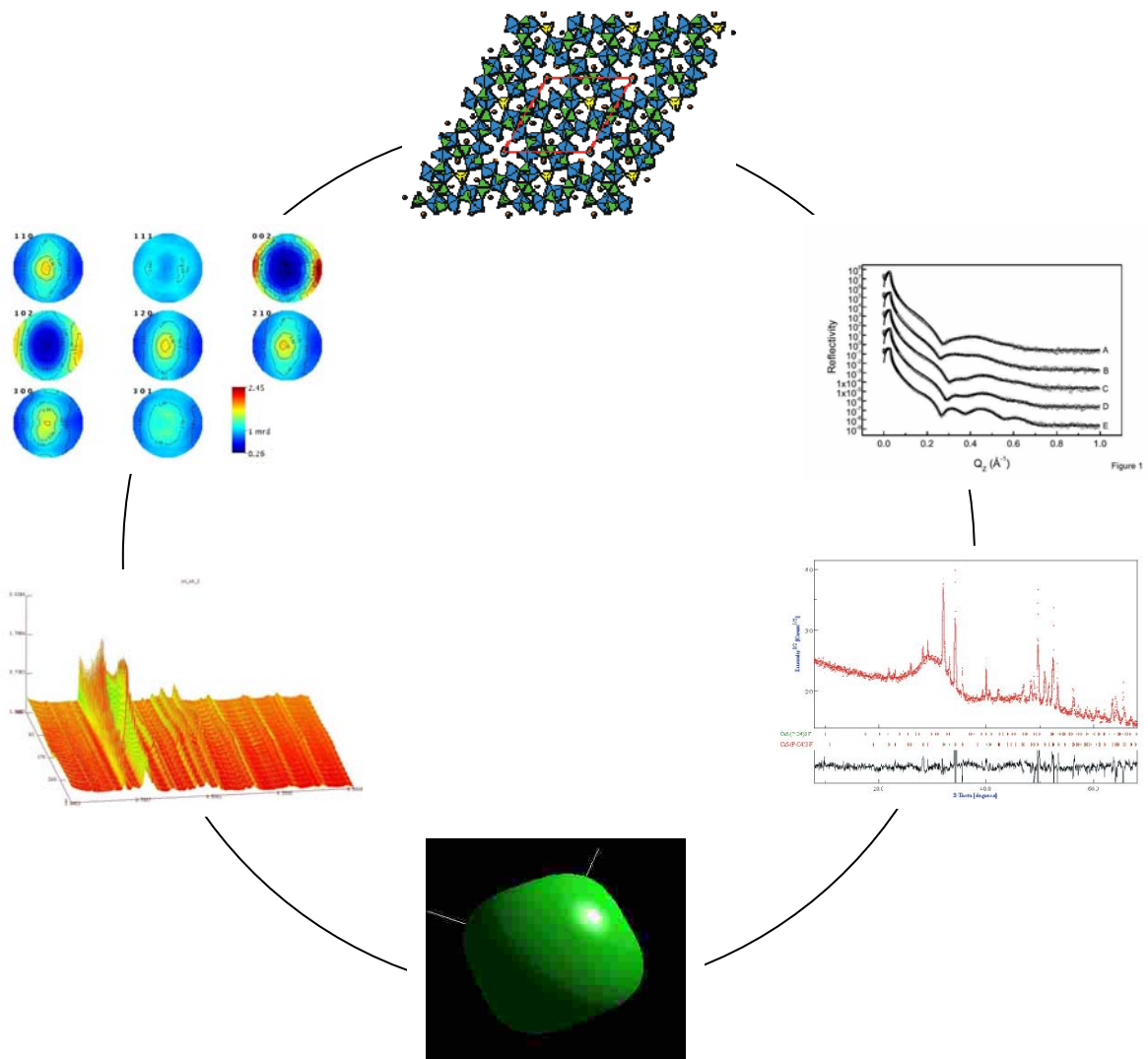
<https://cel.hal.science/cel-00109040v2>

Submitted on 26 Oct 2010

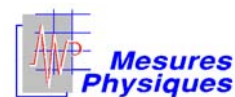
HAL is a multi-disciplinary open access archive for the deposit and dissemination of scientific research documents, whether they are published or not. The documents may come from teaching and research institutions in France or abroad, or from public or private research centers.

L'archive ouverte pluridisciplinaire **HAL**, est destinée au dépôt et à la diffusion de documents scientifiques de niveau recherche, publiés ou non, émanant des établissements d'enseignement et de recherche français ou étrangers, des laboratoires publics ou privés.

Combined Analysis: structure-texture-microstructure-phase- stresses-reflectivity determination by x-ray and neutron scattering



Daniel Chateigner



Combined Analysis: structure-texture-microstructure-phase-stresses-reflectivity determination by x-ray and neutron scattering

Daniel Chateigner

daniel.chateigner@ensicaen.fr

CRISMAT-ENSICAEN, UMR CNRS n°6508, 6 Bd. M. Juin, F-14050 Caen, France

IUT Mesures-Physiques, Université de Caen Basse-Normandie, Caen, France

<http://www.ecole.ensicaen.fr/~chateign/texture/combined.pdf>

0 Introduction	13
1 Some basic notions about powder diffraction	15
1.1 Crystallite, grain, polycrystal and powder.....	15
1.2 Bragg law and harmonic reflections.....	15
1.2.1 Bragg law	15
1.2.2 Monochromator.....	16
1.2.3 Harmonic radiation components	16
1.3 Geometrical conditions of diffraction, Ewald sphere.....	17
1.4 Imperfect powders.....	19
1.5 Main diffraction line profile components.....	19
1.5.1 Origin of $g(x)$	20
1.5.1.1 Laboratory X-rays	20
1.5.1.2 Synchrotron X-rays	21
1.5.1.3 Constant wavelength neutrons.....	21
1.5.1.4 Time Of Flight neutrons	21
1.5.1.5 Constant-wavelength Instrument Resolution Examples.....	21
1.5.2 Origin of $f(x)$	22
1.5.3 Deconvolution-extraction of $f(x)$ and $g(x)$	23
1.6 Peak profile Parameters.....	23
1.7 Modelling of the diffraction peaks	23
1.7.1 Why needing modelling ?	23
1.7.2 Modeling of a powder diffraction pattern	24
1.7.2.1 Decomposition of the diagram (individual adjustment of the peaks).....	24
1.7.2.2 Profile refinement with cell constraint (<i>Whole pattern fitting</i>).....	25
1.7.2.3 Peak-shape Functions for constant wavelength instruments	26
1.7.2.3.1 Gaussian	26
1.7.2.3.2 Lorentzian and Modified Lorentzian (Pearson VII).....	27
1.7.2.3.3 Voigt.....	27
1.7.2.3.4 Pseudo-Voigt.....	27
1.7.2.3.5 Split Pearson VII [Toraya 1986]	27
1.7.2.3.6 Variable pseudo-Voigt	28
1.7.2.3.7 Parameterised pseudo-Voigt [Thompson et al. 1987]	28
1.7.2.3.8 Anisotropic variable pseudo-Voigt [Le Bail et Jouanneaux 1997].....	29
1.7.2.3.9 Anisotropic variable Pearson VII [Le Bail et Jouanneaux 1997]	29
1.7.2.3.10 Anisotropic parameterised pseudo-Voigt [Stephens 1999]	30
1.7.2.4 Peak-shape Functions for TOF neutrons	30
1.7.2.4.1 Convolution of Gaussian and rising and falling exponentials	30
1.7.2.4.2 Convolution of Pseudo-Voigt and back-to-back exponentials	31
1.7.2.4.3 Moderator pulse shape function	32
1.7.2.4.4 Convolution of PV with the Ikeda-Carpenter pulse function	32
1.8 Experimental geometry	33
1.8.1 Curved Position Sensitive detector, asymmetric reflection geometry	33

1.8.2 CCD or image plate detector, transmission geometry	34
1.8.3 Curved-Area Position-Sensitive detector, transmission geometry	35
1.9 Intensity calibration (Flat-Field)	36
1.9.0 Counts and Intensity.....	36
1.9.0.1 Monitored incident intensity	36
1.9.0.2 Counting statistics	37
1.9.0.2.1 Poisson statistics.....	37
1.9.0.2.2 Zero-background peak and best precision	37
1.9.0.2.3 Detection limit.....	38
1.9.0.2.4 Presence of background under peaks.....	38
1.9.1 Flat-Field.....	39
1.9.2 PSD detector.....	39
1.9.3 CAPS detector.....	40
1.10 Standard samples.....	42
1.10.1 Laboratory x-ray standards.....	42
1.10.2 Neutron texture standards.....	43
1.10.2.1 International Round-Robin calcite standard.....	43
1.10.2.2 <i>Belemnite</i> rostrum calcite standard.....	44
1.11 Probed thickness (penetration depth)	45
2 Structure refinement by diffraction profile adjustment (Rietveld method).....	49
2.1 Principle of the Rietveld method.....	49
2.2 Rietveld based codes	50
2.3 Parameters modelling.....	51
2.3.1 Background modelling	51
2.3.1.0 Background components	51
2.3.1.1 Empirical approaches	51
2.3.1.1.1 m^{th} order polynomial function.....	52
2.3.1.1.2 Fourier series.....	52
2.3.1.1.3 Interpolation	52
2.3.1.1.4 2D detectors.....	52
2.3.1.2 Physical approaches	53
2.3.2 Structure factor.....	54
2.3.2.1 Structure factor expression.....	54
2.3.2.1.1 Usual 3-dimensional definition	54
2.3.2.1.2 Higher-space representation	54
2.3.2.2 Scattering factors.....	55
2.3.2.2.1 X-rays scattering factors.....	55
2.3.2.2.2 Neutrons scattering factors	55
2.3.2.2.3 Electrons scattering factors	56
2.3.2.3 Site occupation factors	57
2.3.2.4 Atomic positions	57
2.3.2.5 Thermal vibrations and temperature factors.....	57
2.3.2.5.1 Isotropic.....	57
2.3.2.5.2 Anisotropic.....	58
2.3.2.5.3 Negative thermal displacement parameters.....	58
2.3.2.5.4 Debye temperature to temperature factors.....	59
2.3.3 Crystallites Preferred Orientation (texture) corrections	59
2.3.3.1 Original Rietveld and March approaches	60
2.3.3.2 March–Dollase approach	60
2.3.3.3 Modified March–Dollase approach.....	60
2.3.3.4 Donnet–Jouanneaux function.....	61
2.3.3.5 Arbitrary Texture correction	61
2.3.3.6 Remarks.....	61
2.3.4 Peak asymmetry	62
2.3.4.1 Rietveld's correction [Rietveld 1969]:.....	62
2.3.4.2 Howard's correction [Howard 1982].....	62
2.3.4.3 Finger, Cox et Jephcoat's correction [Finger et al. 1994]	63
2.3.4.4 Bérar-Baldinozzi correction [Bérar et Baldinozzi 1993].....	63
2.3.4.5 TOF neutrons	63
2.3.5 Peak displacements	64

2.3.5.0 Zero-shift.....	64
2.3.5.1 Debye-Scherrer geometry.....	64
2.3.5.2 Flat plate, θ - 2θ Bragg-Brentano symmetrical geometry	64
2.3.5.3 Flat plate at fixed sample angle ω , asymmetrical geometry	64
2.3.5.4 Flat plate transmission geometry.....	64
2.3.5.5 Sample excentricity (Bragg-Brentano geometry).....	64
2.3.5.6 Sample transparency	65
2.3.5.7 Sample planarity (Bragg-Brentano geometry)	65
2.3.6 Lorentz-polarisation correction	65
2.3.6.0 Series of flat co-planar monochromators	65
2.3.6.1 Powder diffraction.....	66
2.3.6.1.1 Bragg-Brentano geometry	66
2.3.6.1.2 2D detector and polarised beams.....	66
2.3.6.2 Time Of Flight neutrons.....	67
2.3.6.3 General remark.....	67
2.3.7 Volume, Absorption, thickness corrections.....	67
2.3.7.1 Schulz geometry, point detector, thin layered structure	67
2.3.7.2 Schulz geometry, CPS detector, thin layered structure	68
2.3.7.3 Transmission geometry, 2D detectors, flat sample.....	69
2.3.8 Localisation corrections	70
2.3.8.1 Schulz reflection geometry, CPS detector.....	70
2.3.8.2 Debye-Scherrer transmission geometry, 2D detectors	70
2.3.8.3 Debye-Scherrer transmission geometry, CAPS detectors	71
2.3.9 Microabsorption/Roughness corrections	72
2.3.9.1 Sparks model, Bragg-Brentano	72
2.3.9.2 Suortti model, Bragg-Brentano	72
2.3.9.3 Pitschke model, Bragg-Brentano.....	73
2.3.9.4 Sidey model, Bragg-Brentano	73
2.3.10 Wavelength	73
2.4 Crystal Structure Databases	74
2.5 Reliability factors in profile refinements.....	74
2.6 Parameter exactness	77
2.7 The Le Bail method.....	77
2.8 Refinement procedures.....	78
2.8.1 Least squares	78
2.8.2 Genetic or evolutionary algorithms.....	79
2.8.3 Derivative difference minimisation (DDM).....	81
2.8.4 Simulated annealing	82
2.9 Refinement Strategy.....	82
2.10 Structural determination by diffraction	83
2.10.1 The phase problem in diffraction	83
2.10.2 Patterson function.....	83
2.10.3 Direct methods	85
2.10.4 Direct space methods	87
2.10.5 Fourier difference map	87
2.10.6 Extension to aperiodic structures	88
2.10.6.1 Generalities	88
2.10.6.2 Superspace formalism principle	88
3 Automatic indexing of powder diagrams.....	90
3.1 Principle	90
3.2 Dichotomy approach	90
3.3 Criteria for quality	91
4 Quantitative Texture Analysis (QTA).....	92
4.0 Classical Texture Analysis	92
4.0.1 Qualitative aspects of texture analysis	92
4.0.2 Effects on diffraction diagrams	94
4.0.2.1 θ - 2θ diagrams.....	94
4.0.2.2 Asymmetric diagrams	95
4.0.2.3 ω -scans: rocking curves	98

4.0.3	Limitations of classical diagrams	100
4.0.3.1	θ - 2θ diagrams.....	100
4.0.3.2	Asymmetric diagrams	101
4.0.3.3	rocking curves	101
4.0.4	The Lotgering factor	105
4.0.5	Representations of textures: pole figures	106
4.0.5.1	Pole Sphere.....	106
4.0.5.2	Equal-angular projection: Stereographic projection.....	107
4.0.5.3	Equal-area projection: Lambert projection.....	108
4.0.5.4	Pole Figures.....	109
4.0.5.5	Coverage of pole figures and scanning strategies	110
4.0.5.5.1	Using point detectors.....	110
4.0.5.5.2	Using 1D detectors	111
4.0.5.5.3	Using 2D CAPS detectors	111
4.0.5.5.4	Pole figure coverage.....	112
4.0.5.5.4.1	Localisation correction effect.....	112
4.0.5.5.4.2	Defocusing effect	114
4.0.5.5.4.3	Absorption effect.....	117
4.0.6	Localisation of crystallographic directions from pole figures.....	118
4.0.6.1	Normal diffraction and Pole Figures	118
4.0.6.2	Grains, Crystallites and Crystallographic planes.....	120
4.0.6.3	Single texture component.....	120
4.0.6.4	Multiple texture component	121
4.0.6.5	Pole figures and $(hk\ell)$ multiplicity.....	122
4.0.6.6	A real example	123
4.0.7	Texture types.....	124
4.0.7.0	Curie groups (limit groups)	124
4.0.7.1	Random texture	125
4.0.7.2	Planar textures.....	126
4.0.7.4	Fibre textures.....	127
4.0.7.5	Three-dimensional textures	128
4.0.7.5.1	3D texture.....	128
4.0.7.5.2	Single crystal texture.....	128
4.1	Orientation Distribution (OD) or Orientation Distribution Function (ODF).....	129
4.1.0	Pole figures and Orientation Spaces.....	129
4.1.0.1	Pole figures and orientation of planes	129
4.1.0.2	Mathematical expression of diffraction pole figures	130
4.1.1	The Orientation Space \mathcal{H}	130
4.1.2	Euler Angles conventions.....	131
4.1.3	Orientations and Pole figures	133
4.1.4	Choice for the sample coordinate system K_A	133
4.1.5	Pole figure, crystal, texture and sample symmetries	135
4.1.6	Orientation distance.....	136
4.2	Distribution density and normalisation	136
4.3	Direct and normalised Pole figures	136
4.3.1	Direct experimental pole figures	137
4.3.2	Normalised pole figures	137
4.3.2.1	Direct normalisation.....	138
4.3.2.2	Normalisation refinement.....	139
4.4	Reduced pole figures.....	139
4.5	Fundamental equation of Quantitative Texture Analysis	139
4.5.1	Fundamental equation	139
4.5.2	Typical OD components.....	140
4.5.2.1	Random OD and random part: FON	140
4.5.2.2	Isolated components.....	141
4.5.2.3	Cyclic components	142
4.5.3	OD plotting	143
4.5.3.1	2D plots.....	143
4.5.3.2	3D plot.....	144
4.5.4	Finding an orientation component in the OD	145

4.6 Resolution of the fundamental equation.....	146
4.6.1 ODF and OD	146
4.6.2 Generalised spherical harmonics.....	146
4.6.2.1 Principle	146
4.6.2.2 Normal Diffraction and Positivity of $f(g)$	148
4.6.2.2.1 Complete, even and odd ODFs.....	148
4.6.2.2.2 Positivity method.....	149
4.6.2.2.3 “GHOST” and quadratic methods.....	149
4.6.2.3 Least-squares refinement.....	150
4.6.3 Vector method [Ruer 1976, Ruer et Baro 1977, Vadon 1981].....	150
4.6.4 Williams-Imhof-Matthies-Vinel (WIMV) method [Williams 1968, Imhof 1982, Matthies et Vinel 1982].....	150
4.6.4.1 Regular WIMV.....	150
4.6.4.2 Extended WIMV (E-WIMV)	151
4.6.5 Arbitrarily Defined Cells (ADC) method [Pawlik 1993]	151
4.6.6 Entropy maximisation method [Schaeben 1988, Schaeben 1991, Schaeben 1991a].....	152
4.6.7 Component method [Helming 1998].....	152
4.6.7.1 Description	152
4.6.7.2 Gaussian components [Bunge 1969, Matthies et al. 1987]	153
4.6.7.3 Elliptical components [Matthies et al. 1987].....	153
4.6.8 Exponential Harmonics [Van Houtte 1991].....	154
4.6.9 Radon transform and Fourier analysis.....	154
4.6.10 Orientation space coverage	154
4.7 OD Refinement reliability estimators.....	155
4.7.1 RP factors	155
4.7.2 RPw Surface weighted factors	157
4.7.3 RB Bragg-like factors.....	157
4.7.4 RBw Bragg-like weighted factors	158
4.7.5 Rw weighted factors.....	159
4.7.6 Visual inspection.....	159
4.8 Inverse pole figures	160
4.8.1 Definition	160
4.8.2 Inverse pole figure sectors.....	161
4.9 Texture strength factors.....	162
4.9.1 Texture Index	162
4.9.1.1 ODF Texture Index	163
4.9.1.2 Pole Figure Texture Index.....	163
4.9.2 Texture Entropy	163
4.9.3 Pole Figure and ODF strengths	163
4.9.4 Correlation between F^2 and S.....	164
4.10 Texture programs	165
4.10.1 Berkeley Texture Package (BEARTEX).....	165
4.10.2 Material Analysis Using Diffraction (MAUD)	165
4.10.3 General Structure Analysis System (GSAS)	165
4.10.4 preferred orientation package, Los Alamos (popLA).....	166
4.10.5 The Texture Analysis software (LaboTex).....	166
4.10.6 Pole Figure Interpretation (POFINT).....	166
4.10.7 Strong Textures (STROTEX and Phiscans).....	167
4.10.8 STEREOPOLE.....	167
4.10.9 MTEX	167
4.11 Limits of the classical texture analysis.....	167
4.12 Magnetic Quantitative Texture Analysis (MQTA)	169
4.12.1 Magnetisation curves and magnetic moment distributions	169
4.12.2 A simple sample holder for MQTA	169
4.12.3 Methodology	170
4.12.3.1 Measured pole figures	170
4.12.3.2 Normalisation conditions	170
4.12.3.3 Nuclear part determination.....	171
4.12.3.4 Normalisation conditions of the ODFs.....	172
4.12.3.5 Absence of external magnetic field	172

4.12.3.6 Application of an external magnetic field	172
4.12.3.7 Magnetic part determination	173
4.12.3.7.1 Magnetic polarisation pole figures	173
4.12.3.7.2 Total Magnetic-scattering pole figures	174
4.12.3.7.2.1 Initially magnetically isotropic sample	174
4.12.3.7.2.2 Initially magnetically anisotropic sample	175
4.12.3.8 Fundamental equations of MQTA	175
4.12.4 From magnetic-scattering to the MODF and magnetic moment distributions	176
4.12.5 One example	176
4.13 Reciprocal Space Mapping (RSM)	178
5 Quantitative Microstructure Analysis (QMA)	180
5.1 Problematic	180
5.2 Microstructure modelling (classical)	181
5.2.1 Integral Breadth, FWHM, volume- and area-weighted sizes	181
5.2.1.1 Integral breadth and apparent linear size	181
5.2.1.2 Area- and volume-weighted sizes	182
5.2.1.3 Relationship between FWHM and Gaussian and Lorentzian components of the integral breadth	183
5.2.1.4 An expression between Gaussian and Lorentzian integral breadth components	183
5.2.2 Scherrer approach	183
5.2.3 Stokes and Wilson microstrains	184
5.2.4 Williamson-Hall approach	184
5.3 Bertaut-Warren-Averbach approach (Fourier analysis)	185
5.3.1 Instrumental contribution removal	185
5.3.2 Broadening due to crystallite size	186
5.3.3 Crystallite size and microdistortion broadening	187
5.3.4 Fourier analysis to integral breadths	189
5.3.5 Integral breadths to distributions, sizes and microstrains	190
5.3.5 Relationships between $\langle R_A \rangle$ and $\langle R_V \rangle$	191
5.4 Anisotropic broadening, Popa approach [Popa 1998]	191
5.4.1 Anisotropic broadening	191
5.4.2 Anisotropic Crystallite sizes	192
5.4.3 Anisotropic Microstrains	197
5.5 Stacking and Twin faults	198
5.5.1 From Line shifts and Fourier analysis	198
5.5.1.1 Face-centered cubic materials	198
5.5.1.2 Hexagonal compact materials	199
5.5.2 Popa approach	199
5.6 Dislocations	199
5.6.1 Dislocation density	200
5.6.1 Wilkens' model and Fourier analysis	200
5.7 Crystallite Size distributions	201
5.7.0 Normal size distribution function	201
5.7.1 Lognormal distribution function	202
5.7.2 Gamma distribution function	202
5.7.3 Anisotropic distribution functions	203
5.8 Rietveld approach	203
5.8.1 Constant wavelength data	203
5.8.2 Time of Flight neutrons	204
6 Quantitative Phase Analysis (QPA)	205
6.0 Standardised experiments	205
6.1 Polycrystalline samples	205
6.2 Amorphous-crystalline aggregates	206
6.2.1 Crystallinity fraction [Ruland 1961]	206
6.2.2 Amorphous modeling [Le Bail 1995]	207
6.3 Detection limit	208
7 Residual Strain-stress Analysis (RSA)	209
7.1 Strain definitions	209

7.2 ϵ_{33} strain determination	210
7.2.1 Isotropic polycrystalline sample	210
7.2.2 Single crystal	210
7.3 Complete strain tensor determination	211
7.3.1 Isotropic polycrystalline samples	211
7.3.1.1 triaxial stress state	211
7.3.1.2 Biaxial stress state	211
7.3.1.3 Uniaxial stress state	211
7.3.2 Single crystal samples	212
7.3.2.1 Cubic and orthorhombic crystal systems	212
7.3.2.2 Stress tensor	212
7.4 Textured samples	213
7.4.1 Generalities	213
7.4.2 Non-linear least-squares fit	213
7.4.3 Strain and stress distribution functions	214
8 X-ray Reflectivity (XRR).....	215
8.1 Introduction	215
8.1.1 Definition of the reflectivity	215
8.1.2 Specular and off-specular reflectivity	215
8.1.3 Combined Specular - off-specular scans	216
8.2 X-rays and neutrons refractive index	217
8.2.1 X-rays	217
8.2.1 Neutrons	218
8.3 The critical angle of reflection	219
8.3.1 X-rays	219
8.3.2 Neutrons	220
8.4 Fresnel formalism (Specular reflectivity)	220
8.4.1 Reflection coefficient and reflectivity	220
8.4.1.1 Reflection coefficient	220
8.4.1.2 Flat sample reflectivity	221
8.4.1.3 Single layer on substrate	222
8.4.1.4 More complex structures	222
8.4.2 Transmission coefficient	223
8.4.3 Yoneda wings	224
8.5 Surface roughness	225
8.5.1 Roughness representation	225
8.5.2 Bulk sample	227
8.5.2 Single layer on substrate	227
8.6 Matrix formalism (specular reflectivity)	228
8.7 Born approximation	229
8.8 Electron density profile	230
8.9 Multilayers reflectivity curves	230
8.10 Instrumental Corrections	231
8.10.1 Correction for irradiated area	231
8.10.2 Imperfectly parallel beam	232
9 Combined Structure-Texture-Microstructure-Stress-Phase-Reflectivity Analysis.....	234
9.1 Problematic	234
9.2 Implementation	237
9.3 Experimental set-up	239
9.4 Instrument calibration	239
9.4.1 Peaks broadening	240
9.4.1.1 χ broadening	241
9.4.1.2 2θ broadening	242
9.4.1.3 ω broadening	242
9.4.1.4 General broadening	243
9.4.2 Peak shifts	243
9.4.3 Background variations	244
9.5 Refinement Strategy	244
9.5.1 Global scheme	244

9.5.2 Solution Examination	245
9.6 Examples	247
9.6.0 QTA of single phased materials	247
9.6.0.1 Single phased bulks	247
9.6.0.1.1 PZT ceramics elaborated by molten flux	247
9.6.0.1.2 Thickness/grain size ratio effect in Thin Rolled Nickel	249
9.6.0.1.3 Mullite ceramics from muscovite-kaolinite alternate layers	256
9.6.0.2 QTA of single layers	258
9.6.0.1.2 Nacre-like electrodeposited CaCO ₃	259
9.6.1 QTA and isotropic QMA	265
9.6.1.1 Magnetically aligned slip-casted Al ₂ O ₃ ceramics	266
9.6.2 Anisotropic crystallite shape, texture, cell parameters and thickness	268
9.6.2.1 Diffraction pattern from single sample orientation	268
9.6.2.2 Nanocrystalline Silicon films on Si-(001) and amorphous SiO ₂	269
9.6.2.3 Gold thin films on Si-(001) single crystal substrates	271
9.6.3 Layering, isotropic shape, microstrains, texture, structure	274
9.6.4 Phase and texture	276
9.6.4.1 Texture removal	276
9.6.4.2 Crystalline multiphase textured compounds	277
9.6.4.2.1 Top-seeded MTG grown YBa ₂ Cu ₃ O _{7-δ} / Y ₂ BaCuO ₅ ensembles	277
9.6.4.2.2 Sinter-Forged Bi2223 / Bi2212 samples	280
9.6.4.3 Amorphous-Crystalline multiphase textured compounds	284
9.6.4.3.1 Irradiated fluorapatite ceramics	284
9.6.4.3.2 GaN-doped SiO ₂ matrices	290
9.6.5 Texture of modulated structures	295
9.6.5.1 Ca ₃ Co ₄ O ₉ ceramics	295
9.6.5.1.1 Hot-forged Magnetically aligned slip-casted Co349 ceramics	296
9.6.5.1.2 Reactive Templated Grain-Growth Co349 ceramics	298
9.6.5.2 Hot-Forged [Bi _{0.81} CaO ₂] ₂ [CoO ₂] _{1.69} misfit ceramics	299
9.6.6 Texture – Residual stresses - Layering	302
9.6.6.1 AlN/Pt/TiO _x /Al ₂ O ₃ /Ni-Co-Cr-Al-Y stacks	302
9.6.7 Texture and Structure	306
9.6.7.1 Biogenic crystals of <i>Charonia lampas lampas</i> shells	307
9.6.7.2 Other mollusc shell layers	316
9.6.7.3 Mimicking nacre in coatings on Ti-4Al-6V substrates	318
10 Macroscopic anisotropic properties	321
10.1 Aniso- and Iso-tropic samples and properties	321
10.2 Macroscopic/Microscopic properties	321
10.2.1 $\overline{\mathcal{T}}^M$ and $\overline{\mathcal{T}}$ tensors	321
10.2.2 Microscopic properties	321
10.2.2.0 Classifications of properties	322
10.2.2.1 Extensive and Intensive variables	322
10.2.2.2 Work element of conjugated variables	322
10.2.2.3 Generalised Thermodynamics	322
10.2.2.3.1 Generalised energy and Free Enthalpy	323
10.2.2.3.2 Linear Generalised total derivatives	324
10.2.2.3.2.1 Constitutive thermodynamic equations	324
10.2.2.3.2.2 Material properties	324
10.2.2.3.3 Property tensor reduction by symmetry operators	326
10.2.2.3.3.0 Curie and Neumann principles	326
10.2.2.3.3.1 Crystallographic groups	326
10.2.2.3.3.2 Polar and axial vectors	327
10.2.2.3.3.3 Time reversal symmetry	329
10.2.2.3.3.3 Space and Time reversal, magnetic groups	329
10.2.2.4 Thermal properties	330
10.2.2.4.1 Heat capacity	330
10.2.2.4.2 Thermal conductivity	331
10.2.2.4.3 Thermal diffusivity	332
10.2.2.5 Electric and Optical properties	332
10.2.2.5.1 Dielectric properties	332

10.2.2.5.2 Optical linear properties	333
10.2.2.5.2.1 Refractive indexes	333
10.2.2.5.2.2 Linear Birefringence.....	334
10.2.2.5.3 Optical rotation properties.....	335
10.2.2.5.3.1 Circular Birefringence.....	335
10.2.2.5.3.2 Optical Rotation (Gyration).....	335
10.2.2.5.3.3 Optical Rotatory Power.....	336
10.2.2.5.4 Electrical Conductivity-Resistivity.....	336
10.2.2.5.5 ElectroOptic effects.....	337
10.2.2.5.5.1 Generalised ElectroOptic polarisation formulation.....	337
10.2.2.5.5.2 Quadratic non-linear electrical effect.....	337
10.2.2.5.5.3 Linear ElectroOptic (Pockels) effect.....	338
10.2.2.5.5.4 Second Harmonic Generation (SGH).....	339
10.2.2.5.5.5 Kerr effect.....	339
10.2.2.5.5.6 Electric-field induced SGH.....	341
10.2.2.5.6 Four-wave mixing.....	341
10.2.2.6 Magnetic properties.....	341
10.2.2.6.1 Magnetic Induction, Field and Magnetisation.....	341
10.2.2.6.2 Diamagnetics.....	342
10.2.2.6.3 Paramagnetics.....	342
10.2.2.6.4 Ferro- and ferrimagnetics.....	343
10.2.2.7 Mechanical properties.....	344
10.2.2.7.1 Static mechanical properties.....	344
10.2.2.7.2 Bulk Acoustic Waves (BAW).....	349
10.2.2.8 ThermoElectric (TE) properties.....	352
10.2.2.8.1 Pyroelectricity.....	352
10.2.2.8.2 Seebeck and Peltier effects.....	352
10.2.2.8.2.1 Non-magnetic Crystal, $H = 0$	352
10.2.2.8.2.2 Crystal under H	354
10.2.2.8.3 Power Factor.....	354
10.2.2.8.4 Figure of Merit.....	354
10.2.2.9 ThermoMechanic (TMe) properties.....	355
10.2.2.10 ElectroMechanic (EMe) properties.....	356
10.2.2.10.1 Piezoelectric effect.....	356
10.2.2.10.2 Acoustic waves propagation in piezoelectrics.....	362
10.2.2.10.3 2 nd order Piezoelectric effect.....	363
10.2.2.10.4 Electrostriction.....	364
10.2.2.11 MagnetoMechanic (MMe) properties.....	365
10.2.2.11.1 PiezoMagnetic effect.....	365
10.2.2.11.2 Acoustic waves propagation in piezomagnetics.....	366
10.2.2.11.3 2 nd order Piezomagnetic effect.....	367
10.2.2.11.4 Magnetostriction.....	367
10.2.2.12 MagnetoElectric (ME) properties.....	368
10.2.2.12.1 Linear magnetoelectric effect.....	368
10.2.2.12.2 Non-Linear magnetoelectric effect.....	369
10.2.2.12.3 Hall effect and magnetoresistance.....	370
10.2.2.13 MagnetoOptic (MO) effects and magnetic birefringence.....	370
10.2.2.13.1 Generalised MagnetoOptic formulation.....	370
10.2.2.13.2 Faraday rotation.....	370
10.2.2.13.3 Cotton-Mouton effect.....	371
10.2.2.13.4 Magnetic birefringence.....	371
10.2.2.13.5 Induced Gyrotropic Birefringence (IGB).....	371
10.2.2.14 Mechano-Optic (MeO) properties.....	371
10.2.2.14.1 Linear Photoelastic effect.....	371
10.2.2.14.2 AcoustoOptic effect.....	373
10.2.2.15 Atomic diffusion.....	373
10.2.2.16 PiezoMagnetoElectric (PME) properties.....	373
10.2.2.17 Multiferroics.....	374
10.2.3 Macroscopic properties anisotropy and modelling.....	374
10.2.3.1 Averaging of tensors.....	374

10.2.3.1.1 Volume average.....	374
10.2.3.1.2 Arithmetic average over orientations	375
10.2.3.1.3 Geometric average over orientations	375
10.2.3.1.3.1 Scalar case	375
10.2.3.1.3.2 2 nd order tensors case.....	376
10.2.3.2 Heat capacity	376
10.2.3.3 Thermal expansion	376
10.2.3.4 Electric polarisation.....	376
10.2.3.5 Mechanical properties	377
10.2.3.5.1 The Voigt model.....	377
10.2.3.5.2 The Reuss model	378
10.2.3.5.3 The Hill model	378
10.2.3.5.4 The geometric mean model	379
10.2.3.5.5 Some examples.....	380
10.2.3.5.5.1 Constant elastic stiffness tensor in Ni thin rolled sheets with different grain sizes ..	380
10.2.3.5.5.2 Geometric mean applied to mollusc shell's mineral	380
10.2.3.5 Bulk Acoustic Waves from OD and $C^{i/mn}$	382
10.2.3.5.1 Photoexcited acoustic waves in Fibre textured Au films.....	383
10.2.3.5.2 Hetero-epitaxial and fibre textured LiNbO ₃ films	386
10.2.3.6 Thermoelectric properties.....	388
10.2.3.6.1 RTGG Co349 ceramics	388
10.2.3.6.2 Hot-Forged [Bi _{0.81} CaO ₂] ₂ [CoO ₂] _{1.69} misfit ceramics	389
10.2.3.7 Magnetisation in oriented easy-plane ErMn ₄ Fe ₈ C	390
10.2.3.8 Dielectric constant.....	395
References.....	396
General Bibliography	415
Glossary	418
Abbreviations	420
Mathematical operators	421
Acknowledgements	423
Warnings and comments.....	424
Figures caption.....	425
Tables caption	433

Some typographical mistakes may have been introduced throughout this document.
Suggestions and corrections are very welcome.

0 Introduction

Solid state chemistry and technology recent developments gave rise to the necessity of intensive structural analysis from single crystal diffraction. However for many solids, single crystal growth is not easy to manage and sometimes impossible. When this is the case, or when structural defects cannot be overcome, the corresponding phases have often been forsaken, due to the inherent difficulties to carry out crystallographic characterisations on polycrystals. But in the last decades powder diffraction techniques progressed significantly, notably due to the Rietveld approach (Rietveld, 1969) and computer science developments. Undoubtedly these developments are of prior importance in the study of solids that do not form large crystals, but also of all materials elaborated by classical solid state reactions, thin deposited structures, natural materials like clays and more recently nanomaterials in which the required properties are intimately linked to the stabilisation of small crystals.

Since the Rietveld method's birth, several ten thousands of structures have been refined and some thousands have been resolved *ab-initio* from the only diffraction data of powder samples. The number of laboratories and industries using this technique, still fairly new when dealing with the incorporation of various formalisms like in the combined approach, does not stop increasing.

However, materials having specific properties are often elaborated from low symmetry phases, which are consequently anisotropic. Property's optimisation is then conditioned by the elaboration processes which have to keep the intrinsic microscopic anisotropy of the constituting crystals at the macroscopic level. These elaboration techniques are complex (alignment under uniaxial pressure, magnetic or electric fields, thermal gradients, flux or substrate growing ... and combinations) and often sample preparation is a hard, time consuming, matter. Naturally, non-destructive characterisations are then required. Unfortunately, when samples are oriented, which was not often the case until recently, most of the characterisation techniques (as the Rietveld analysis of concerns here) require samples grinding. Very often this grinding is not acceptable, for the previously described reasons, but also in the case of rare samples (fossils, comets ...) or simply when grinding modifies the physical behaviour of the samples themselves (thin films, residual stress materials ...). Sometimes grinding is simply not possible, imagine peeling off a 10 nm thick film on a substrate !

In all these cases, the combined analysis becomes essential.

The first part of this document is dedicated to some basic notions concerning diffraction by polycrystals. The various peak profiles used are described and some, most common combined analysis instrumental set-up detailed.

In the second part, powder diffraction data treatment is introduced. In particular, the Rietveld analysis is detailed, including treatment of all the information provided by diffraction diagrams, when texture is not present in the sample or simple to treat.

The third part deals with the automatic phase indexing, necessary step to solve a structure *ab-initio*.

Since its effect prevails on real samples where textures are often stabilised, quantitative texture analysis is detailed in the fourth part.

The fifth part is dedicated to microstructural aspects (isotropic and anisotropic crystal sizes and microdistortions) of the powder diffraction profiles.

In part six, quantitative phase analysis from Rietveld analysis is introduced.

Part seven describes residual stress analysis for isotropic and anisotropic materials.

The eighth part focuses on specular x-ray reflectivity and the various models associated.

Part nine introduces the combined analysis concept, showing all the dilemma that show up when one looks at only one part of the analyses, and case examples are shown as illustration of the methodology.

The 10th part is dedicated to the anisotropic and tensorial macroscopic properties and their simulations to account for the distribution of crystallite orientations in samples.

This book is not intended to provide the reader a complete description of all the **approaches** dealt within it, though quantitative texture analysis is more deeply detailed than others since texture appears to be the largest signal biaser, but a red wire to follow the many concepts introduced through so many years and necessary to understand scattering patterns.

References

- Abeles F. (1948). Sur la propagation des ondes électromagnétiques dans les milieux stratifiés. *Annales de Physique* **3(4)** 504-520
- Agranovich V.M., Ginzburg V.C. (1984). "Crystal Optics with Spatial Dispersion, and Excitons". Springer, Berlin.
- Akaike H. (1974). New look at statistical-model identification. *IEEE Transactions on Automatic Control* **AC 19(6)** 716-723
- Akamatsu S., Komatsu H., Koizumi C., Nonaka J. (1977). A comparison of sugar components of yellow and white pearls. *Nippon Suisan Gakkaishi (Bulletin of the Japanese Society of Scientific Fisheries)* **43** 773–777
- Alexander L.E. (1948). Geometrical factors affecting the contours of x-ray spectrometer maxima. I. Factors causing asymmetry. *Journal of Applied Physics* **19(11)** 1068-1071
- Alexander L.E. (1950). Geometrical factors affecting the contours of x-ray spectrometer maxima. II. Factors causing broadening. *Journal of Applied Physics* **21(2)** 126-136
- Alexander L.E. (1955). The synthesis of x-ray spectrometer line profiles with application to crystallite size measurements. *Journal of Applied Physics* **25(2)** 155-161
- Als-Nielsen J. (1985). The liquid vapour interface. *Zeitschrift für Physik B* **61(4)** 411-414
- Anil T.V., Menon C.S., Shree Krishna Kumar K., Jayachandran K.P. (2004). Third-order elastic constants of ZnS and ZnSe. *Journal of Physics and Chemistry of Solids* **65(6)** 1053-1057
- Antoniadis A., Berruyer J., Filhol A. (1990). Maximum-likelihood methods in powder diffraction refinements. *Acta Crystallographica A* **46** 692-711
- Aouinti M., Chateigner D., Gibaud A., Poncin-Epaillard F. (2002). Planar texture developed in plasma treated polypropylene films. *Materials Science Forum* **408-412** 1579-1584
- Aouinti M., Gibaud A., Chateigner D., Poncin-Epaillard F. (2004). Morphology of polypropylene films treated in CO₂ plasma. *Journal of Polymer Science Part B: Polymer Physics* **42** 2007-2013
- Apostol M. (2008). Generalized theory of thermoelectric figure of merit. *Journal of Applied Physics* **104** 053704
- Armstrong N., Leoni M., Scardi P. (2006). Considerations concerning Wilkens' theory of dislocation line-broadening. *Zeitschrift für Kristallographie* **23(1)** 81-86
- Armstrong R.W. (1961). On size effects in polycrystal plasticity. *Journal of the Mechanics and Physics of Solids* **9(3)** 196–199
- Atlan G., Balmain N., Berland S., Vidal B., Lopez E. (1997). Reconstruction of human maxillary defects with nacre powder: histological evidence for bone regeneration. *Comptes Rendus de l'Académie des Sciences III, Sciences de la Vie* **320** 253-258
- Auzary S., Badawi F., Bimbault L., Rabier J., Gaboriaud R.J., Goudeau P. (1997). An x-ray diffraction study of microstructural and mechanical state of superconducting YBCO thin film. *Journal de Physique III* **7(1)** 35-46
- Badawi F., Durand N., Goudeau P., Pelosin V. (1994). Residual stresses and microstructure of Ag-Ni multilayers. *Applied Physics Letters* **65(24)** 3075-3077
- Balzar D. (1992). Profile fitting of X-ray diffraction lines and Fourier analysis of broadening. *Journal of Applied Crystallography* **25** 559-570
- Balzar D. (1999). Voigt-function model in diffraction line-broadening analysis. In "Defect and Microstructure Analysis by Diffraction". R L Snyder, J. Fiala, H.-J. Bunge (Eds.), International Union of Crystallography Monographs on Crystallography, n° 10, Oxford University Press, 808 pages. Pp 94-126
- Balzar D., Ledbetter H. (1993). Voigt-function modeling in Fourier analysis of size- and strain-broadened X-ray diffraction peaks. *Journal of Applied Crystallography* **26** 97-103
- Balzar D., Popovic S. (1996). Reliability of the simplified integral-breadth methods in diffraction line-broadening analysis. *Journal of Applied Crystallography* **29** 16-23
- Ban Z.-G., Alpay S.P. (2002). Phase diagrams and dielectric response of epitaxial barium strontium titanate films: a theoretical analysis. *Journal of Applied Physics* **91(11)** 9288-9296
- Banerjee S., Gibaud A., Chateigner D., Ferrari S., Fanciulli M. (2002). Structural and chemical characterization of 4.0 nm thick oxynitride films. *Journal of Applied Physics* **91(1)** 540-542
- Banerjee S., Gibaud A., Chateigner D., Ferrari S., Wiemer C., Dekadjevi D.T. (2002a). Study of the effect of plasma treatment on TiN films in N₂/H₂ atmosphere using x-ray reflectivity and secondary ion mass spectroscopy. *Applied Physics Letters* **80(3)** 512-514
- Basinski Z.S. (1977). "Surface effects in crystal plasticity", R.M. Latanision et J.T. Fourie (Ed), *Nato Advanced Study Institutes Series*, p 433-467
- Baumbach T., Mikulik P. (1999). X-ray reflectivity by rough multilayers. In "X-ray and neutron reflectivity: principles and applications", J. Daillant et A. Gibaud (Ed), Springer M58, p 232-280

- Beauvy M., Duverneix T., Berlanga C., Mazoyer R., Duriez C. (1998). Actinide transmutation : new investigation on some actinide compounds. *Journal of Alloys and Compounds* **271** 557-562
- Bérar J.-F., Baldinozzi G. (1993). Modeling of line-shape asymmetry in powder diffraction. *Journal of Applied Crystallography* **26** 128-129
- Berlincourt D., Cook Jr. W.R., Rander M.E. (1963). Piezoelectric, dielectric, and pyroelectric constants of $\text{LiH}_3(\text{SeO}_3)_2$. *Acta Crystallographica* **16** 163-165
- Berlincourt D., Jaffe H., Shiozawa L.R. (1963). Electroelastic properties of the sulfides, selenides, and tellurides of zinc and cadmium. *Physical Review* **129** 1009-1017
- Bernouilli D., Allen C.G. (1961). The most probable choice between several discrepant observations and the formation therefrom of the most likely induction. *Biometrika* **48(1-2)** 3-18
- Bertaut F. (1949a). Signification de la dimension cristalline mesurée d'après la largeur de raie Debye-Scherrer. *Comptes Rendus de l'Académie des Sciences* **228** 187-189
- Bertaut F. (1949b). Etude aux rayons X de la répartition des dimensions des cristallites dans une poudre cristalline. *Comptes Rendus de l'Académie des Sciences* **228** 492-494
- Bertaut E.F. (1950). Raies de Debye-Scherrer et répartition des dimensions des domaines de Bragg dans les poudres polycristallines. *Acta Crystallographica* **3** 14-18
- Bertaut E.F. (1952). Sur la correction de la transformée de Fourier d'une raie de Debye-Scherrer dans la mesure de dimensions cristallines. *Acta Crystallographica* **5** 117-121
- Bethe H.A. (1953). Molière's theory of multiple scattering. *Physical Review* **89** 1256-1266
- Beu A.G. (1985). A classification and catalogue of living world Ranellidae (=Cymatiidae) and Bursidae. *Conchologists of America Bulletin* **13(4)** 55-66
- Beu A.G. (1987). Taxonomy of gastropods of the families Ranellidae (=Cymatiidae) and Bursidae. Part 1. Adoption of Ranellidae, and review of *Linatella* Gray, 1857. *New Zealand Journal of Zoology* **13** 241-266
- Bienville T., Robillard J.-F., Belliard L., Roch-Jeune I., Devos A., Perrin B. (2006). Individual and collective vibrational modes of nanostructures studied by picosecond ultrasonics. *Ultrasonics* **44(1)** e1289-e1294
- Birsan M., Szpunar A., Tun Z., Root J.H. (1996). Magnetic texture determination using nonpolarized neutron diffraction. *Physical Review B* **53(10)** 6412-6417
- Birss R.R. (1964). "Symmetry and Magnetism", Birss (Ed.). North Holland, Amsterdam.
- Bobbio A. (1972). The first endosseous alloplastic implant in the history of man. *Bulletin of the History of Dentistry* **20** 1-6
- Böcker A., Bunge H.-J., Huber J., Krahn W. (1994). Texture formation in Al_2O_3 substrates. *Journal of the European Ceramics Society* **14(4)** 283-293
- Born M., Huang K. (2002). "Dynamical Theory of Crystal Lattices". Oxford University Press, Oxford
- Born, M., Wolf, E. (1980). "Principles of Optics - electromagnetic theory of propagation interference and diffraction of light", Pergamon Press, London 6Pth Edition, 808 pages
- Bornand V., Huet I., Chateigner D., Papet Ph. (2002). Oriented Growth of LiNbO_3 Thin Films for SAW properties. *Materials Science Forum* **408-412** 1573-1578
- Bornand V., Huet I., Bardeau J.-F., Chateigner D., Papet Ph. (2002a). An alternative route for the synthesis of oriented LiNbO_3 thin films. *Integrated Ferroelectrics*, **43** 51-64
- Bouchet P., Rocroi J.-P. (2005). Classification and Nomenclator of Gastropod Families. *Malacologia* **47(1-2)** 1-397
- Bouguerra M., Belkhir M.A., Chateigner D., Samah M., Gerbous L., Nouet G. (2008). Blue and yellow luminescence of GaN nanocrystals-doped SiO_2 matrix. *Physica E* **41** 292-298
- Boultif A., Louër D. (1991). Indexing of powder diffraction patterns for low-symmetry lattices by the successive dichotomy method. *Journal of Applied Crystallography* **24** 987-993
- Boultif A., Louër D. (2004). Powder pattern indexing with the dichotomy method. *Journal of Applied Crystallography* **37** 724-731
- Bowen D.K., Wormington M. (1993). Grazing Incidence X-Ray Characterization of Materials. *Advances in X-ray Analysis* **36** 171-184
- Bowman K.J., Mendendorp M.N. (1994). Texture Measurement of Sintered Alumina Using the March-Dollase Function. *Advanced in X-ray Analysis* **37** 473-478
- Bragg W.L., Thomson J.J. (1914). The diffraction of short electromagnetic waves by a crystal. *Proceedings of the Cambridge Philosophical Society* **17** 43-57
- Bragg, W.L. (1937). "Atomic Structures of Minerals". Cornell University Press: Ithaca, USA. pp 114-126
- Bravais A. (1850). Mémoire sur les systèmes formés par des points distribués régulièrement sur un plan ou dans l'espace. *Journal de l'Ecole Polytechnique* **19** 1-128
- Brentano J.C.M. (1946). Parafocusing properties of microcrystalline powder layers in x-ray diffraction applied to the design of x-ray goniometers. *Journal of Applied Physics* **17** 420-434
- Brosnan K.H., Messing G.L., Meyer Jr. R.J., Vaudin M.D. (2006). Texture measurements in <001> fiber-oriented PMN-PT. *Journal of the American Ceramics Society* **89(6)** 1965-1971

- Brükner S. (2000). Estimation of the background in powder diffraction patterns through a robust smoothing procedure. *Journal of Applied Crystallography* **33** 977-979
- Bunge H.-J. (1969). "Mathematische Methoden der Texturanalyse", Berlin, Akademie Verlag, 330 pages
- Bunge H.-J. (1982). "Texture Analysis in Materials Science", P.R. Morris Transactions, Butterworths, London.
- Bunge H.-J. (1989). Texture and magnetic properties. *Textures and Microstructures* **11** 75-91
- Bunge H.-J., Esling C. (1982). "Quantitative Texture Analysis", Bunge and Esling (Eds.), DGM, Germany.
- Bunge H.-J., Wenk H.-R., Pannetier J. (1982). Neutron diffraction texture analysis using a 2 θ position sensitive detector. *Textures and Microstructures* **5** 153-170
- Burenkov Y.A., Botaki A.A., Davydov S.Y., Nikanorov S.P. (1977). Temperature effect on elastic properties of zinc selenide. *Fizika Tverdogo Tela* **19(9)** 1726-1730
- Çağın T. (1999). Thermal and mechanical properties of some fcc transition metals. *Physical Review B* **59(5)** 3468-3473
- Caglioti G., Paoletti A., Ricci F.P. (1958). Choice of collimators for a crystal spectrometer for neutron diffraction. *Nuclear Instruments and Methods* **3(4)** 223-228
- Canova G.R., Kocks U.F. (1984). The development of deformation textures and resulting properties of fcc metals. In "7th International Conference on Textures of Materials", Brakman C.M., Jongenburger P., Mittermeijer E.J. (Eds). Netherlands, Society for Materials Science, p573-579
- Capkova P., Peschar R., Schenk H. (1993). Partial multiplicity factors for texture correction of cubic structures in the disc-shaped crystallite model. *Journal of Applied Crystallography* **26** 449-452
- Cardwell D.A. (1998). Processing and properties of large grain (RE)BCO. *Materials Science and Engineering B* **53(1-2)** 1-10
- Cariolou M.A., Morse D. (1988). Purification and characterization of calcium-binding conchiolin shell peptides from the mollusc *Haliotis rufescens*, as a function of development. *Journal of Comparative Physiology B* **157** 717-729
- Carisey T., Levin I., Brandon D.G. (1995). Microstructure and mechanical-properties of textured Al₂O₃. *Journal of the European Ceramics Society* **15(4)** 283-289
- Carter J.G., Clark II G.R. (1985). Classical and phylogenetic significance of molluscan shell microstructure, in "Molluscs, notes for a short course" Bottjer D.J., Hickman C.S., Ward P.D., Broadhead T.W. (Eds) Department of Geological Science Studies in Geology; University of Tennessee: Knoxville, USA, pp 50-71
- Cartwright J.H.E., Checa A.G. (2007). The dynamics of nacre self-assembly. *Journal of the Royal Society Interface* **4** 491-504
- Casali R.A., Christensen N.E. (1998). Elastic constants and deformation potentials of ZnS and ZnSe under pressure. *Solid State Communications* **108(10)** 793-798
- Caspi E.N., Pokroy B., Lee P.L., Quintana J.P., Zolotoyabko E. (2005). On the structure of aragonite. *Acta Crystallographica B* **61** 129-132
- Cerný R., Valvoda V., Chládek M. (1995). Empirical texture corrections for asymmetric diffraction and inclined textures. *Journal of Applied Crystallography* **28** 247-253
- Chan S.K., Fang Y., Grimsditch M., Li Z., Nevitt M.V., Robertson W.M., Zouboulis E.S. (1991). Temperature-dependence of the elastic-moduli of monoclinic zirconia. *Journal of the American Ceramic Society* **74(7)** 1742-1744
- Chang S.H., Rogacheva N.N., Chou C.C. (1995). Analysis of methods for determining electromechanical coupling coefficients of piezoelectric elements. *Transactions on Ultrasonics Ferroelectrics and Frequency Control, IEEE* **42(4)** 630-640
- Chateigner D. (1994), "Texture cristallographique de céramiques et de couches minces supraconductrices YBa₂Cu₃O_{7- δ} en relation avec les propriétés physiques", Thesis, Université J. Fourier, Grenoble-France
- Chateigner D. (2002), POFINT: a MS-DOS program for Pole Figure Interpretation. <http://www.ecole.ensicaen.fr/~chateign/qta/pofint/>
- Chateigner D. (2002a), STROTEX and Phiscans: MS-DOS programs for pole figure visualisation and integration.
- Chateigner D. (2005). Reliability criteria in Quantitative Texture Analysis with Experimental and Simulated Orientation Distributions. *Journal of Applied Crystallography* **38** 603-611
- Chateigner D., Erler B. (1997). Preferred orientations and epitaxial relationships of HgI₂ thin films on (001) oriented KCl and Mica single crystals. *Material Science & Engineering: B* **45** 152-161
- Chateigner D., Germi P., Pernet M. (1992). Texture analysis by the Schulz reflection method: defocalisation correction for thin films. *Journal of Applied Crystallography* **25** 766-769
- Chateigner D., Germi P., Pernet M. (1994). X-ray texture analysis in films by the reflection method: principal aspects and applications. *Materials Science Forum* **157-162** 1379-1386
- Chateigner D., Germi P., Pernet M. (1994a). X-ray texture analysis of thin films by the reflection method: intermediate regime in defocusing corrections. *Journal of Applied Crystallography* **27** 278-282

- Chateigner D., Germi P., Pernet M., Fréchar P., Andrieu S. (1995). Fluorescence corrections in thin film texture analysis. *Journal of Applied Crystallography* **28** 369-374
- Chateigner D., Hedegaard C., Wenk H.-R. (1996). Texture analysis of a gastropod shell: *Cypraea testudinaria*. In "11th International Conference on Textures of Materials", Z. Liang, L. Zuo, Y. Chu (Eds.), Int. Academic Publishers **Vol. 2** 1221-1226
- Chateigner D., Hedegaard C., Wenk H.-R. (1999). Quantitative characterisation of mollusc shell textures. In "Textures of Materials", J.A. Szpunar (Ed.), NRC Research Press, **Vol. 2** 1495-1500
- Chateigner D., Hedegaard C., Wenk H.-R. (2000). Mollusc shell microstructures and crystallographic textures. *Journal of Structural Geology* **22(11-12)** 1723-1735
- Chateigner D., Kaptein R., Dupont-Nivet M. (2009). Relevance of X-ray Quantitative Texture Analysis of *Helix aspersa aspersa* (Mollusca: Pulmonata) shells selected or not for an increased weight. Accepted *American Malacological Bulletin*
- Chateigner D., Lutterotti L., Hansen T. (1998). Quantitative phase and texture analysis on ceramics-matrix composites using Rietveld texture analysis. *ILL Highlights* **1997** 28-29
- Chateigner D., Morales M., Harper E.M. (2002). QTA of prismatic calcite layers of some bivalves, a link to trichite ancestrals. *Materials Science Forum* **408-412** 1687-1692
- Chateigner D., Ouladdiaf B., Léon F. (2010). Magnetic Quantitative texture analysis using isotropic thermal neutron beams. *Solid State Phenomena* **160** 75-82
- Chateigner D., Ricote J. (2010). Quantitative Texture Analysis of ferro- and pyro-electric films and ceramics. In "Multifunctional Polycrystalline Ferroelectric Materials: Processing and Properties", Pardo et Ricote (Eds), 804 pages
- Chateigner D., Wenk H.-R., Patel A., Todd M., Barber D.J. (1997). Analysis of preferential orientations in PST and PZT thin films on various substrates. *Integrated Ferroelectrics* **19** 121-140
- Chateigner D., Wenk H.-R., Pernet M. (1997a). Orientation analysis of bulk YBCO from incomplete neutron diffraction data. *Journal of Applied Crystallography* **30** 43-48
- Chatterjee S.K., Sen Gupta S.P. (1974). X-ray Fourier line-shape analysis in cold-worked hexagonal zirconium. *Journal of Materials Science* **9** 953-960
- Chattopadhyay S.K., Chatterjee S.K., Sen Gupta S.P. (1990). An x-ray Fourier line shape analysis in cold-worked hexagonal magnesium base alloys. *Journal of Materials Research* **5(10)** 2120-2125
- Cheary R.W., Cline J.P. (1994). An analysis of the effect of different instrumental conditions on the shapes of x-ray powder line profiles. *Advances in X-ray analysis* **38** 75-82
- Checa A.G., Rodriguez-Navarro A.B. (2005). Self-organisation of nacre in the shells of Pterioidea (Bivalvia: Mollusca). *Biomaterials* **26** 1071-1079
- Chen B., Peng X., Wang J., Sun S. (2008). Investigation of interlaced microstructure of aragonite sheets of *Chamidae* shell. *Computational Materials Science* **44(1)** 201-205
- Chen F.H., Koo H.S., Tseng T.Y. (1991). Effect of Ca₂PbO₄ additions on the formation of the 110K phase in Bi-Pb-Sr-Ca-O superconducting ceramics. *Applied Physics Letters* **58(6)** 637-639
- Chen T., Neville A., Yuan M. (2005). Assessing the effect of Mg²⁺ on CaCO₃ scale formation-bulk precipitation and surface deposition. *Journal of Crystal Growth* **275(1-2)** e1341-e1347
- Chernock W.P., Beck P.A. (1952). Analysis of certain errors in the x-ray reflection method for the quantitative determination of preferred orientations. *Journal of Applied Physics* **23(3)** 341-345
- Choi M.G., Koh H.S., Klues D., O'Connor D., Mathur A., Truskey G.A., Rubin J., Zhou D.X.F., Sung K.-L.P. (2005). Effects of titanium particle size on osteoblast functions *in vitro* and *in vivo*. *Proceedings of the National Academy of Sciences of the USA* **102(12)** 4578-4583
- Clarke R., Whatmore R.W. (1976). The growth and characteristics of PbZr_xTi_{1-x}O₃ single crystals. *Journal of Crystal Growth* **33** 29-38
- Clemens B.M., Bain J.A. (1992). Stress determination in textured thin films using x-ray diffraction. *Materials Research Society Bulletin* **17 (July)** 46-51
- Cochran W. (1955). Relations between the phases of structure factors. *Acta Crystallographica* **8** 473-478
- Cohen J.B., Wagner C.N.J. (1962). Determination of twin fault probabilities from diffraction patterns of fcc metals and alloys. *Journal of Applied Physics* **33(6)** 2073-&
- Compton A.H. (1923). The total reflexion of x-rays. *Philosophical Magazine* **45** 1121-1129
- Cont L., Chateigner D., Lutterotti L., Ricote J., Calzada M.L., Mendiola J. (2002). Combined X-ray Texture-Structure-Microstructure Analysis applied to ferroelectric ultrastructures: a case study on Pb_{0.76}Ca_{0.24}TiO₃. *Ferroelectrics* **267** 323-328
- Courtois C., Devemy S., Champagne P., Lippert M., Rguiti M., Leriche A., Chateigner D., Guilmeau E. (2007). Comparison of two molten flux process for the elaboration of textured PZT thin plates. *Journal of the European Ceramic Society* **27** 3779-3783
- Couterne J.C., Cizeron G. (1971). Phénomène de défocalisation lié à la géométrie de la chambre de texture de Schulz et incidence sur l'intensité mesurée. *Journal of Applied Crystallography* **4** 461-472

- Cransvick L. (1999). Collaborative Computational Project Number 14 (CCP14): single crystal and powder diffraction (freely available crystallographic software for students and academia). <http://www.ccp14.ac.uk/>
- Croce P., Névot L. (1976). Etude des couches minces et des surfaces par réflexion rasante, spéculaire ou diffuse, de rayons X. *Revue de Physique Appliquée* **11(1)** 113-125
- Cullity B.D. (1978). "Elements of X-ray diffraction", p. 447. 2nd. Edition, Cullity (Ed.), Addison-Wesley Publishing Company, Reading MA. 547 pages.
- Currey J.D. (1977). Mechanical Properties of Mother of Pearl in Tension. *Proceedings of the Royal Society of London B, Biological Sciences* **196** 443-463
- Dahms M., Bunge H.-J. (1988). A positivity method for the determination of complete orientation distribution functions. *Textures and Microstructures* **10(1)** 21-35
- Daillat J., Bérorgey O. (1992). Surface scattering of x-rays in thin films. Part I. Theoretical treatment. *Journal of Chemical Physics* **97(8)** 5824-5835
- De Boer D.K.G. (1994). Influence of the roughness profile on the specular reflectivity of x-rays and neutrons. *Physical Review B* **49** 5817-5820
- De Keijser Th.H., Langford J.I., Mittemeijer E.J., Vogels A.B.P. (1982). Use of the Voigt function in a single-line method for the analysis of X-ray diffraction line broadening. *Journal of Applied Crystallography* **15** 308-314
- Dele-Dubois M.L., Merlin J.C. (1981). Etude par spectroscopie Raman de la pigmentation du squelette calcaire du corail. *Revue de Gemmologie* **68** 10-13
- Delhez R., de Keijser Th.H., Langford J.I., Louër D., Mittemeijer E.J., Sonneveld E.J. (1993). Crystal imperfection broadening and peak shape in the Rietveld method. In "The Rietveld Method". Young R.A. (Ed.), IUCr/Oxford University Press. Pp132-166
- Delhez R., de Keijser Th.H., Mittemeijer E.J. (1980). Accuracy in powder diffraction. *National Bureau of Standards Special Publications* **567** 213-253
- De Rango P., Lees M.R., Lejay P., Sulpice A., Tournier R., Ingold M., Germi P., Pernet M. (1991). Texturing of magnetic materials at high temperature by solidification in a magnetic field. *Nature* **349** 770-771
- Derniaux E. (2007). "Etude de structures NiCoCrAlY / Al₂O₃ / TiO_x / Pt / AlN déposées par pulvérisation cathodique sur superalliage base Ni pour capteurs de pression haute température". PhD Thesis, Université de Caen Basse-Normandie.
- Derniaux E., Kayser P., Gageant C., Boivin D., Thobois P., Chateigner D., Gréville D. (2010). Effect of RF bias sputtering on texture and residual stress of AlN films deposited on Pt/TiO_x/Al₂O₃ multilayer structures using the X-ray combined analysis. To be published
- Deutsch M., Ocko B.M. (1998). X-ray and neutron reflectivity. In "Encyclopedia of Applied Physics", G.L. Trigg (Ed.), VCH New-York, vol. **23** pp 479-489
- De Wolff P.M. (1957). On the determination of unit-cell dimensions from powder diffraction patterns. *Acta Crystallographica* **10** 590-595
- De Wolff P.M. (1968). A simplified criterion for the reliability of a powder pattern indexing. *Journal of Applied Crystallography* **1** 108-113
- Dickson J.I., Boutin J., Handfield L. (1984). A comparison of two simple methods for measuring cyclic internal and effective stresses. *Materials Science and Engineering* **64(1)** L7-L11
- Dietrich S., Haase A. (1995). Scattering of x-rays and neutrons at interfaces. *Physics Reports* **260(1-2)** 1-138
- Dimos D., Chaudhari P., Mannhart J., LeGoues F.K. (1988). Orientation dependence of grain-boundary critical currents in YBa₂Cu₃O_{7-d} bicrystals. *Physical Review Letters* **61(2)** 219-222
- Dollase W.A. (1986). Correction of intensities for preferred orientation in powder diffractometry: application of the March model. *Journal of Applied Crystallography* **19** 267-272
- Dong C., Wu F., Chen H. (1999). Correction of zero shift in powder diffraction patterns using the reflection-pair method. *Journal of Applied Crystallography* **32** 850-853
- Dragomir I.C., Ungár T. (2002). Contrast factors of dislocations in hexagonal crystal system. *Journal of Applied Crystallography* **35** 556-564
- Durand L., Kircher F., Régnier P., Chateigner D., Pellerin N., Gotor F.J., Simon P., Odier P. (1995). Orientation of Y₂BaCuO₅ precipitates during unidirectional solidification of YBa₂Cu₃O_{7-δ} under a magnetic field. *Superconductor Science and Technology* **8** 214-218
- Dusek M., Petříček V., Wunschel M., Dinnebier R.E., van Smaalen S. (2001). Refinement of modulated structures against x-ray powder diffraction data with JANA2000. *Journal of Applied Crystallography* **34** 398-404
- Eastman J., Bausmeister P. (1974). The microstructure of polished optical surfaces. *Optics Communications* **12(4)** 418-420

- Eberhart J.-P. (1989), "*Analyse Structurale et Chimique des Matériaux (diffraction des rayons X, électrons et neutrons, spectrométrie des rayons X, électrons et ions, microscopie électronique)*", Eberhart J.-P. (Ed.), Dunod, 614 pages
- Ewing R.C., Weber W.J., Clinard Jr F.W. (1995). Radiation effects in nuclear waste forms for high-level radioactive waste. *Progress in Nuclear Energy* **29(2)** 63-127
- Esling C., Muller J., Bunge H.-J. (1982). An integral formula for the even part of the texture function or "the apparition of the f_n and f_0 ghost distributions". *Journal de Physique* **43(2)** 189-196
- Essmann U., Mughrabi H. (1979). Annihilation of dislocations during tensile and cyclic deformation and limits of dislocation densities. *Philosophical Magazine A* **40(6)** 731-756
- Ewald P.P. (1940). X-ray diffraction by finite and imperfect crystal lattices. *Proceedings of the Physical Society* **52** 167-174
- Fabris S., Paxton A.T., Finnis M.W. (2000). Relative energetics and structural properties of zirconia using a self-consistent tight-binding model. *Physical Review B* **61(10)** 6617-6630
- Falini G., Albeck S., Weiner S., Addadi L. (1996). Control of Aragonite or Calcite Polymorphism by Mollusk Shell Macromolecules. *Science* **271** 67-69
- Feaugas X., Haddou H. (2003). Grain-size effects on tensile behaviour of nickel and AlSi 316L stainless steel. *Metallurgical and Materials Transactions A-Physical Metallurgy and Materials Science* **34(10)** 2329-2340
- Feng C. (1965). Determination of relative intensity in x-ray reflection study. *Journal of Applied Physics* **36(11)** 3432-3435
- Feng Y., Zhu M., Liu F., Liu J., Han H., Han Y. (2001). Structural evaluation of polycrystalline silicon thin films by hot-wire-assisted PECVD. *Thin Solid Films* **395(1-2)** 213-216
- Field M., Merchant M.E. (1949). Reflection method of determining preferred orientation on the Geiger-counter spectrometer. *Journal of Applied Physics* **20** 741-745
- Finger L.W., Cox D.E., Jephcoat A.P. (1994). A correction for powder diffraction peak asymmetry due to axial divergence. *Journal of Applied Crystallography* **27** 892-900
- Fischer R.X., Schmucker M., Angerer P., Schneider H. (2001). Crystal structures of Na and K aluminate mullites. *American Mineralogist* **86(11-12)** 1513-1518
- Fisher R.A. (1922). On the mathematical foundations of theoretical statistics. *Philosophical Transactions of the Royal Society of London A* **222** 309-368
- Flinn J.E., Field D.P., Korth G.E., Lillo T.M., Macheret J. (2001). The flow stress behavior of OFHC polycrystalline copper. *Acta Materialia* **49(11)** 2065-2074
- Fourie J.T. (1968). Flow stress gradient between surface and centre of deformed copper single crystals. *Philosophical Magazine* **17** 735-756
- Fourie J.T. (1970). Sub-surface dislocation structure of deformed copper. *Philosophical Magazine* **21** 977-985
- Fourie J.T., Dent N.C.G. (1972). The soft surface effect in deformed a-phase Cu-5.8 at % Al. *Acta Metallurgica* **20(11)** 1291-1296
- Gale B., Griffiths D. (1960). Influence of instrumental aberrations on the Schultz technique for the measurement of pole figures. *British Journal of Applied Physics* **11(3)** 96-102
- Gau J.-T., Principe C., Wang J. (2007). An experimental study on size effects on flow stress and formability of aluminum and brass for microforming. *Journal of Materials Processing Technology* **184(1-3)** 42-46
- Gehrke R., Zachmann H.G. (1981). Determination of the degree of crystallinity and of crystal-lattice defects in poly(ethylene-terephthalate) using the x-ray method of Ruland. *Macromolecular Chemistry and Physics – Makromolekulare Chemie* **182(2)** 627-635
- Gergaud P. (1992). "Analyse mécanique et microstructurale de dépôts de molybdène et molybdène carboné élaborés par pulvérisation cathodique magnétron". PhD Thesis, E.N.S.A.M. of Paris, France
- Germain G., Main P., Woolfson M.M. (1971). On the application of phase relationships to complex structures III. The optimum use of phase relationships. *Acta Crystallographica A* **27** 368-376
- Gibaud A. (1999). Specular reflectivity from smooth and rough surfaces. "*X-ray and neutron reflectivity: principles and applications*", J. Daillant et A. Gibaud (Eds.), Springer-Verlag, Lecture Notes in Physics Monographs 58, p 87-120
- Gibaud A., Vignaud G., Sinha S.K. (1993). The correction of geometrical factors in the analysis of x-ray reflectivity. *Acta Crystallographica A* **49** 642-648
- Grahn H.T., Maris H.J., Tauc J. (1989). Picoseconds ultrasonics. *IEEE Journal of Quantum Electronics* **25(12)** 2562-2569
- Gražulis S., Chateigner D., Downs R.T., Yokochi A.F.T., Quirós M., Lutterotti L., Manakova E., Butkus J., Moeck P., Le Bail A. (2009). Crystallography Open Database – an open access collection of crystal structures. *Journal of Applied Crystallography* **42(4)** 726-729 <http://www.crystallography.net/>
- Grebille D., Lambert S., Bourée F., Petricek V. (2004). Contribution of powder diffraction for structure refinements of aperiodic misfit cobalt oxides. *Journal of Applied Crystallography* **37** 823-831

- Grebille D., Muguerra H., Pérez O., Guilmeau E., Rousselière H., Funahashi R. (2007). Superspace crystal symmetry of thermoelectric misfit cobalt oxides and predicted structural models. *Acta Crystallographica B* **63** 373-383
- Gridi-Bennadji F., Chateigner D., Di Vita G., Blanchart P. (2009). Mechanical properties of textured ceramics from muscovite-kaolinite alternate layers. *Journal of the European Ceramic Society* **29(11)** 2177-2184
- Grimmer H. (1992). The piezomagnetolectric effect. *Acta Crystallographica A* **48** 266-271
- Grimmer H. (1993). General relations for transport properties in magnetically ordered crystals. *Acta Crystallographica A* **49** 763-771
- Grimmer H. (1994). The forms of tensors describing magnetic, electric and toroidal properties. *Ferroelectrics* **161** 181-189
- Grimmer H. (2007). The piezoelectric effect of second order in stress and strain: its form for crystals and quasicrystals of any symmetry. *Acta Crystallographica A* **63** 441-446
- Guilmeau E., Chateigner D., Noudem J. (2002). Sinter-forging of strongly textured Bi2223 discs with large J_c : nucleation and growth of Bi2223 from Bi2212 crystallites. *Superconductor Science and Technology* **15** 1436-1444
- Guilmeau E., Chateigner D., Noudem J.G. (2003). Effect of the precursor powders on the final properties of hot-forged Bi2223 textured discs. *Superconductor Science and Technology* **16** 484-491
- Guilmeau E., Chateigner D., Noudem J.G., Funahashi R., Horii S., Ouladdiaf B. (2005). Rietveld texture analysis of complex oxides: examples of polyphased Bi2223 superconducting and Co349 thermoelectric textured ceramics characterization using neutron and X-ray diffraction. *Journal of Applied Crystallography* **38** 199-210
- Guilmeau E., Chateigner D., Suzuki T.S., Sakka Y., Henrist C., Ouladdiaf B. (2005). Rietveld texture analysis of alumina ceramics by neutron diffraction. *Chemistry of Materials* **17** 102-106
- Guilmeau E., Lambert S., Chateigner D., Noudem J.G., Ouladdiaf B. (2003). Quantitative texture analysis of polyphased oxides by diffraction: example of Bi-2223 sinter-forged ceramic and Y123 foam superconductors. *Materials Science and Engineering B* **104** 107-112
- Guilmeau E., Mikami M., Funahashi R., Chateigner D. (2005). Synthesis and Thermoelectric properties of $\text{Bi}_{2.5}\text{Ca}_{2.5}\text{Co}_2\text{O}_x$ layered cobaltites. *Journal of Materials Research* **20(4)** 1002-1008
- Guilmeau E., Pollet M., Grebille D., Chateigner D., Vertruyen B., Cloots R., Funahashi R., Ouladdiaf B. (2008). Neutron diffraction texture analysis and thermoelectric properties of BiCaCoO misfit compounds. *Material Research Bulletin* **43** 394-400
- Guinier A. (1956). "Théorie et technique de la radiocristallographie", Guinier (Ed.), Dunod, Paris
- Guinier A. (1994). "X-ray Diffraction", Guinier (Ed.), Dover Publications, Inc., New York
- Hall W.H. (1949). X-ray line broadening in metals. *Proceedings of the Physical Society of London section A* **62(359)** 741-743
- Hamley I.W., Pedersen J.S. (1994). Analysis of neutron and x-ray reflectivity data. I. Theory. *Journal of Applied Crystallography* **27** 29-35
- Hansen N. (1977). The effect of grain size and strain on the tensile flow stress of aluminium at room temperature. *Acta Metallurgica* **25(8)** 863-869
- Hare P.E., Abelson P.H. (1965). Amino acid composition of some calcified proteins. Year book-Carnegie Institute, Washington **65** 223-232
- Hatanaka T., Hasegawa H. (1995). Dielectric properties of $\text{Pb}(\text{Zr}_x\text{Ti}_{1-x})\text{O}_3$ single crystals including monoclinic zirconia. *Japanese Journal of Applied Physics* **34** 5346-5348
- Hauk V. (1997). "Structural and residual stress analysis by non-destructive methods: evaluation, application, assessment", Hauk (Ed.), Amsterdam, Elsevier
- Hauk V., Vaessen G. (1985). Residual-stresses in groups of crystallites of steels having preferred orientation. *Zeitschrift für Metallkunde* **76(2)** 102-107
- Hauptman H., Karle J. (1953). Solution of the Phase Problem I. The Centrosymmetric Crystal. *American Crystallographic Association monograph n°3*, New-York, 87 p
- Hauptman H., Karle J. (1953a). The probability distribution of the magnitude of a structure factor. II. The non-centrosymmetric crystal. *Acta Crystallographica* **6** 136-141
- Hearmon R.F.S. (1946). The elastic constants of anisotropic materials. *Reviews of Modern Physics* **18(3)** 409-440
- Hearmon R.F.S. (1956). The elastic constants of anisotropic materials 2. *Advances in Physics* **5(19)** 323-&
- Hedegaard C., Bardeau J.-F., Chateigner D. (2006). Molluscan shell pigments: An in situ resonance Raman study. *Journal of Molluscan Studies* **72** 157-162
- Heidelbach F., Riekel C., Wenk H.-R. (1999). Quantitative texture analysis of small domains with synchrotron radiation x-rays. *Journal of Applied Crystallography* **32** 841-849
- Heizmann, J.-J., Laruelle, C. (1986). Simultaneous measurement of several x-ray pole figures. *Journal of Applied Crystallography* **19** 467-472

- Helming K. (1992). Minimal pole figure ranges for quantitative texture analysis. *Texture and Microstructure* **19** 45-54
- Helming K. (1998). Texture approximations by model components. *Materials Structure* **5(1)** 3-9
- Hermida J.D. (1982). Influence of the sample radius and irradiated zone width on the defocusing phenomenon in the Schulz technique. *Materials Science and Engineering* **56** 135-141
- Hielscher R., Schaeben H. (2008). A novel pole figure inversion method: specification of the MTEX algorithm. *Journal of Applied Crystallography* **41** 1024-1037. <http://code.google.com/p/mtex/>
- Hielscher R., Schaeben H., Chateigner D. (2007). On the entropy to texture index relationship in quantitative texture analysis. *Journal of Applied Crystallography* **40** 371-375
- Hill R. (1952). The elastic behaviour of a crystalline aggregate. *Proceedings of the Physical Society of London* **A65(389)**, 349-354
- Hill R.J., Fischer R.X. (1990). Profile agreement indices in Rietveld and pattern-fitting analysis. *Journal of Applied Crystallography* **23** 462-468
- Hill R.J., Flack H.D. (1987). The use of the Durbin-Watson d statistic in Rietveld analysis. *Journal of Applied Crystallography* **20** 356-361
- Hill R.J., Howard C.J. (1987). Quantitative phase analysis from neutron powder diffraction data using the Rietveld method. *Journal of Applied Crystallography* **20** 467-474
- Hirao, M., Ogi H. (2003). "*EMATs for Science and Industry*", Kluwer, Boston.
- Hodgins C.G., Irwin, J.C. (2006). Elastic constants of ZnSe. *Physica Status Solidi A* **28** 647-652
- Holland J.R. (1964). Quantitative determinations and descriptions of preferred orientation. *Advances in X-ray Analysis* **7** 86-93
- Horning R.D., Staudenmann J.-L. (1988). The Debye-Waller factor for polyatomic solids. Relationships between X-ray and specific-heat Debye temperatures. The Debye-Einstein model. *Acta Crystallographica A* **44** 136-142
- Hosemann R. (1950). Röntgeninterferenzen an stoffen mit flüssigkeitsstatistischen gitterstörungen. *Zeitschrift für Physik A* **128(1)** 1-35
- Hosemann R. (1951). Die parakristalline Feinstruktur natürlicher und synthetischer Eiweisse. Visuelles Näherungsverfahren zur Bestimmung der Schwankungstensenoren von Gitterzellen. *Acta Crystallographica* **4** 520-530
- Hosoda N., Sugawara A., Kato T. (2003). Template effect of crystalline poly(vinyl alcohol) for selective formation of aragonite and vaterite CaCO₃ thin films *Macromolecules* **36(17)** 6449-6452
- Houben L, Luysberg M, Carius R. (2003). Microtwinning in microcrystalline silicon and its effect on grain-size measurements. *Physical Review B* **67** 045312 [10 pages]
- Howard C.J. (1982). The approximation of asymmetric neutron powder diffraction peaks by sums of Gaussians. *Journal of Applied Crystallography* **15** 615-620
- Huijser-Gerits E.M.C., Rieck G.D. (1974). Defocusing effects in the reflexion technique for the determination of preferred orientation. *Journal of Applied Crystallography* **7** 286-290
- Hurley D.H., Wright O.B., Matsuda O., Gusev V.E., Kolosov O.V. (2000). Laser picosecond acoustics in isotropic and anisotropic materials. *Ultrasonics* **38(1-8)** 470-474
- Ibers J.A. (1958). Atomic scattering amplitudes for electrons. *Acta Crystallographica* **11** 178-183
- Ikeda S., Carpenter J.M. (1985). Wide-energy-range, high-resolution measurements of neutron pulse shapes of polyethylene moderators. *Nuclear Instruments and Methods in Physics Research A* **239(3)** 536-544
- Imhof J. (1982). The resolution of orientation space with reference to pole figure resolution. *Textures & Microstructures* **4** 189-200
- Isaure M.-P., Laboudigue A., Manceau A., Sarret G., Tiffreau C., Trocellier P., Lamble G., Hazemann J.-L., Chateigner D. (2002). Quantitative Zn speciation in a contaminated dredge sediment by μ -PIXE, μ -EXAFS spectroscopy and principal component analysis. *Geochimica et Cosmochimica Acta* **66** 1549-1567
- Itahara H., Sugiyama J., Tani T. (2004). Enhancement of electrical conductivity in thermoelectric [Ca₂CoO₃]_{0.62}[CoO₂] ceramics by texture improvement. *Japanese Journal of Applied Physics* **43(8A)** 5134-5139
- Itahara H., Tajima S., Tani T. (2002). Synthesis of beta-Co(OH)₂ platelets by precipitation and hydrothermal methods. *Journal of the Ceramics Society of Japan* **110(12)** 1048-1052
- Itahara H., Xia C.T., Sugiyama J., Tani T. (2004). Fabrication of textured thermoelectric layered cobaltites with various rock salt-type layers by using beta-Co(OH)₂ platelets as reactive templates. *Journal of Materials Chemistry* **14(1)** 61-66
- Ito T. (1949). A general powder x-ray photography. *Nature* **164(4174)** 755-756
- Jackson A.P., Vincent J.F.V., Turner R.M. (1990). Comparison of nacre with other ceramic composites. *Journal of Material Sciences* **25** 3173-3178

- Jain S.C., Willander M., Narayan J., van Overstraeten R. (2000). III-nitrides: growth, characterization, and properties. *Journal of Applied Physics* **87(3)** 965-1006
- Janner A. (1995). Towards a more comprehensive crystallography. *Acta Crystallographica B* **51(4)** 386-401
- Jansen E., Schäfer W., Will G. (1994). R values in analysis of powder diffraction data using Rietveld refinement. *Journal of Applied Crystallography* **27** 492-496
- Janssen P.J.M., de Keijser Th. H., Geers M.G.D. (2006). An experimental assessment of grain size effects in the uniaxial straining of thin Al sheet with a few grains across the thickness. *Materials Science and Engineering A* **419(1-2)** 238-248
- Janssen T., Janner A., Looijenga-Vos A., de Wolff P.M. (2006). Incommensurate and commensurate modulated structures. *International Tables for Crystallography*, vol. C, Prince E. (Ed.). Dordrecht: Kluwer Academic Publishers, 907-955
- Jin S., Sherwood R.C., Gyorgy E.M., Tiefel T.H., van Dover R.B., Nakahara S., Schneemeyer L.F., Fastnacht R.A., Davis M.E. (1989). Large magnetic hysteresis in a melt-textured Y-Ba-Cu-O superconductor. *Applied Physics Letters* **54** 584-586
- Jones F.W. (1938). The measurement of particle size by the X-ray method. *Proceedings of the Royal Society* **166(A924)** 16-43
- Jones P., Silver J. (1979). Red and blue-green bile pigments in the shell of *Astraea tuber* (Mollusca: Archaeogastropoda). *Comparative Biochemistry and Physiology Series B* **63** 185-188
- Jorgensen J.D., Johnson D.H., Mueller M.H., Peterson S.W., Worlton J.G., von Dreele R.B. (1978). Proceedings of the Conference on Diffraction Profile Analysis, Cracow, Poland, 14-15 August 1978, pp 20-22
- Jouanneaux A. (1999). WinMProf: a visual Rietveld software. International Union of Crystallography, *Commission on Powder Diffraction Newsletter* **21** 13
- Kakuta K., Tsurumi T., Fukunaga O. (1995). Dielectric Properties of Flux-Grown PbTiO₃ Single Crystal. *Japanese Journal of Applied Physics* **34** 5341-5345
- Kals T.A., Eckstein R. (2000). Miniaturization in sheet metal working. *Journal of Materials Processing Technology* **103(1)** 95-101
- Kamat S., Su X., Ballarini R., Heuer A.H. (2000). Structural basis for the fracture toughness of the shell of the conch *Strombus gigas*. *Nature* **405** 1036-1040
- Karle J., Hauptman H. (1956). A theory of phase determination for the four types of non-centrosymmetric space groups 1P222, 2P22, 3P₁2, 3P₂2. *Acta Crystallographica* **9** 635-651
- Kayser P., Thobois P., Gageant C. (2003). Pt/AlN/Pt Piezoelectric Transducer for Unsteady Pressure Sensor in Rotating Machines. 2002 Activities Report ONERA 3-21.
- Kazan M., Moussaed E., Nader R., Masri P. (2007). Elastic constants of aluminum nitride. *Physica Status Solidi C* **4(1)** 204-207
- Keller C., Hug E., Chateigner D. (2008). On the origin of the stress decrease for nickel polycrystals with few grains across the thickness. *Materials Science and Engineering A* **500** 207-215
- Khattak C.P., Cox D.E. (1977). Profile analysis of x-ray powder diffractometer data: structural refinement of La_{0.75}Sr_{0.25}CrO₃. *Journal of Applied Crystallography* **10** 405-411
- Kim D.-K., Kriven W.M. (2006). Oxide laminated composites with aluminum phosphate (AlPO₄) and alumina platelets as crack deflecting materials. *Composites Part B Engineering* **37(6)** 509-514
- Kingery W.D., Bowen H.K., Uhlmann D.R. (1976). "Introduction to Ceramics", 2nd Ed., Kingery, Bowen, Uhlmann (Eds.), John Wiley & Sons
- Klein H.H., Stern W.B., Weber W. (1982). On physical and chemical properties of ruby muscovite used in the electrical industry. *Schweizerische Mineralogische und Petrographische Mitteilungen* **62(1)** 145-173
- Klug H.P., Alexander L.E. (1974). "X-ray diffraction procedures for polycrystalline and amorphous materials" Wiley, New York
- Kocks U.F. (1988). A symmetric set of Euler angles and oblique orientation space sections. In "8th International Conference on Textures of Materials", Kallend J.S. et Gottstein G. (Eds). Warrendale, PA, USA: The Metallurgical Society, p31-36
- Kocks U.F., Kallend J.S., Wenk H.-R., Rollet A.D., Wright S.I. (1994). popLA, preferred orientation package – Los Alamos. Technical Report LA-CC-89-18, Los Alamos National Laboratory, USA
- Kocks F., Tomé C., Wenk H.-R. (1998). "Texture and Anisotropy", Kocks F., Tomé C., Wenk H.-R. (Eds.), Cambridge University Press
- Kohlbeck F., Hörl E.M. (1976). Indexing program for powder patterns especially suitable for triclinic, monoclinic and orthorhombic lattices. *Journal of Applied Crystallography* **9** 28-33
- Kohlbeck F., Hörl E.M. (1978). Trial and error indexing program for powder patterns of monoclinic substances. *Journal of Applied Crystallography* **11** 60-61
- Koizumi C., Nonaka J. (1970). Yellow pigments of pearl I. Carotenoid pigment in yellow nacre. *Nippon Suisan Gakkaishi (Bulletin of the Japanese Society of Scientific Fisheries)* **36** 1054-1058

- Kolb K., Macherauch E. (1962). Flow stress of surface layers of polycrystalline nickel and its influence on residual stresses in deformed specimens. *Philosophical Magazine* **7(75)** 415–426
- Kong L.B., Zhang T.S., Ma J., Boey F. (2003). Some main group oxides on mullite phase formation and microstructure evolution. *Journal of Alloys and Compounds* **359(1-2)** 292-299
- Konings R.J.M., Haas D. (2002). Fuels and targets for transmutation. *Comptes Rendus Physique* **3(7-8)** 1013-1022
- Koptsik V.A. (1966). "Shubnikov groups", Koptsik (Ed.). Izd. MGU Pub., Moscow.
- Krauss C., Chateigner D., Gil O. (2008). Fully inorganic electrodeposition of pure aragonite prismatic-like textured layers on titanium foils. *Crystal Growth and Design* **8(12)** 4378-4382
- Krishnamurty T.S.G., Gopalakrishnamurty P. (1969). Piezomagnetic coefficients. *Acta Crystallographica A* **25** 332-333
- Kroll U., Meier J., Torres P., Pohl J., Shah A. (1998). From amorphous to microcrystalline silicon films prepared by hydrogen dilution using the VHF (70 MHz) GD technique. *Journal of Non-Crystalline Solids* **227-230(1)** 69-72
- Kuskov V.I., Rusakov A.P., Mentser A.N. (1973). Elastic-constants of ZnSe. *Soviet Physics Solid State* **14** 1869-
- Labat S., Gergaud P., Thomas O., Gilles B., Marty A. (2000). Interdependence of elastic strain and segregation in metallic multilayers: an x-ray diffraction study of {111} Au/Ni multilayers. *Journal of Applied Physics* **87(3)** 1172-1181
- Lambert S., Leligny H., Grebille D. (2001). Three Forms of the Misfit Layered Cobaltite $[\text{Ca}_2\text{CoO}_3][\text{CoO}_2]_{1.62}\cdot\text{A}$ 4D Structural Investigation. *Journal of Solid State Chemistry* **160(2)** 322-331
- Landau L.D., Lifshitz E.M. (1967). "Theory of Elasticity". Mir, Moscow. 207 pages
- Landolt-Börnstein (1966). "Numerical data and functional relationships in science and technology", group III, Elastic, piezoelectric, piezooptic and electrooptic constants of crystals, vol 1., K.-H. Hellwege and A.M. Hellwege (Eds.), Springer-Verlag, Berlin, 150p
- Langford J.I. (1978). A rapid method for analysing the breadths of diffraction and spectral lines using the Voigt function. *Journal of Applied Crystallography* **11** 10-14
- Langford J.I. (1992). "Proceedings of the International Conference on Accuracy in powder Diffraction II", NIST special publications **846** 110-126
- Langford J.I., Boultif A., Auffrédic A., Louër D. (1993). The use of pattern decomposition to study the combined x-ray diffraction effects of crystallite size and stacking faults in ex-oxalate zinc oxide. *Journal of Applied Crystallography* **26** 22-33
- Langford J.I., Louër D. (1982). Diffraction line profiles and Scherrer constants for materials with cylindrical crystallites. *Journal of Applied Crystallography* **15** 20-26
- Langford J.I., Louër D., Scardi P. (2000). Effect of a crystallite size distribution on x-ray diffraction line profiles and whole-powder-pattern fitting. *Journal of Applied Crystallography* **33** 964-974
- Langford J.I., Louër D., Sonneveld E.J., Visser J.W. (1986). Applications of Total Pattern Fitting to a Study of Crystallite Size and Strain in Zinc Oxide Powder. *Powder Diffraction* **1(3)** 211-221
- Larson A.C., Von Dreele R.B. (2000), "General Structure Analysis System (GSAS)", Los Alamos National Laboratory Report LAUR 86-748. <http://www.ncnr.nist.gov/programs/crystallography/software/gsas.html>
- Le Bail A. (1992). Modelling crystallite size/microstrain in Rietveld analysis. National Institute of Standards and Technology Special Publication **846**. Proceedings of the *International Conference on Accuracy in Powder Diffraction II*, NIST, Gaithersburg, MD, May 26-29, 142-153
- Le Bail A. (1995). Modelling the silica glass structure by the Rietveld method. *Journal of Non-Crystalline Solids* **183** 39-42
- Le Bail A. (2005). Whole powder pattern decomposition methods and applications – a retrospection. *Powder Diffraction* **20** 316-326
- Le Bail A., Joux A. (1997). A qualitative account for anisotropic broadening in whole-powder-diffraction-pattern fitting by second-rank tensors. *Journal of Applied Crystallography* **30** 265-271
- Ledbetter H., Ogi H., Nakamura N. (2004). Elastic, anelastic, piezoelectric coefficients of monocystal lithium niobate. *Mechanics of Materials* **36** 941-947
- Legrand B., Chateigner D., Perrier de la Bathie R., Tournier R. (1997). Orientation by solidification in a magnetic field: a new process to texture SmCo compounds used as permanent magnets. *Journal of Magnetism and Magnetic Materials* **173** 20-28
- Legrand C., Yi J.H., Thomas P., Guinebrière R., Mercurio J.-P. (1999). Structural characterisation of sol-gel $\text{SrBi}_2\text{Nb}_2\text{O}_9$ thin film deposited on (001) SrTiO_3 single crystal. *Journal of the European Ceramic Society* **19** 1379-1381
- Leibfried G., Ludwig W. (1961). *Solid State Physics* **12** 275-
- Leisure R.G., Foster K., Hightower J.E., Agosta D.S. (2004). *Material Science and Engineering A* **370** 34-

- Léon F., Chateigner D., Ouladdiaf B., Zucali M., Lutterotti L., Richard D. (2009). Quantitative texture analysis at the D19-ILL beamline using a 120° curved area position sensitive detector. Submitted *Journal of Applied Crystallography*
- Li S., Funahashi R., Matsubara I., Ueno K., Yamada H. (1999). High temperature thermoelectric properties of oxide $\text{Ca}_9\text{Co}_{12}\text{O}_{28}$. *Journal of Materials Chemistry* **9** 1659-
- Li S., Jiang F., Han G., Wang L., Xiong C., Peng X., Mo H. (2005). Relationship between structure characteristic and blue luminescence in unintentional doped GaN layers. *Materials Science and Engineering B* **122(1)** 72-75
- Liu Y.S., Depre L., de Buyser L., Wu T.B., van Houtte P. (2003). Intensity correction in texture measurement of polycrystalline thin films by x-ray diffraction. *Textures and Microstructures* **35(3)** 283-290
- Lopez E., Vidal B., Berland S., Camprasse S., Camprasse G., Silve C. (1992). Demonstration of the capacity of nacre to induce bone formation by human osteoblasts maintained *in vitro*. *Tissues and Cells* **24(5)** 667-679
- Lotgering F.K. (1959). Topotactical reactions with ferrimagnetic oxides having hexagonal crystal structures-I. *Journal of Inorganic and Nuclear Chemistry* **9** 113-123
- Louër D., Langford J.I. (1988). Peak shape and resolution in conventional diffractometry with monochromatic x-rays. *Journal of Applied Crystallography* **21** 430-437
- Louër D., Louër M. (1972). Méthode d'essais et erreurs pour l'indexation automatique des diagrammes de poudre. *Journal of Applied Crystallography* **5** 271-275
- Louër D., Vargas R. (1982). Indexation automatique des diagrammes de poudre par dichotomie successive. *Journal of Applied Crystallography* **15** 542-545
- Lowenstam H. A. (1967). Lepidocrocite, an Apatite Mineral, and Magnetite in Teeth of Chitons (Polyplacophora). *Science* **156** 1373-1375
- Lutterotti L., Scardi P. (1994). Simultaneous structure and size-strain refinement by the Rietveld method. *Journal of Applied Crystallography* **23** 246-252
- Lutterotti L., Matthies S., Wenk H.-R. (1999). MAUD (Material Analysis Using Diffraction): a user friendly Java program for Rietveld texture analysis and more. National Research Council of Canada, Ottawa 1999, 1599-1604. <http://www.ing.unitn.it/~luttero/maud/>
- Lutterotti L., Chateigner D., Ferrari S., Ricote J. (2004). Texture, residual stress and structural analysis of thin films using a combined X-ray analysis. *Thin Solid Films* **450** 34-41
- Lutterotti L., Matthies S., Chateigner D., Ferrari F., Ricote J. (2002). Rietveld texture and stress analysis of thin films by x-ray diffraction. *Materials Science Forum* **408-412** 1603-1608
- Maeder G. (1986). X-ray diffraction and stress measurement. *Chemica Scripta* **26(A)** 23-31
- Maignan A., Hébert S., Hervieu M., Michel C., Pelloquin D., Khomskii D. (2003). Magnetoresistance and magnetothermopower properties of Bi/Ca/Co/O and Bi(Pb)/Ca/Co/O misfit layer cobaltites. *Journal of Physics: Condensed Matter* **15(7)** 2711-2724
- Maistrelli P., Lutterotti L., Scardi P. (1993). Low temperature x-ray powder diffraction of ceria-stabilised zirconia. *Materials Science Forum* **133-136** 783-788
- Maistrelli P., Lutterotti L., Scardi P. (1994). Thermal behaviour of monoclinic zirconia at low temperature by XRPD full pattern analysis. *Materials Science Forum* **166-169** 495-500
- Malmros G., Thomas J.O. (1977). Least-squares structure refinement based on profile analysis of powder film intensity data measured on an automatic microdensitometer. *Journal of Applied Crystallography* **10** 7-11
- Manceau A., Chateigner D., Gates W.P. (1998). Polarized EXAFS, distance-valence least-squares modeling (DVLS), and quantitative texture analysis approaches to the structural refinement of Garfield nontronite. *Physics and Chemistry of Minerals* **25** 347-365
- Mann S. (1988). Molecular recognition in biomineralization. *Nature* **332(10)** 119-124
- March A. (1932). Mathematische theorie der regelung nach der korngestalt bei affiner deformation. *Zeitschrift für Kristallographie* **81** 285-297
- Markelov V.A., Novikov M.A., Turkin A.A. (1977). Experimental observation of a new nonreciprocal magneto-optical effect. *Journal of Experimental and Theoretical Physics Letters* **25** 378-380
- Matsuda O., Wright O.B., Hurley D.H., Gusev V.E., Shimizu K. (2004). Coherent shear phonon generation and detection with ultrashort optical pulses. *Physical Review Letter* **93(9)** 095501 [4 pages]
- Matthies S. (1979). Reproducibility of the orientation distribution function of texture samples from pole figures (ghost phenomena). *Physica Status Solidi B* **92(2)** K135-K138
- Matthies S., Chateigner D. (2000). Definition of spectrometer/diffraction related parameters, angles, rotation directions and coordinate systems. http://www.ecole.ensicaen.fr/~chateign/texture/working_formulaes.pdf
- Matthies S., Humbert M. (1995). On the principle of a geometric mean of even-rank symmetric tensors for textured polycrystals. *Journal of Applied Crystallography* **28** 254-266
- Matthies S., Lutterotti L., Wenk H.-R. (1997). Advances in texture analysis from diffraction spectra. *Journal of Applied Crystallography* **30**, 31-42.

- Matthies S., Vinel G.W. (1982). On the reproduction of the orientation distribution function of texturized samples from reduced pole figures using the conception of a conditional ghost correction. *Physica Status Solidi B* **112** K111-K114
- Matthies S., Vinel G.W., Helming K. (1987), "Standard Distributions in Texture Analysis". Vol 1, Ed. Matthies, Akademie Verlag, Berlin. 449p
- Matthies S., Wenk H.-R. (1985). ODF reproduction with conditional ghost correction. In "Preferred orientation in deformed metals and rocks: an introduction to modern texture analysis", H.-R. Wenk (Ed.), Academic Press inc. pp 139-147
- Matthies S., Wenk H.-R. (1992). Optimization of texture measurements by pole figure coverage with hexagonal grids. *Physica Status Solidi A* **133** 253-257
- Matthies S., Wenk H.-R., Vinel G.W. (1988). Some basic concepts of texture analysis and comparison of three methods to calculate orientation distributions from pole figures. *Journal of Applied Crystallography* **21** 285-304
- Matulis C.E., Taylor J.C. (1993). A theoretical model for the correction of intensity aberrations in Bragg-Brentano x-ray diffractometers – detailed description of the algorithm. *Journal of Applied Crystallography* **26** 351-356
- Mayanovic R.A., Sladek R.J., Debska U. (1988). Elastic constants of $Zn_{1-x}Mn_xSe$: tetrahedral bond weakening due to Mn 3d(t₂)-Se 4p hybridization. *Physical Review* **B38(2)** 1311-1315
- McCusker L.B., von Dreele R.B., Cox D.E., Louer D., Scardi P. (1999). Rietveld refinement guidelines. *Journal of Applied Crystallography* **32** 36-50
- McSkimin H.J., Andreatch Jr. P. (1964). Elastic Moduli of Silicon vs Hydrostatic Pressure at 25.0°C and – 195.8°C. *Journal of Applied Physics* **35(7)** 2161-2165
- Mecking H. (1977). "Work Hardening in Tension and Fatigue", A.W. Thompson (Ed.), TMS-AIME, New York p 67-89
- Mecking H., Kocks U.F. (1981). Kinetics of flow and strain-hardening. *Acta Metallurgica* **29(11)** 1865-1875
- Michel J.F., Picart P. (2003). Size effects on the constitutive behaviour for brass in sheet metal forming. *Journal of Materials Processing Technology* **141** 439–446
- Migliori A., Sarro J. (1997). "Resonant Ultrasound Spectroscopy", Wiley-Interscience, New-York
- Mikami M., Guilmeau E., Funahashi R., Chong K., Chateigner D. (2005). Enhancement of electrical properties of the thermoelectric compound $Ca_3Co_4O_9$ through use of Large-Grained Powder. *Journal of Materials Research* **20(9)** 2491-2497
- Miro S., Grébillé D., Chateigner D., Pelloquin D., Stoquert J.-P., Grob J.-J., Costantini J.-M., Studer F. (2005). X-ray diffraction study of damage induced by swift heavy ion irradiation in fluorapatite. *Nuclear Instruments and Methods in Physics Research B* **227** 306-318
- Mittemeijer E.J., Scardi P. (2004). "Diffraction analysis of the microstructure of materials". Springer, Berlin
- Miyazaki S., Shibata K., Fujita H. (1979). Effect of specimen thickness on mechanical properties of polycrystalline aggregates with various grain sizes. *Acta Metallurgica* **27(5)** 855–862
- Morales M., Artigas M., Bacmann M., Fruchart D., Skolozdra R., Soubeyroux J.-L., Wolfers P. (1999). Comparison of the magnetic properties of $ErMn_{12-x}Fe_x$ series with their related hydrides and carbides. *Journal of Magnetism and Magnetic Materials* **196-197** 703-704
- Morales M., Bacmann M., Wolfers P., Fruchart D., Ouladdiaf B. (2001). Magnetic properties and interactions in the $RMn_{12-x}Fe_x$ series (R = Y, Ho, Er, Nd and $x \leq 9$). *Physical Review B* **64(14)** 144426
- Morales M., Bacmann M., Fruchart D., Wolfers P., Ouladdiaf B. (2001a). Impact of hydrogen and carbon insertion on the fundamental characteristics of the $ErMn_{12-x}Fe_x$ compounds. *Journal of Magnetism and Magnetic Materials* **236(1-2)** 83-92
- Morales M., Chateigner D., Fruchart D. (2003). Texture and magneto-crystalline anisotropy analysis of an oriented $ErMn_4Fe_8C$ powder sample. *Journal of Magnetism and Magnetic Materials* **257(2)** 258-269
- Morales M., Chateigner D., Lutterotti L., Ricote J. (2002). X-ray Combined QTA using a CPS applied to a ferroelectric ultrastructure. *Materials Science Forum* **408-412**, 113-118.
- Morales M., Leconte Y., Rizk R., Chateigner D. (2004). Anisotropic crystallite size analysis of textured nanocrystalline silicon thin films probed by x-ray diffraction. *Thin Solid Films* **450** 216-221
- Morales M., Leconte Y., Rizk R., Chateigner D. (2005). Structural and microstructural characterization of nanocrystalline silicon thin films obtained by radio-frequency magnetron sputtering. *Journal of Applied Physics* **97** 034307
- Mughrabi H. (1970). Investigations of Plastically Deformed Copper Single Crystals in the Stress-Applied State. I. A Study of the Dislocation Behaviour in the Surface Region and in the Bulk. *Physica Status Solidi B* **39(1)** 317-327
- Mughrabi H. (1971). Some consequences of surface and size effects in plastically deformed copper single crystals. *Physica Status Solidi B* **44(1)** 391-402

- Mutvei H. (1980). The nacreous layer in molluscan shells, in "The Mechanisms of Biomineralization in Animals and Plant". Omori M., Watabe N. (Eds.), Tokai University Press: Tokyo, JP. pp 49-56
- Mutvei H., Dunca E. (2008). Structural relationship between interlamellar organic sheets and nacreous tablets in gastropods and the cephalopod *Nautilus*. *Palaeontologische Zeitschrift* **82(1)** 85-94
- Nakahara H. (1983). "Biomineralization and biological metal accumulation" Westbroek P., Jong E.W. (Ed) Reidel: Dordrecht, NL, pp 225-230
- Nakahara H. (1991). "Mechanisms and phylogeny of mineralization in biological systems" Suga S., Nakahara H. (Ed) Springer: Berlin, DE, chap. 4.2, pp 343-350
- Nakamura S. (1999). InGaN-based violet laser diodes. *Semiconductor Science and Technology* **14** R27-R40
- Narutani T., Takamura J. (1991). Grain-size strengthening in terms of dislocation density measured by resistivity. *Acta Metallurgica et Materiala* **39(8)** 2037-2049
- Nassif N., Pinna N., Gehrke N., Antonietti M., Jäger C., Cölfen H. (2005). Amorphous layer around aragonite platelets in nacre. *Proceedings of the National Academy of Sciences of the USA* **102(36)** 12653-12655
- Nemat-Nasser S., Maximenko A., Olevsky E. (2006). Modeling the plastic response of thin metal membranes. *Journal of the Mechanics and Physics of Solids* **54(11)** 2474-2494
- Neville A., Morizot A.P. (2002). Calcareous scales formed by cathodic protection—an assessment of characteristics and kinetics. *Journal of Crystal Growth* **243(3-4)** 490-502
- Nevitt M.V., Chan S.K., Liu J.Z., Grimsditch M.H., Fang Y. (1988). The elastic properties of monoclinic ZrO₂. *Physica B & C* **150(1-2)** 230-233
- Névoit L., Croce P. (1980). Caractérisation des surfaces par réflexion rasante de rayons X. Application à l'étude du polissage de quelques verres silicates. *Revue de Physique Appliquée* **15(3)** 761-779
- Noudem J.-G., Beille J., Bourgault D., Chateigner D., Tournier R. (1996). Bulk textured Bi-Pb-Sr-Ca-Cu-O (2223) ceramics by solidification in a magnetic field. *Physica C* **264** 325-330
- Noudem J.G., Guilmeau E., Chateigner D., Lambert S., Reddy E.S., Ouladdiaf B., Schmitz G.J. (2004). Properties of YBa₂Cu₃O_y-textured superconductor foams. *Physica C* **408** 655-656
- Noudem J.G., Harnois C., Chateigner D., Chaud X. (2003). Melt textured YBCO bulks with artificially patterned holes. "Applied Superconductivity", *Inst. Phys. Conf. ser n°181, IOP Publishing Ltd.*, 1426-1431
- Noudem J.G., Meslin S., Harnois C., Chateigner D., Chaud X. (2004). Melt textured YBa₂Cu₃O_y bulks with artificially patterned holes: a new way of processing c-axis fault current limiter meanders. *Superconductor Science and Technology* **17** 931-936
- Noyan I.C., Cohen J.B. (1987). "Residual Stress: measurement by diffraction and interpretation". Noyan, Cohen (Eds.), Springer-Verlag
- Noyan I.C., Huang T.C., York B.R. (1995). Residual stress/strain analysis in thin films by x-ray diffraction. *Critical Reviews in Solid State and Materials Sciences* **20(2)** 125-177
- Nye J.-F. (1985), "Physical Properties of Crystals: their representation by tensors and matrices", Lavoisier publishers, 330 p.
- O'Connor B.H., Li D.Y., Sitepu H. (1991). Strategies for preferred orientation corrections in x-ray powder diffraction using line intensity ratios. *Advances in X-ray Analysis* **34** 409-415
- O'Connor B.H., Li D.Y., Sitepu H. (1992). Texture characterization in x-ray powder diffraction using the March formula. *Advances in X-ray Analysis* **35** 277-283
- Ogi H., Ohmori T., Nakamura N., Hirao M. (2006). Elastic, anelastic, and piezoelectric coefficients of alpha-quartz determined by resonance ultrasound spectroscopy. *Journal of Applied Physics* **100(5)** 053511
- Okada K. (2008). Activation energy of mullitization from various starting materials. *Journal of the European Ceramic Society* **28(2)** 377-382
- Orton J.W., Foxon C.T. (1998). Group III nitride semiconductors for short wavelength light-emitting devices. *Reports on Progress in Physics* **61(1)** 1-75
- Ouchani S, Dran J.C., Chaumont J. (1997). Evidence of ionization annealing upon helium-ion irradiation of pre-damaged fluorapatite. *Nuclear Instruments and Methods in Physics section B: Beam Interactions with Materials and Atoms* **132(3)** 447-451
- Ouhenia S., Chateigner D., Belkhir M.A., Guilmeau E. (2008). Microstructure and Crystallographic Texture of *Charonia lampas lampas* Shell. *Journal of Structural Biology* **163** 175-184
- Park Y.S. (1999). Current status of group III-nitride semiconductors and future prospects. *Journal of the Korean Physical Society* **34** S199-S219
- Parrat L.G. (1954). Surface studies of solids by total reflection of x-rays. *Physical Review* **95(2)** 359-369
- Patterson A.L. (1934). A Fourier Series Method for the Determination of the Components of Interatomic Distances in Crystals. *Physical Review* **46(5)** 372-376
- Patterson A.L. (1939). The diffraction of x-rays by small crystalline particles. *Physical Review* **56(10)** 972-977
- Paul T.A., Fitzgerald P.G. (1992). Transmission electron-microscopic investigation of fission tracks in fluorapatite. *American Mineralogist* **77(3-4)** 336-344

- Pawley G.S., Mackenzie G.A., Dietrich O.W. (1977). Neutron powder diffraction and constrained refinement. The structures of p-dibromo and p-diiodotetrafluorobenzene. *Acta Crystallographica A* **33** 142-145
- Pawley G.S. (1981). Unit-cell refinement from powder diffraction scans. *Journal of Applied Crystallography* **14** 357-361
- Pawlik K. (1993). Application of the ADC method for ODF approximation in cases of low crystal and sample symmetries. *Materials Science Forum* **133-136** 151-156
- Pawlik K., Ozga P. (1999), LaboTex: The texture analysis software, "Göttinger Arbeiten zur Geologie und Paläontologie", SB4. <http://www.labosoft.com/pl/>
- Pernet M., Chateigner D., Germi P., Dubourdieu C., Thomas O., Sénateur J.-P., Chambonnet D., Belouet C. (1994). Texture influence on critical current density of YBCO films deposited on (100)-MgO substrates. *Physica C* **235-240** 627-628
- Petricek V., Dusek M., Palatinus L. (2006). *The crystallographic computing system*. Institute of Physics, Praha, Czech Republic
- Pézeril T. (2005). *Génération et détection d'ondes acoustiques transverses picosecondes: Théories et Expériences*. PhD Thesis, Université du Maine – Le Mans, <http://tel.archivesouvertes.fr/tel-00011291/fr/>
- Pézeril T., Chigarev N., Ruello P., Gougeon S., Mounier D., Breteau J.-M., Picart P., Gusev V.E. (2006). Laser acoustics with picosecond collimated shear strain beams in single crystals and polycrystalline materials. *Physical Review B* **73(13)** 132301 [4 pages]
- Pézeril T., Ruello P., Gougeon S., Chigarev N., Mounier D., Breteau J.-M., Picart P., Gusev V.E. (2007). Generation and detection of plane coherent shear picosecond acoustic pulses by lasers: experiment and theory. *Physical Review B* **75(17)** 174307 [19 pages]
- Pézeril T., F. Leon, D. Chateigner, S. Kooi, K.A. Nelson (2008). Picosecond photoexcitation of acoustic waves in locally canted gold films. *Applied Physics Letters* **92** 061908
- Pitschke W., Hermann H., Mattern N. (1993). The influence of surface roughness on diffracted X-ray intensities in Bragg-Brentano geometry and its effect on the structure determination by means of Rietveld analysis. *Powder Diffraction* **8(2)** 74-83
- Pokroy B., Quintana J.P., Caspi E.N., Berner A., Zolotoyabko E. (2004). Anisotropic lattice distortions in biogenic aragonite. *Nature Materials* **3** 900-902
- Pokroy B., Fitch A.N., Lee P.L., Quintana J. P., Caspi E.N., Zolotoyabko E. (2006). Anisotropic lattice distortions in mollusc-made aragonite: A widespread phenomenon. *Journal of Structural Biology* **153** 145-150
- Pokroy B., Fieramosca J.S., Von Dreele R.B., Fitch A.N., Caspi E.N., Zolotoyabko E. (2007). Atomic structure of biogenic aragonite. *Chemistry of Materials* **19** 3244-3251
- Ponce F.A., Bour D.P. (1997). Nitride-based semiconductors for blue and green light-emitting devices. *Nature* **386(6623)** 351-359
- Ponder W.F., Lindberg D.L. (1997). Towards a phylogeny of gastropod molluscs: An analysis using morphological data. *Zoological Journal of the Linnean Society* **119(2)** 83-265
- Popa N.C. (1992). Texture in Rietveld refinement. *Journal of Applied Crystallography* **25** 611-616
- Popa N.C. (1998). The (hkl) dependence of diffraction-line broadening caused by strain and size for all Laue groups in Rietveld refinement. *Journal of Applied Crystallography* **31** 176-180
- Popa N.C., Balzar D. (2002). An analytical approximation for a size-broadened profile given by the lognormal and gamma distributions. *Journal of Applied Crystallography* **35** 338-346
- Popa N.C., Balzar D. (2008). Size-broadening anisotropy in whole powder pattern fitting. Application to zinc oxide and interpretation of the apparent crystallites in terms of physical models. *Journal of Applied Crystallography* **41** 615-627
- Press W.H., Teukolsky S.A., Vetterling W.T., Flannery B.P. (2010). *Numerical Recipes* Third Edition, Press, Teukolsky, Vetterling, Flannery (Eds.), Cambridge University Press
- Prevel M., Lemonnier S., Klein Y., Hébert S., Chateigner D., Ouladdiaf B., Noudem J.G. (2005). Textured Ca₃Co₄O₉ thermoelectric oxides by thermo-forging process. *Journal of Applied Physics* **98** 093706
- Prince E. (1989). *The Rietveld Method*. Vol. 9, Workshop Notes, available from the *American Crystallographic Association*, PO Box 96, Ellicott station, Buffalo, NY 14205
- Radon J.H. (1986). On the determination of functions from their integral values along certain manifolds. *IEEE Transactions on Medical Imaging* **5(4)** 170-176
- Raulea L.V., Goijaerts A.M., Govaert L.E., Baaijens F.P.T. (2001). Size effects in the processing of thin metal sheets. *Journal of Materials Processing Technology* **115(1)** 44-48
- Raymond (2000). *"Elaboration par pulvérisation cathodique et caractérisation des propriétés physico-chimiques de couches de nitrure d'aluminium piézo-électriques: application à la mesure à haute température de fluctuations de pression"*. PhD Thesis, Université de Nantes.
- Reiter G. (1994). Dewetting as a probe of polymer mobility in thin-films. *Macromolecules* **27(11)** 3046-3052

- Reshchikov M.A., Morkoç H. (2005). Luminescence properties of defects in GaN. *Journal of Applied Physics* **97** 061301
- Reuss A (1929). Account of the liquid limit of mixed crystals on the basis of the plasticity condition for single crystal. *Zeitschrift für Angewandte Mathematik und Mechanik* **9** 49-58
- Ribarik G., Ungar T., Gubicza J. (2001). MWP-fit: a program for multiple whole-profile fitting of diffraction peak profiles by ab initio theoretical functions. *Journal of Applied Crystallography* **34(5)** 669-676
- Richardson W.H. (1972). Bayesian-based iterative method of image restoration. *Journal of the Optical Society of America* **62(1)** 55-59
- Richardson J.W. Jr. (1993). Background modelling in Rietveld analysis. In "The Rietveld Method". Young R.A. (Ed.), IUCr/Oxford University Press, pp102-110
- Ricote J., Chateigner D. (1999). Quantitative texture analysis applied to the study of preferential orientations in ferroelectric thin films. *Boletín de la Sociedad Española de Cerámica y Vidrio*, **38(6)** 587-591
- Ricote J., Chateigner D. (2004). Quantitative microstructural and texture characterisation by X-ray diffraction of polycrystalline ferroelectric thin films. *Journal of Applied Crystallography* **37** 91-95
- Ricote J., Chateigner D., Morales M., Calzada M.L., Wiemer C. (2004). Application of the x-ray combined analysis to the study of lead titanate based ferroelectric thin films. *Thin Solid Films* **450** 128-133
- Ricote J., Poyato R., Alguero M., Pardo L., Calzada M.L., Chateigner D. (2003). Texture development in modified lead titanate thin films obtained by chemical solution deposition on Silicon-based substrates. *Journal of the American Ceramic Society* **86(9)** 1571-1577
- Riello P., Fagherazzi G., Clemente D., Canton P. (1995). X-ray Rietveld analysis with a physically based background. *Journal of Applied Crystallography* **28** 115-120
- Riello P., Fagherazzi G., Canton P., Clemente D., Signoretto M. (1995a). Determining the degree of crystallinity in semicrystalline materials by means of the Rietveld analysis. *Journal of Applied Crystallography* **28** 121-126
- Riello P., Fagherazzi G., Canton P. (1998). Scale factor in powder diffraction. *Acta Crystallographica A* **54** 219-224
- Riello P., Canton P., Fagherazzi G. (1998a). Quantitative phase analysis in semicrystalline materials using the Rietveld method. *Journal of Applied Crystallography* **31** 78-82
- Rietveld H.M. (1967). Line profiles of neutron powder-diffraction peaks for structure refinement. *Acta Crystallographica* **22** 151-152
- Rietveld H.M. (1969). A profile refinement method for nuclear and magnetic structures. *Journal of Applied Crystallography* **2** 65-71
- Robinson I.K., Tweet D.J. (1992). Surface x-ray diffraction. *Reports on Progress in Physics* **55(5)** 599-651
- Rodriguez-Carvajal J. (2003). Recent advances in magnetic structure determination by neutron powder diffraction. *Physica B* **192(1-2)** 55-69. <http://www.ill.eu/sites/fullprof/index.html>
- Roe R.-J. (1965). Description of crystallite orientation in polycrystalline materials III, general solution to pole figure inversion. *Journal of Applied Physics* **36** 2024-2031
- Rollett J.S. (1965). "Computing Methods in Crystallography". Rollett (Ed.), Pergamon Press, Oxford. 256 pages
- Rousseau M., Pereira-Mouries L., Almeida M.J., Milet C., Lopez E. (2003). The water-soluble matrix fraction from the nacre of *Pinctada maxima* produces earlier mineralization of MC3T3-E1 mouse pre-osteoblasts. *Comparative Biochemistry and Physiology B-Biochemistry & Molecular Biology* **135(1)** 1-7
- Ruer D. (1976). "Méthode vectorielle d'analyse de la texture", Thesis Université de Metz, France
- Ruer D., Baro R. (1977). A New Method for the Determination of the Texture of Materials of Cubic Structure from Incomplete Reflection Pole Figures. *Advances in X-ray Analysis* **20** 187-200
- Ruland W. (1961). X-ray determination of crystallinity and diffuse disorder scattering. *Acta Crystallographica* **14** 180-1185
- Runge C. (1917). The classification of a crystal system through x-rays. *Physikalische Zeitschrift* **18** 509-515
- Russell T.P. (1996). On the reflectivity of polymers: Neutrons and X-rays. *Physica B* **221(1-4)** 267-283
- Sabine T.M. (1980). Neutron-diffraction – The total powder-pattern. *Australian Journal of Physics* **33(3)** 565-572
- Sakaguchi T., Burgess J. G., Matsunaga (1993). Magnetite formation by a sulphate-reducing bacterium T. *Nature* **365** 47-49
- Salzmann I., Resel R. (2004). STEREOPOLE: software for the analysis of x-ray diffraction pole figures with IDL. *Journal of Applied Crystallography* **37** 1029-1033
- Savitzky A., Golay M.J.E. (1964). Smoothing and differentiation of data by simplified least-squares procedures. *Analytical Chemistry* **36** 1627-1639
- Sayre D. (1952). The squaring method: a new method for phase determination. *Acta Crystallographica* **5** 60-65
- Scardi P., Leoni M. (2001). Diffraction line profiles from polydisperse crystalline systems. *Acta Crystallographica A* **57** 604-613

- Schaeben H. (1988). Entropy Optimisation in quantitative texture analysis. *Journal of Applied Physics* **64** 2236-2237
- Schaeben H. (1991). Determination of complete ODF using the maximum entropy method. In "*Advances and applications of quantitative texture analysis*", Bunge H.-J., Esling C. Eds, DGM, Oberursel, Germany. pp109-118
- Schaeben H. (1991a). Entropy optimization in quantitative texture analysis. II. Application to pole-to-orientation density inversion. *Journal of Applied Physics* **69(3)** 1320-1329
- Schaeben H., van den Boogaart K.G. (2003). Spherical harmonics in texture analysis. *Tectonophysics* **370(1-4)** 253-268
- Scherrer P. (1918). Bestimmung der Grösse und der inneren Struktur von Kolloidteilchen mittels Röntgenstrahlen. *Göttinger Nachrichten Gesellschaft* **2** 98-100
- Schreuer J., Hildmann B., Schneider H. (2006). Elastic properties of mullite single crystals up to 1400°C. *Journal of the American Ceramics Society* **89(5)** 1624-1631
- Schulz L.G. (1949a). Determination of preferred orientation in flat reflection samples using a Geiger counter x-ray spectrometer. *Journal of Applied Physics* **20(11)** 1030-1033
- Schulz L.G. (1949b). Determination of preferred orientation in flat transmission samples using a Geiger counter x-ray spectrometer. *Journal of Applied Physics* **20(11)** 1033-1036
- Schwarz G. (1978). Estimating dimension of a model. *Annals of Statistics* **6(2)** 461-464
- Seabaugh M.M., Messing G.L., Vaudin M.D. (2000). Texture development and microstructure evolution in liquid-phase-sintered alpha-alumina ceramics prepared by templated grain growth. *Journal of the American Ceramics Society* **83(12)** 3109-3116
- Searle C.W., Davis V., Hutchens R.D. (1982). Magnetically determined particle alignment factors of sintered rare-earth cobalt permanent magnets. *Journal of Applied Physics* **53(3)** 2395-2397
- Segmuller A. (1972). Correction for defocusing in the Schulz technique for pole figure determination. *Journal of Applied Physics* **43(6)** 2907
- Sellinger A., Weiss P.M., Nguyen A., Lu Y., Assink R.A., Gong W., Brinker C.J. (1998). Continuous self-assembly of organic-inorganic nanocomposite coatings that mimic nacre. *Nature* **394** 256-260
- Shannon C.E. (1948). A mathematical theory of communication. *Bell System Technical Journal* **27(3)** 379-423
- Shannon C.E. (1948a). A mathematical theory of communication. *Bell System Technical Journal* **27(4)** 623-656
- Shannon C.E., Weaver W. (1963), "*The mathematical theory of communication*", Univ. of Illinois Press, Urbana, 125 pages
- Shi D., Boley M.S., Chen J.G., Xu M., Vandervoort K., Liao Y.X., Zangvil A., Akujieze J., Segre C. (1989). Origin of enhanced growth of the 110K superconducting phase by Pb doping in the Bi-Sr-Ca-Cu-O system. *Applied Physics Letters* **55(7)** 699-701
- Shikano M., Funahashi R. (2003). Electrical and thermal properties of single-crystalline $(\text{Ca}_2\text{CoO}_3)_{0.7}\text{CoO}_2$ with a $\text{Ca}_3\text{Co}_4\text{O}_9$ structure. *Applied Physics Letters* **82(12)** 1851-1853
- Shim S.H., Shim K.B., Yoon J.W., Shimizu Y., Sasaki T., Koshizaki N. (2005). Blue luminescence from amorphous GaN films deposited by pulsed-laser ablation at room temperature. *Thin Solid Films* **472(1-2)** 11-15
- Shimada M., Azuma Y., Okuyama K., Hayashi Y., Tanabe E. (2006). Plasma synthesis of light emitting gallium nitride nanoparticles using a novel microwave-resonant cavity. *Japanese Journal of Applied Physics* **45(1A)** 328-332
- Shirane G. (1959). A note on the magnetic intensities of powder diffraction. *Acta Crystallographica* **12** 282-285
- Shirley R. (1978). Indexing powder diagrams. In "*Computing in crystallography*", H. Shenk, R. Olthoff-Hazekamp, H. van Koningsveld, G.C. Bassi (Eds.); Delft University Press, p221-234
- Shirley R. (1980). Data accuracy for powder indexing. In "*Accuracy in powder diffraction*", S. Block, C.R. Hubbard (Eds.) *National Bureau of Standards (US) special Publications* N° **567**, p361-382
- Shuvalov L.A., Belov N.V. (1962). The symmetry of crystals in which ferromagnetic and ferroelectric properties appear simultaneously. *Kristallografiya* **7** 192-197
- Sidey V. (2004). A simplified correction function for the effect of surface roughness in x-ray powder diffraction. *Journal of Applied Crystallography* **37** 1013-1014
- Silve C., Lopez E., Vidal B., Smith D.C., Camprasse S., Camprasse G., Couly G. (1992). Nacre initiates biomineralization by human osteoblasts maintained in vitro. *Calcified Tissue International* **51** 363-369
- Simons G., Weippert Ch., Dual J., Villain J. (2006). Size effects in tensile testing of thin cold rolled and annealed Cu foils. *Materials Science and Engineering A* **416(1-2)** 290-299
- Sirotine A., Chaskolskaia M. (1984). "*Fondements de la physique des cristaux*", Sirotine, Chaskolskaia (Eds.), MIR Publishers, Moscow. 695 pp
- Smith B.L., Schaffer T.E., Viani M., Thompson J.B., Frederick N.A., Kind J., Belcher A., Stucky G.D., Morse D.E., Hansman P.K. (1999). Molecular Mechanistic Origin of the Toughness of Natural Adhesives, Fibres and Composites. *Nature* **399** 761-763

- Smith D.K. (1989). Computer-analysis of diffraction data. *Reviews in Mineralogy* **20** 183-216
- Smith G.S. (1977). Estimating the unit-cell volume from one line in a powder diffraction pattern: the triclinic case. *Journal of Applied Crystallography* **10** 252-255
- Smith G.S., Snyder R.L. (1979). F_N : a criterion for rating powder diffraction patterns and evaluating the reliability of powder-pattern indexing. *Journal of Applied Crystallography* **12** 60-65
- Snyder R.L., Condrate R.A., Johnson P.F. (1985). *Advances in Material Characterisation II*, Snyder, Condrate, Johnson (Eds.), Plenum Press ED.
- Solovyov L.A. (2004). Full-profile refinement by derivative difference minimization. *Journal of Applied Crystallography* **37** 743-749. <http://krsk.info/icct/en/cont/persons/sol/ddm.html>
- Sonneveld E.J., Visser J.W. (1975). Automatic collection of powder data from photographs. *Journal of Applied Crystallography* **8** 1-7
- Sörgel J., Scherz U. (1998). Ab initio calculation of elastic constants and electronic properties of ZnSe and ZnTe under uniaxial strain. *European Physics Journal B* **5(1)** 45-52
- Soubeyroux J.-L., Fruchart D., Isnard O., Miraglia S., Tomey E. (1995). Role of the (H,C,N) interstitial elements on the magnetic properties of iron-rare earth permanent magnet alloys. *Journal of Alloys and Compounds* **19** 16-24
- Soulet S., Carpena J., Chaumont J., Kaitasov O., Ruault M.O., Krupa J.C. (2001). Simulation of the alpha-annealing effect in apatitic structures by He-ion irradiation: Influence of the silicate/phosphate ratio and of the OH/F- substitution. *Nuclear Instruments and Methods in Physics section B: Beam Interactions with Materials and Atoms* **184(3)** 383-390
- Sparks C.J., Kumar R., Specht E.D., Zschack P, Ice G.E., Shiraishi T., Hisatsune K. (1992). Effect of powder sample granularity on fluorescent intensity and on thermal parameters in x-ray diffraction Rietveld analysis. *Advances in X-ray Analyses* **35** 57-62
- Stearns D.G. (1989). The scattering of x-rays from nonideal multilayer structures. *Journal of Applied Physics* **65(2)** 491-506
- Stearns D.G. (1992). X-ray scattering from interfacial roughness in multilayer structures. *Journal of Applied Physics* **71(9)** 4286-4298
- Steiner T. (2004). “*Semiconductor Nanostructures for Optoelectronic Applications*”, Editor Todd Steiner, Artech House, Inc, Boston.
- Stephens P.W. (1999). Phenomenological model of anisotropic peak broadening in powder diffraction. *Journal of Applied Crystallography* **32** 281-289
- Stoev K.N., Sakurai K. (1999). Review on grazing incidence x-ray spectrometry and reflectometry. *Spectrochimica Acta B* **54(1)** 41-82
- Stokes A.R. (1948). A numerical Fourier-analysis method for the correction of widths and shapes of lines on x-ray powder photographs. *Proceedings of the Physical Society of London B* **61** 382-391
- Stokes G.K., Keown S.R., Dyson D.J. (1968). The construction of stereographic projections by computer. *Journal of Applied Crystallography* **1** 68-70
- Stokes A.R., Wilson A.J.C. (1944). The diffraction of x rays by distorted crystal aggregates – I. *Proceedings of the Physical Society* **56(1)** 174-181
- Suchicital C.T.A., Payne D.A. (1990). Flux growth of single crystal lead titanate. *Journal of Crystal Growth* **104** 211-217
- Suortti P. (1972). Effect of porosity and surface roughness on the x-ray intensity reflected from a powder specimen. *Journal of Applied Crystallography* **5** 325-331
- Suvaci E., Messing G.L. (2000). Critical factors in the templated grain growth of textured reaction-bonded alumina. *Journal of the American Ceramics Society* **83(8)** 2041-2048
- Suzuki H., Ikeda S., Takeuchi S. (1956). Deformation of thin copper crystals. *Journal of the Physical Society of Japan* **11(4)** 382-393
- Suzuki T.S., Uchikoshi T., Okuyama H., Sakka Y., Hiraga K. (2006). Mechanical properties of textured, multilayered alumina produced using electrophoretic deposition in a strong magnetic field. *Journal of the European Ceramic Society* **26** 661–665
- Swann P.R. (1966). The dislocation distribution near the surface of deformed copper. *Acta Metallurgica* **14(7)** 900-903
- Tampieri A., Celotti G.C., Calestani G., Lesca S. (1997). New Technology to Improve Texturing and Transport Current in Bulk (2223) BSCCO Superconductors. *Key Engineering Materials* **132-136** 1247-1250
- Tani T., Itahara H., Xia C., Sugiyama J. (2003). Topotactic synthesis of highly-textured thermoelectric cobaltites. *Journal of Materials Chemistry* **13** 1865-1867
- Tarumi R., Ledbetter H., Shiomi S., Ogi H., Hirao M., Tsai A.P. (2010). Elastic constants and anisotropic internal frictions of decagonal $Al_{72}Ni_{18}Co_8$ single quasicrystal at low temperatures. *Journal of Applied Physics* **108(1)** 013514(1-5)
- Taupin D. (1973). A powder-diagram automatic-indexing routine. *Journal of Applied Crystallography* **6** 380-385

- Tavger B.A., Zaitsev V.M. (1956). Magnetic symmetry of crystals. *Soviet Physics Journal of Experimental and Theoretical Physics* **3** 430-436
- Taylor J.C., Miller S.A., Bibby D.M. (1985). A study of decomposition methods for refinement of H⁺-ZSM5 zeolite with powder diffraction data. *Zeitschrift für Kristallographie* **176(3-4)** 183-192
- Tenckhoff E. (1970). Defocusing for the Schulz technique of determining preferred orientation. *Journal of Applied Physics* **41(10)** 3944-3948
- Terasaki I., Sasago Y., Uchinokura K. (1997). Large thermoelectric power in NaCo₂O₄ single crystals. *Physical Review B* **56(20)** 12685-12687
- Thompson A.W. (1973). Fatigue crack morphology at surfaces. *Scripta Metallurgica* **7(2)** 211-213
- Thompson A.W. (1977). Effect of grain-size on work-hardening in nickel. *Acta Metallurgica* **25(1)** 83-86
- Thompson P., Cox D.E., Hastings J.B. (1987). Rietveld refinement of Debye-Scherrer synchrotron x-ray data from Al₂O₃. *Journal of Applied Crystallography* **20** 79-83
- Thomsen C., Strait J., Vardeny Z., Maris H.J., Tauc J., Hauser J.J. (1984). Coherent phonon generation and detection by picosecond light pulses. *Physical Review Letter* **53(10)** 989-992
- Thomsen C., Grahn H.T., Maris H.J., Tauc J. (1986). Surface generation and detection of phonons by picosecond light pulses. *Physical Review B* **34(6)** 4129-4138
- Toraya H. (1986). Whole-powder-pattern fitting without reference to a structural model: application to x-ray powder diffraction data. *Journal of Applied Crystallography* **19** 440-447
- Tuchman J.A., Sui Z., Herman I.P., Gunshor R.L., Kolodziejewski L.A., Cammack D.A., Shone M. (1990). "Properties of II-VI Semiconductors MRS Symposia Proceedings No. 161" F.J. Bartoli, H.F. Schaake, J.F. Schetzina (Eds.), Materials Research Society, Pittsburg
- Ungár T., Castelnau O., Ribárik G., Drakopoulos M., Béchade J.-L., Chauveau T., Snigirev A., Snigireva I., Schroer C., Bacroix B. (2007). Grain to grain slip activity in plastically deformed Zr determined by X-ray micro-diffraction line profile analysis. *Acta Materialia* **55** 1117-1127
- Ungár T., Dragomir I.C., Révész A., Borbély A. (1999). The contrast factors of dislocations in cubic crystals: the dislocation model of strain anisotropy in practice. *Journal of Applied Crystallography* **32** 992-1002
- Uzumaki T., Yamanaka K., Kamehara N., Niwa K. (1989). The effect of Ca₂PbO₄ addition on superconductivity in a Bi-Sr-Cu-O system. *Japanese Journal of Applied Physics Letters* **28(1)** L75-L77
- Vadon A. (1981), "Généralisation et optimisation de la méthode vectorielle d'analyse de la texture". Thesis, Université de Metz, France
- Vallat-Sauvain E., Kroll U., Meier J., Shah A. (2000). Evolution of the microstructure in microcrystalline silicon prepared by very high frequency glow-discharge using hydrogen dilution. *Journal of Applied Physics* **87(6)** 3137-3142
- Van den Hoogenhof W.W., de Boer D.K.G. (1994). Glancing incidence X-ray analysis: Forgotten or to be discovered? *Surface and Interface Analysis* **22(1)** 572-575
- Van Houtte P. (1983). The Use of a Quadratic Form for the Determination of Non-negative Texture Functions. *Textures and Microstructures* **6(1)** 1-19
- Van Houtte P. (1991). A method for the generation of various ghost correction algorithms – The example of the positivity method and the exponential method. *Textures and Microstructures* **13** 199-212
- Vidal B., Vincent P. (1984). Metallic multilayers for x rays using classical thin-film theory. *Applied Optics* **23(11)** 1794-1801
- Vignaud G., Gibaud A., Grübel G., Joly S., Ausserré D., Legrand J.F., Gallot Y. (1998). Ordering of diblock PS-PBMA thin films: An X-ray reflectivity study. *Physica B* **248(1-4)** 250-257
- Visser J.W. (1969). A fully automatic program for finding the unit cell from powder data. *Journal of Applied Crystallography* **2** 89-95
- Voigt W. (1928). "Lehrbuch der Kristallphysik". Teubner Verlag, Leipzig
- Von Dreele R.B., Jorgensen J.D., Winsdor C.G. (1982). Rietveld refinement with spallation neutron powder diffraction data. *Journal of Applied Crystallography* **15** 581-589
- Von Laue M. (1926). The Lorentz factor and distribution of intensity in Debye-Scherrer fringes. *Zeitschrift für Kristallographie* **64(1)** 115-142
- Wagner C.N.J. (1957). Stacking faults by low-temperature cold work in copper and alpha-brass. *Acta Metallurgica* **5(8)** 427-434
- Wagner C.N.J. (1966). Analysis of the Broadening and Changes in Position of Peaks in an X-Ray Powder Pattern. In "Local atomic arrangements studied by X-ray diffraction", J.B. Cohen, J.E. Hilliard (Eds.), New York: Gordon and Breach Science Publishers, *Metallurgical Society Conferences* **36** 219-268
- Wagner F., Dahms M. (1991). Determination of complete O.D.F.s with an optimized positivity method. In "Advances and applications of quantitative texture analysis", Bunge H.-J. et Esling C. (Eds), DGM, p101-108
- Walther K., Heinitz J., Ullemeyer K., Betzl M., Wenk H.-R. (1995). Time-of-Flight texture analysis of limestone standard: Dubna results. *Journal of Applied Crystallography* **28** 503-507.

- Wang M., Xiong G., Tang X., Hong Z. (1993). The formation mechanism of $\text{Bi}_2\text{Sr}_2\text{Ca}_2\text{Cu}_3\text{O}_x$ superconducting phase. *Physica C* **210(3-4)** 413-416
- Wang S.X., Lumpkin G.R., Wang L.M., Ewing R.C. (2000). Ion irradiation-induced amorphization of six zirconolite compositions. *Nuclear Instruments and Methods in Physics section B: Beam Interactions with Materials and Atoms* **166-167** 293-298
- Wang T., Cölfen H., Antonietti M. (2005). Nonclassical crystallization: Mesocrystals and morphology change of CaCO_3 crystals in the presence of a polyelectrolyte additive. *Journal of the American Chemical Society* **127(10)** 3246-3247
- Warren B.E. (1938). A simplified derivation of the Laue particle size equation. *Zeitschrift für Kristallographie* **99(5)** 448-452
- Warren B.E. (1959). X-ray studies of deformed metals. In "Progress in Metal Physics", Vol. 8, Chalmers B., King R. (Eds.), New-York: Pergamon. pp 147-202
- Warren B.E. (1969). "X-ray diffraction", Warren (Ed.), Addison-Wesley, Reading, Massachusetts
- Warren B.E., Averbach B.L. (1950). The effect of cold-work distortion on x-ray patterns. *Journal of Applied Physics* **21(6)** 595-599
- Warren B.E., Averbach B.L. (1952). The separation of cold-work distortion and particle size broadening in x-ray patterns. *Journal of Applied Physics* **23(4)** 497-497
- Weislak L., Bunge H.-J., Nauer-Gerhardt C.U. (1993). X-ray diffraction texture analysis with a position sensitive detector. *Zeitschrift für Metallkunde* **84(7)** 479-493
- Weber W.J., Williford R.E., Sickafus K.E. (1997). Total displacement functions for SiC. *Journal of Nuclear Materials* **244(3)** 205-211
- Weber W., Ewing R.C., Catlow C.R.A., Diaz de la Rubia T., Hobbs L.W., Kinoshita C., Matzke H.J., Motta A.T., Nastasi M., Salje E.H.K., Vance E.R., Zinkle S.J. (1998). Radiation effects in crystalline ceramics for the immobilization of high-level nuclear waste and plutonium. *Journal of Materials Research* **13(6)** 1434-1484
- Weiner S., Talmon Y., Traub W. (1983). Electron diffraction of mollusc shell organic matrices and their relationship to the mineral phase. *International Journal of Biological Macromolecules* **5** 325-328
- Weiner S., Traub W. (1980). X-ray diffraction study of the insoluble organic matrix of mollusk shells. *FEBS Letters* **111(2)** 311-316
- Weiner S., Traub W. (1981). Organic-Matrix-Mineral relationships in mollusk-shell nacreous layers. In "Structural aspects of recognition and assembly in biological macromolecules". Balaban M., Sussman J.L., Traub W., Yonath A. (Eds.). Balaban ISS, Rehovot and Philadelphia pp 467-482
- Welzel U., Ligot J., Lamparter P., Vermeulen A.C., Mittermeyer E.J. (2005). Stress analysis of polycrystalline thin films and surface regions by x-ray diffraction. *Journal of Applied Crystallography* **38** 1-29
- Welzel U., Mittermeyer E.J. (2003). Diffraction stress analysis of macroscopically elastically anisotropic specimens: on the concepts of diffraction elastic constants and stress factors. *Journal of Applied Physics* **93(11)** 9001-9011
- Wenk H.-R. (1985). "Preferred orientation in deformed metals and rocks: an introduction to modern texture analysis", H.-R.Wenk (Ed.), Academic Press inc..
- Wenk H.-R. (1991). Standard project for pole-figure determination by neutron diffraction. *Journal of Applied Crystallography* **24**, 920-927
- Wenk H.-R. (1992). Advantages of monochromatic x-rays for texture determination of superconducting thin films. *Journal of Applied Crystallography* **25** 524-530
- Wenk H.-R., Chateigner D., Pernet M., Bingert J., Hellstrom E., Ouladdiaf B. (1996). Quantitative texture analysis of Bi-2212 and 2223 tapes and wires using neutron diffraction. *Physica C* **272** 1-12
- Wenk H.-R., Heidelbach F., Chateigner D., Zontone F. (1997). Laue orientation imaging. *Journal of Synchrotron Radiation* **4** 95-101
- Wenk H.-R. (1998). Pole figure measurements by diffraction techniques. In "Texture and Anisotropy", Kocks U.F., Tomé C.N., Wenk H.-R. (Eds), Cambridge University Press, pp 167-177
- Wenk H.-R., Bunge H.-J., Kallend J.S., Lücke K., Matthies S., Pospiech J., Van Houtte P. (1988). Orientation Distributions: Representation and Determination. *Proceedings of the eighth International Conference on Textures of Materials*, Kallend et Gottstein (Eds.), The Metallurgical Society, Warrendale, Pennsylvania, pp17-30
- Wenk H.-R., Lutterotti L., Vogel S. (2003). Texture analysis with the new HIPPO TOF diffractometer. *Nuclear Instruments and Methods in Physics Research A* **515** 575-588
- Wenk H.-R., Matthies S., Donovan J., Chateigner D. (1998). BEARTEX: A Windows based program for quantitative texture analysis. *Journal of Applied Crystallography* **31** 262-269
- Wenk H.-R., Matthies S., Lutterotti L. (1994). Texture analysis from diffraction spectra *Materials Science Forum*, **157-162**, 473-479.

- Wenk H.-R., Pawlik K., Pospiech J., Kallend J.S. (1994). Deconvolution of superposed pole figures by discrete ODF methods: comparison of ADC and WIMV for quartz and calcite with trigonal crystal and triclinic specimen symmetry. *Texture & Microstructure* **22** 233-260
- Werner P. (1964). Trial-and-error computer methods for indexing of unknown powder patterns. *Zeitschrift für Kristallographie* **120(4-5)** 375-387
- Werner P.-E., Eriksson L., Westdahl M. (1985). TREOR, a semi-exhaustive trial-and-error powder indexing program for all symmetries. *Journal of Applied Crystallography* **18** 367-370
- Widmann F., Simon J., Daudin B., Feuillet G., Rouvière J.-L., Pelekanos N.T., Fishman G. (1998). Blue-light emission from GaN self-assembled quantum dots due to giant piezoelectric effect. *Physical Review B* **58(24)** R15989-R15992
- Wiles D.B., Young R.A. (1981). A new computer program for Rietveld analysis of x-ray powder diffraction patterns. *Journal of Applied Crystallography* **14** 149-151
- Wilkins M. (1970). The determination of density and distribution of dislocations on deformed single crystals from broadened x-ray diffraction profiles. *Physica Status Solidi A* **2** 359-370
- Wilkins M. (1970a). In "*Fundamental aspects of dislocation theory*", Simmons J.A., de Wit R., Bulloughs R. (Eds.). National Bureau of Standards special publications n°317, US department of Commerce, Washington D.C.. pp1195-1221
- Will G., Merz P., Schäfer W., Dahms M. (1990). Application of position sensitive detectors for neutron diffraction texture analysis of hematite ores. *Advances in X-ray Analysis* **33** 277-283. Barrett C.S. et al. (Ed.) Plenum Press, New-York 1990.
- Willemse P.F., Naughton B.P., Verbraak C.A. (1982). X-ray residual stress measurements on cold-drawn steel wire. *Materials Science and Engineering* **56(1)** 25-37
- Williams R.O. (1968). Analytical methods for representing complex textures by biaxial pole figures. *Journal of Applied Physics* **39(9)** 4329-4335
- Williamson G.K., Smallman R.E. (1956). Dislocation densities in some annealed and cold-worked metals from measurements on the x-ray Debye-Scherrer spectrum. *Philosophical Magazine* **1(1)** 34-46
- Wilson A.J.C. (Ed.) (1962). "*X-ray Optics. The diffraction of X-rays by finite and imperfect crystals*", London: Methuen & Co, J. Wiley & Sons (London, New-York), 2nd Edition.
- Wilson A.J.C. (Ed.) (1963). "*Mathematical Theory of x-ray Powder Diffractometry*", Eindhoven: Philips Technical Library. 128 pages
- Woolfson M., Hai-fu F. (1995). "*Physical and non-physical methods of solving crystal structures*". Woolfson et Hai-fu (Eds.), Cambridge University Press, New-York, 272p
- Wright S.I. (1993). A review of automated orientation imaging microscopy (OIM). *Journal of Computer-Assisted Microscopy* **5(3)** 207-221
- Wright S.I., Adams B.L. (1992). Automatic analysis of electron backscatter diffraction patterns. *Metallurgical transactions A, Physical metallurgy and materials science* **23(3)** 759-767
- Wulf R. (1990). Experimental distinction of elements with similar atomic number using anomalous dispersion (δ synthesis): an application of synchrotron radiation in crystal structure analysis. *Acta Crystallographica A* **46** 681-688
- Yao Z.Q., Ye Q., Li Y.Q., Zou Y.S., Zhang W.J., Lee S.T. (2007). Microstructure analysis of c-axis oriented aluminium nitride thin films by high-resolution transmission electron microscopy. *Applied Physics Letters* **90** 121907
- Yoneda Y. (1963). Anomalous surface reflection of x-rays. *Physical Review* **131(5)** 2010-2013
- Yoneda A., Kubo A. (2006). Simultaneous determination of mean pressure and deviatoric stress based on numerical tensor analysis: a case study for polycrystalline x-ray diffraction of gold enclosed in a methanol-ethanol mixture. *Journal of Physics: Condensed Matter* **18(25)** S979-S994
- Young R.A., Desai P. (1989). Crystallite Size and Microstrain Indicators in Rietveld Refinement. *Archiwum Nauki o Materialach* **10** 71-90
- Young R.A., Larson A.C., Paiva-Santos C.O. (1999). DBWS-9807a, *Program for Rietveld analysis of x-ray and neutron powder diffraction patterns*. School of Physics, Georgia Institute of Technology, Atlanta, Georgia, USA
- Young R.A., Mackie P.E., Von Dreele R.B. (1977). Application of the pattern-fitting structure-refinement method of x-ray powder diffractometer patterns. *Journal of Applied Crystallography* **10** 262-269
- Zhou Y., Matsubara I., Shin W., Izu N., Murayama N. (2004). Effect of grain size on electric resistivity and thermopower of $(\text{Ca}_{2.6}\text{Bi}_{0.4})\text{Co}_4\text{O}_9$ thin films. *Journal of Applied Physics* **95(2)** 625-628

General Bibliography

- Authier A. (2003). International Tables for Crystallography, "*Physical Properties of Crystals*", Volume D, Published for IUCr, Kluwer Academic Publishers, 522 pages
- Azaroff L.V. (1968). "*Elements of x-ray crystallography*", McGraw-Hill
- Azaroff L.V., Buerger M.J. (1958). "*The powder method in x-ray crystallography*", McGraw-Hill
- Bacon G.E. (1966). "*X-ray and Neutron diffraction*", Pergamon
- Bacon G.E. (1975). "*Neutron diffraction*", 3rd Edition, Clarendon Press, Oxford, UK. 636 pages
- Bijvoet J.M., Kolkmeier N.H., MacGillavry C.H. (1951). "*X-ray analysis of crystals*", Butterworths
- Birkholz M. (2006). "*Thin film analysis by x-ray scattering*", Wiley-VCH, 356 pages
- Birss R.R. (1964). "*Symmetry and Magnetism*", North Holland, Amsterdam.
- Born M., Huang K. (2002). "*Dynamical Theory of Crystal Lattices*". Oxford University Press, Oxford**
- Born, M., Wolf, E. (1980). "*Principles of Optics - electromagnetic theory of propagation interference and diffraction of light*", Pergamon Press, London 6th Edition, 808 pages
- Bragg, W.L. (1937). "*Atomic Structures of Minerals*". Cornell University Press: Ithaca, USA
- Buerger M.J. (1953). "*X-ray Crystallography*", Wiley
- Buerger M.J. (1959). "*Vector space*", Wiley
- Buerger M.J. (1960). "*Crystal-Structure analysis*", John Wiley & Sons, Inc., 668 pages
- Buerger M.J. (1963). "*Elementary crystallography*", Wiley
- Bunge H.-J. (1969). "*Mathematische Methoden der Texturanalyse*", Berlin, Akademie Verlag, 330 pages
- Bunge H.-J. (1982). "*Texture Analysis in Materials Science*", P.R. Morris Transactions, Butterworths, London
- Bunge H.-J. (1986). "*Experimental techniques of Texture Analysis*", DGM, Oberursel, Germany
- Bunge H.-J. (1987). "*Theoretical Methods of Texture Analysis*", DGM, Oberursel, Germany
- Bunge H.-J., Esling C. (1982). "*Quantitative Texture Analysis*", DGM, Germany, 551 pages
- Bunge H.-J., Esling C. (1991). "*Advances and applications of quantitative texture analysis*", DGM, 308p
- Bunge H.-J., Siegesmund S., Skrotzki W., Weber K. (1994). "*Textures of Geological Materials*", DGM, 399 pages
- Carpenter G.B. (1969). "*Principles of crystal structure determination*", Benjamin
- Compton A.H., Allison S.K. (1935). "*X-rays in theory and experiment*", Van Nostrand
- Coulomb P. (1982). "*Les textures dans les métaux de réseaux cubiques*". Dunod, Paris
- Cowley J.M. (1995). "*Diffraction Physics*", 3rd edition, Elsevier Science, Amsterdam
- Cullity B.D. (1978). "*Elements of X-ray diffraction*", 2nd Edition, Addison-Wesley Publishing Company, Reading MA. 547 pages
- Dailland J., Gibaud A. (1999). "*X-ray and neutron reflectivity: principles and applications*", Springer-Verlag, Lecture Notes in Physics Monographs 58, 331 pages
- Dinnebier R.E., Billinge S.J.L. (2008). "*Powder Diffraction. Theory and Practice*", the Royal Society of Chemistry Publishing, 582 pages
- Ducros P. (1971). "*Radiocristallographie*", Dunod
- Eberhart J.-P. (1989). "*Analyse Structurale et Chimique des Matériaux (diffraction des rayons X, électrons et neutrons, spectrométrie des rayons X, électrons et ions, microscopie électronique)*", Dunod, 614 pages
- Engler O., Randle V. (2010). "*Introduction to Texture Analysis. Macrotexture, Microtexture and Orientation Mapping*", 2nd Edition, CRC Press, Taylor and Francis Group, 456 pages
- Esling C., Humbert M., Schwarzer R.A., Wagner F. (2005). "*Texture and Anisotropy of Polycrystals II*", Trans Tech Publications Ltd., 478 pages
- Gay R. (1958). "*Cours de cristallographie*", Gauthier-Villars
- Guinebreteire R. (2007). "*X-ray diffraction by polycrystalline materials*", ISTE Ltd., 351 pages
- Guinier A. (1964). "*Théorie et technique de la radiocristallographie*", Dunod, Paris, 740 pages
- Guinier A. (1994). "*X-ray Diffraction*", Dover Publications, Inc., New York
- Hahn T. (2002). International Tables for Crystallography, "*Space-group symmetry*", Volume A, 5th Edition, Kluwer Academic Publisher.
- Hammond Christopher 2001. "*The basics of crystallography and diffraction*", 2nd Edition, Oxford University Press.
- Hauk V. (1997). "*Structural and residual stress analysis by non-destructive methods: evaluation, application, assessment*", Hauk (Ed.), Amsterdam, Elsevier
- Hilton H. 1963. "*Mathematical crystallography*", Dover.
- Hirao, M., Ogi H. (2003). "*EMATs for Science and Industry*", Kluwer, Boston.**
- James R.W. (1965). "*The optical principles of the diffraction of x-rays*", G. Bell, London.
- Jeffery J.W. (1971). "*Methods in x-ray crystallography*", Academic Press.
- Kittel C. (1983). "*Physique de l'Etat Solide*", 5th Edition, Dunod Université, 593 pages
- Klug H.P., Alexander L.E. (1974). "*X-ray diffraction procedures for polycrystalline and amorphous materials*" Wiley, New York, 966 pages
- Kocks U.F., Tomé C.N., Wenk H.-R. (1998). "*Texture and Anisotropy*", Cambridge University Press, 676 pages
- Koptsik V.A. (1966). "*Shubnikov groups*", Izd. MGU Pub., Moscow.

- Landau L.D., Lifshitz E.M. (1967). "*Theory of Elasticity*". Mir, Moscow. 207 pages
- Légrand C. (1967). "*La radiocristallographie*", Presses universitaires de France
- Lipson H., Cochran W. (1953). "*The determination of crystal structures*", G. Bell and Sons
- Lipson H., Steeple H. (1970). "*Interpretation of x-ray powder diffraction pattern*", MacMillan
- Liang L., Rinaldi R., Schober H. (2009). "*Neutron applications in earth, energy and environmental sciences*", Springer, 634 pages
- Matthies S., Vinel G.W., Helming K. (1987), "*Standard Distributions in Texture Analysis*", Vol 1, Akademie Verlag, Berlin. 449p
- Migliori A., Sarro J. (1997). "*Resonant Ultrasound Spectroscopy*", Wiley-Interscience, New-York
- Mittemeijer E.J., Scardi P. (2004). "*Diffraction analysis of the microstructure of materials*". Springer, Berlin
- Morawiec A. (2004). "*Orientations and Rotations. Computations in Crystallographic Textures*", Springer-Verlag, 200 pages
- Noyan I.C., Cohen J.B. (1987). "*Residual Stress: measurement by diffraction and interpretation*". Noyan, Cohen (Eds.), Springer-Verlag
- Nye J.-F. (1985), "*Physical Properties of Crystals: their representation by tensors and matrices*", Lavoisier publishers, 330 pages
- Pecharsky V.K., Zavalij P.Y. (2005). "*Fundamentals of powder diffraction and structural characterization of materials*". Springer. 713 pages
- Peiser H.S., Rooksby H.P., Wilson A.J. (1955). "*X-ray diffraction by polycrystalline materials*", IOP, London, 725 pages
- Press W.H., Flannery B.P., Teukolsky S.A., Vetterling W.T. (1986). "*Numerical Recipes*" Cambridge University Press.
- Rollett J.S. (1965). "*Computing Methods in Crystallography*". Rollett (Ed.), Pergamon Press, Oxford. 256 pages
- Rousseau J.-J. (2000). "*Cristallographie géométrique et radiocristallographie*", Dunod Publishers, 370 pages
- Rousseau J.-J. (1998). "*Basic crystallography*", Wiley J. Publishers. 414 pages
- Shannon C.E., Weaver W. (1963), "*The mathematical theory of communication*", Univ. of Illinois Press, Urbana, 125 pages
- Shenk H. (1990). "*Computing in Crystallography*", Delf University Press 221p
- Shmueli U. (2001). International Tables for Crystallography, "*Reciprocal Space*", Volume B, Published for IUCr, Kluwer Academic Publishers
- Sirovine A., Chaskolskaia M. (1984). "*Fondements de la physique des cristaux*", MIR Publishers, Moscow. 695 pp
- Snyder R.L., Condrate R.A., Johnson P.F. (1985). *Advances in Material Characterisation II*, Snyder, Condrate, Johnson (Eds.), Plenum Press ED.
- Snyder R.L., Fiala J., Bunge H.-J. (1999). "*Defect and microstructure analysis by diffraction*", Oxford University Press.
- Stout G.H., Jensen L.H. ((1968). "*X-ray Structure Determination. A practical Guide*", The McMillan Company, 467 pages
- Van Meerssche M., Feneau-Dupont J. (1973). "*Introduction à la cristallographie et à la chimie structurale*", Vander, Louvain. 752 pages
- Warren B.E. (1969). "*X-ray diffraction*", Addison-Wesley, Reading, Massachusetts
- Wenk H.-R. (1985). "*Preferred orientation in deformed metals and rocks: an introduction to modern texture analysis*", Academic Press inc., 610 pages
- Wilson A.J.C. (1962). "*X-ray Optics*", London: Methuen
- Wilson A.J.C., Prince E. (1999). International Tables for Crystallography, "*Mathematical, physical and chemical tables*", Volume C, 2nd Edition, Kluwer Academic Publisher.
- Woolfson M.M. 1961. "*Direct methods in crystallography*", Oxford.
- Woolfson M.M. 1970. "*An introduction to x-ray crystallography*", Cambridge University Press.
- Woolfson M., Hai-fu F. (1995). "*Physical and non-physical methods of solving crystal structures*", Cambridge University Press, New-York, 272p
- Young R.A. (1993). "*The Rietveld Method*". IUCr/Oxford University Press. 298 pages
- Zachariasen W.H. 1945. "*Theory of x-ray diffraction in crystals*", Wiley.

Glossary

ρ	Material density
ρ_e	Material electron density
dS	Surface element of the Pole Sphere
$a, b, c, \alpha_c, \beta_c, \gamma_c$	Unit-cell parameters
$\mathbf{a}, \mathbf{b}, \mathbf{c}$	Unit vectors of the unit-cell
$\Delta\mathbf{k}$	Scattering vector
\mathbf{n}	Normal to the sample surface
\mathcal{S}	Spectrometer (Diffractometer) space
\mathcal{S}_p	Physical 3D space
\mathcal{S}_e	External (reciprocal) 3D space
\mathcal{S}_i	Internal (reciprocal) superspace orthogonal to \mathcal{S}_e
χ	Polar angle in the diffractometer space
φ	Azimuthal angle in the diffractometer space
\mathcal{V}	Pole figure space
ϑ_y	Polar angle in the pole figure space
φ_y	Azimuth of pole figures
hkl	Miller indices
(hkl)	Crystallographic plane hkl
$\{hkl\}$	Crystallographic planes hkl and diffracting equivalents
$[hkl]$	Crystallographic direction hkl
$[hkl]^*$	Crystallographic direction hkl of the reciprocal space
$\langle hkl \rangle$	Crystallographic direction hkl and diffracting equivalents
$\langle hkl \rangle^*$	Crystallographic direction hkl and diffracting equivalents of the reciprocal space
L_{hkl}	Lotgering factor
p, p_0	ratio entering the Lotgering factor for a textured and a random sample respectively
\mathbf{h}	$\langle hkl \rangle^*$ directions
\mathbf{y}	ϑ_y, φ_y direction in \mathcal{V}
$I_h(\mathbf{y})$	Direct pole figure
$P_h(\mathbf{y})$	Normalised pole figure
K_A	Sample reference frame
$(\mathbf{x}_A, \mathbf{y}_A, \mathbf{z}_A)$	Unit-vectors of the sample reference frame
$\mathbf{X}_A, \mathbf{Y}_A, \mathbf{Z}_A$	Sample axes aligned with $\mathbf{x}_A, \mathbf{y}_A, \mathbf{z}_A$ respectively
$[\mathbf{XYZ}]$	Vector of the sample reference frame
K_B	Crystal reference frame
$(\mathbf{x}_B, \mathbf{y}_B, \mathbf{z}_B)$	Unit-vectors of the crystal reference frame
$\mathbf{X}_B, \mathbf{Y}_B, \mathbf{Z}_B$	Crystal axes aligned with $\mathbf{x}_B, \mathbf{y}_B, \mathbf{z}_B$ respectively
\mathcal{H}	Orientation space
\mathbf{g}	Set of three Euler angles defining one orientation
g	Orientation distance
dg	Orientation element in the \mathcal{H} -space
α, β, γ	Euler angles in the \mathcal{H} -space in the Roe-Matthies convention
$\varphi_1, \Phi, \varphi_2$	Euler angles in the \mathcal{H} -space in the Bunge convention

$f(\mathbf{g})$	Orientation Distribution of crystallites
$f_f(\mathbf{g})$	OD of for ferroelectric domains
$d_{hk\ell}$	Inter-reticular distance between $(hk\ell)$ planes
ω	Angle between the incident beam and the sample surface: incidence angle
θ	Angle between the incident beam and the scattering planes $\{hk\ell\}$: Bragg angle
δ	Angle running along the Debye ring on a 2D detector
V	Irradiated volume of the sample
$dV(\mathbf{y})$	Volume of crystallites having \mathbf{h} between \mathbf{y} and $\mathbf{y} + d\mathbf{y}$
$dV(\mathbf{g})$	Volume of crystallites which orientation is between \mathbf{g} and $\mathbf{g} + d\mathbf{g}$
J_c	Superconducting transport critical current density
F_d	Damaged (amorphous) fraction of an irradiated sample
F_c	Crystalline fraction of a sample
$\overline{\mathcal{T}}$	Microscopic tensor for a property
$\overline{\mathcal{T}}^M$	Macroscopic tensor
$\langle \overline{\mathcal{T}} \rangle$	Arithmetic average of the tensor $\overline{\mathcal{T}}$
\mathbf{p}_h	electric polarisation vector of a ferroelectric domain
ε_{ij}	strain tensor
ε_{ij}^M	macroscopic strain tensor
σ_{ij}	stress tensor
σ_{ij}^M	macroscopic stress tensor
$S_{ijk\ell}$	elastic compliance tensor
$S_{ijk\ell}^M$	macroscopic elastic compliance tensor
$S_{ijk\ell}^{V,R,H}$	macroscopic elastic compliance tensor calculated using the Voigt, Reuss, Hill models
$C_{ijk\ell}$	elastic stiffness tensor
$C_{ijk\ell}^M$	macroscopic elastic stiffness tensor
$C_{ijk\ell}^{V,R,H}$	macroscopic elastic stiffness tensor calculated using the Voigt, Reuss, Hill models
ξ	mixing parameter of the Hill model
$\chi_{m,ij}$	Magnetic susceptibility tensor
$\mu_{r,ij}$	Magnetic relative permeability tensor
$\varepsilon_{r,ij}$	Dielectric relative permittivity tensor
ε_0	Dielectric permittivity of vacuum
\mathbf{L}	Atomic orbital angular momentum
\mathbf{S}	Atomic spin angular momentum
\mathbf{J}	Atomic total magnetic momentum
g_{ij}	Anisotropic Landé factor
μ_B	Bohr magneton
k_B	Boltzman constant
c	light speed
N	Avogadro number

Abbreviations

14:24	$(\text{Sr,Ca})_{14}\text{Cu}_{24}\text{O}_{41}$
BAW	Bulk Acoustic Waves
Bi2223	$(\text{Bi,Pb})_2\text{Sr}_2\text{Ca}_2\text{Cu}_3\text{O}_{10+x}$
Bi2212	$(\text{Bi,Pb})_2\text{Sr}_2\text{Ca}_1\text{Cu}_2\text{O}_{8+x}$
CAPS	Curved-Area Position Sensitive detector
CCL	Comarginal Crossed Lamellar layer
CPS	Curved Position Sensitive detector
CSL	Coincidence Site Lattices
EBSD	Electron Back-Scattering Diffraction
EDX	Energy Dispersive X-ray
ESR	Electron Spin Resonance
FAp	$\text{Ca}_{10}(\text{PO}_4)_6\text{F}_2$
FWHM	Full Width at Half Maximum
HAp	$\text{Ca}_{10}(\text{PO}_4)_6(\text{OH})_2$
HRTEM	High-Resolution TEM
HWHM	Half Width at Half Maximum
HWHD	Half Width at Half maximum of the distribution Density
ILL	<i>Institut Laue-Langevin</i>
LN	LiNbO_3
MPB	Morphotropic Phase Boundary
MQTA	Magnetic Quantitative Texture Analysis
m.r.d.	multiple of a random distribution
MTG	Melt Texture Growth
NMR	Nuclear Magnetic Resonance
ODF	Orientation Distribution Function
PSD	Position Sensitive Detector
PZT	$\text{Pb}(\text{Zr,Ti})\text{O}_3$
PL	PhotoLuminescence
PLE	PhotoLuminescence Excitation
QMA	Quantitative Microstructure Analysis
QPA	Quantitative Phase Analysis
QTA	Quantitative Texture Analysis
RCL	Radial Crossed Lamellar layer
RSA	Residual Strain-stress Analysis
RTGG	Reactive Templated Grain-Growth
SBN	$\text{SrBi}_2\text{Nb}_2\text{O}_9$
SEM	Scanning Electron Microscope
TEM	Transmission Electron Microscope
TGG	Templating Grain Growth
TSMTG	Top-Seeded Melt Texture Growth
XRR	X-Ray specular Reflectivity
Y123	$\text{YBa}_2\text{Cu}_3\text{O}_{7-\delta}$
Y211	Y_2BaCuO_5

Constants

We used in this book the following values of the constants of physics:

Avogadro number	$N = 6.022 \cdot 10^{23}$	
Electron charge	$e = -1,6021892 \cdot 10^{-19}$	C
Boltzmann constant	$k_B = 1,380662 \cdot 10^{-23}$	J.K ⁻¹
Planck constant	$h = 6,626176 \cdot 10^{-34}$	J.s
Rydberg constant	$R_H = 1.1 \cdot 10^7$	m ⁻¹
Electron mass	$m_e = 9,109534 \cdot 10^{-31}$	kg
Free-space permittivity	$\epsilon_0 = 8,8541878 \cdot 10^{-12}$	A s A ⁻¹ m ⁻¹
Free-space permeability	$\mu_0 = 4\pi \cdot 10^{-7}$	V s A ⁻¹ m ⁻¹
Free-space light speed	$c = 299792458$	m.s ⁻¹

Acknowledgements

I am indebted to Magali Morales (CIMAP-Caen) whom constantly comes with new issues, criticisms, advices and proposals. She suffered the first times of building the Combined Analysis when taking part into the ESQUI European project. This work should be understood within hers.

Luca Lutterotti (DIM-Trento) is entirely devoted to this thematic and programing, without him nothing could have been carried out.

Jesus Ricote (DMF-Madrid), Michele Zucali and Emmanuel Guilmeau (CRISMAT-Caen), provided some of the worst samples to test, Salim Ouhenia (Physics Dept. Bejaia) for his work on CaCO₃-PAA films and *Charonia* shell, Hans-Rudolf Wenk (DEPS-Berkeley) and Siegfried Matthies, are pioneers in the field with the so-called "Rietveld-Texture Analysis", Bachir Ouladdiaf was of so much constant help during the multiple stays at ILL needed to achieve these works. Please receive my warmest sympathy and friendship.

I wish to thank in particular M.L. Calzada (DMF-Madrid) for the preparation of PCT ferroelectric films, E. Derniaux and P. Kayser (ONERA-Paris) for the elaboration of AlN films, G. Leclerc, R. Bouregba and G. Poullain (CRISMAT-Caen) for the PZT film elaboration and hysteresis characterisation, R. Whatmore (Cranfield University) for the elaboration of the spin coated PZT films, V. Bornand (Univ. Montpellier) for the elaboration of the LiNbO₃ films, M. Bouguerra for the GaN-SiO₂ composite elaboration and PL and PLE characterisation, R. Kaptein and C. Krauss for the CaCO₃ thin layer electrodeposition, C. Keller and E. Hug (CRISMAT-Caen) for the mechanical characterisation of the polycrystalline Ni samples, S. Deniel and P. Blanchart (ENSCI-Limoges) for the elaboration of mullite composites and their mechanical characterisation, F. Léon for his experimental help in MQTA, O. Pérez (CRISMAT-Caen) for the fruitful discussions around superspaces.

The work has been periodically ameliorated through remarks and notifications of mistakes. I would like to thank Piotr Ozga for this.

This work could not have been carried out without supports from the following institutions and organisms, through constant financial or contracts:

- Ministère de l'Enseignement Supérieur et de la Recherche
- Délégation Régionale à la Recherche et à la Technologie, Conseil Régional de Basse-Normandie
- GdR Nomade: Groupement de Recherche "NOUVEAUX MATériaux pour les DEchets radioactifs"
- CNRS-CSIC French-Spanish cooperation "Crystallographic texture influence on polycrystalline ferroelectric materials properties" (contract n° 16215, 2004-2005, 2004FR0030)
- The European Union project ESQUI "X-ray Expert System for microelectronic films Quality Improvements" within the GROWTH program (G6RD-CT99-00169)
- CNRS-CSIC French-Spanish cooperation "PTL, SBT and PTC ferroelectric film characterisation" (contract n° 8540, 2000-2001, 2000FR0021)
- European Concerted Action "ELENA: ELEctrocERamics from NAnopowders produced by innovative methods" (COST n° 539, 2005-2009)
- European Concerted Action "Application of ferroelectric thin-films for SAW devices" (COST n° 514, 1998)
- The Spanish advanced fellowship program "Ramón y Cajal" of the Spanish MCyT
- The Spanish MCyT projects MAT2000-1925-CE and MAT2002-00463
- The Spanish FINNOVA program (CAM)
- The MIND Network of Excellence "*Multifunctional & Integrated Piezoelectric Devices*" NoE 515757-2.
- The Mat 2005-01304 FEDER-MEC-Spain: "Materiales ceramicos ferroelectricos con alta deformacion bajo el campo electrico nuevas soluciones solidas con frontera de fases morfotropica y texturacion"

Warnings and comments

This text is appended regularly. If you detect any incoherence, mistake, typos, lost or missing reference or whatsoever, or if you miss some explanation or development, please warn the author directly by email at daniel.chateigner@ensicaen.fr

Figures caption

Figure 1: Definitions of grains (green), crystallites (black and red) and crystallographic planes (dashes) in a polycrystalline sample.....	15
Figure 2: Schematic illustration of Bragg's law	16
Figure 3: Simulated x-ray diffraction diagrams for a Si powder, for $\lambda = 1.5406 \text{ \AA}$ (a) and for $\lambda/2 = 0.7703 \text{ \AA}$ (b). Intensities for the $\lambda/2$ contributions have been enhanced for visibility.	17
Figure 4: Ewald and pole sphere, Debye-Scherrer rings, geometrical interpretation of diffraction.....	19
Figure 5: Instrument resolution curves for a neutron (D1B-ILL, calcite rostrum sample) and a x-ray (CRISMAT, LaB ₆ standard powder) constant wavelength diffractometer set-up.....	22
Figure 6: Least-squares result on a polypropylene sample	25
Figure 7: Refinement of an anatase/rutile powder operated by Whole Pattern Fitting using Fullprof.....	26
Figure 8: 4-circles reflection Geometry using a CPS detector	34
Figure 9: 4-circles transmission Geometry using a 2D detector	34
Figure 10: a) View of the D19-ILL CAPS detector (Sax Mason, ILL courtesy), and b) Schematic of the CAPS detector geometry. The Ewald (largest) and Pole (smallest) spheres are drawn, together with detector and angle coordinates.....	36
Figure 11: Intensity calibration using a CPS 120 detector, by moving the detector in front of the direct x-ray beam.	40
Figure 12: a) Intensity response of the D19-ILL CAPS detector under vanadium flat-field scatterer exposure, b) Raw and c) intensity-corrected Debye-Scherrer diagram obtained on a calcite standard	41
Figure 13: Series of diffractograms measured on the LaB ₆ standard from NIST, with corresponding simulated diagrams (lines). Tilt angle χ is 0 for the bottom diagram, 60° for the top. Line broadening as χ increases is due to beam defocusing, as explained later.	43
Figure 14: Experimental and recalculated normalised pole figures for the limestone Round-Robin neutron texture standard obtained at the D20 ILL beamline. Equal-area projections, Logarithmic density scale (multiplied by 100).....	44
Figure 15: {006} and {300} normalised pole figures of the <i>Belemnite</i> rostrum from the Cretaceous (Lambda=2.4Å, D20-ILL beamline).	45
Figure 16: Thicknesses $T(\omega, \mu, I_T/I_\infty)$ as calculated from Equation - 45, in function of 2θ . a) increasing ω angles (1, 5, 10 and 20°), for $\mu = 208 \text{ cm}^{-1}$ and $I_T/I_\infty = 0.95$. b): increasing μ (208 and 2000 cm^{-1}), for $\omega = 20^\circ$ and $I_T/I_\infty = 0.95$. c): increasing I_T/I_∞ (0.63 and 0.95), for $\omega = 10^\circ$ and $\mu = 208 \text{ cm}^{-1}$	48
Figure 17: Debye-Scherrer of the Belemnite rostrum of Figure 3b represented in the pole figure frame K_S . The vertical axis correspond to the number of the discretised diagrams using a 5° grid.....	72
Figure 18: Model functions for surface roughness corrections from various authors. The parameters used in the models are not intended to fit the closest same solution.	73
Figure 19: Schematic of a diffraction experiment using the θ - 2θ geometry. The plane of the figure is the scattering plane.	94
Figure 20: Calculated diagrams of α -SiO ₂ for a) a bulk powder without preferred orientation and b): an oriented powder showing strong orientation with {00 l } planes parallel to the sample surface.	95
Figure 21: Asymmetric geometry of measurement	97
Figure 22: Asymmetric geometry using a PSD or a CPS.....	98
Figure 23: ω -scan (rocking curves arrangement) for measuring orientations	99
Figure 24: ω -scan of a single crystal having a 0.1° FWHM of its {002} reflection centred at $2\theta = 18^\circ$	100
Figure 25: Theoretical diagram in the 20-165° 2θ -range, for diamond measured with Cr K α_1 radiation	101
Figure 26: Two texture components differing only by their orientation in the sample plane	101
Figure 27: Illustration of crystallographic planes rotation when planes are perpendicular (dotted or continuous lines) or parallel (rectangles) to the diffraction plane.....	102
Figure 28: Two orientation components, represented by their c axes.....	104
Figure 29: Two orientation components, Gaussians with 0.1° FWHMs, as described in	104
Figure 30: Representation of a crystallite orientation on the Pole Sphere	107
Figure 31: (a) Stereographic projection of Figure 30 and (b) Wulff net to manually read angles in the projection	108
Figure 32: Lambert projection of Figure 30	109
Figure 33: Stereographic (a) and Equal-area (b) projections of 1368 points located at every 5° in χ and ϕ on the Pole Sphere	109

Figure 34: Scanning strategy for the complete coverage of the pole figures using the D19-ILL CAPS detector. χ_{plate} is the sample orientation given by the goniometer, χ is the equivalent χ in terms of pole figures uncorrected for localisation..... 112

Figure 35: Illustration of the pole figure coverage. (a) for an initial $10^\circ \times 10^\circ$ grid scan in χ and ϕ in the diffractometer space and for a pole figure at $2\theta = 2\omega$ (symmetric position) using a CPS detector, (b) for the same ω position as previously but for a pole figure at $\theta - \omega = 10^\circ$. (c) using a CAPS detector and an azimuthal scan step of 30° and $\chi_{\text{plate}} = 30^\circ$ and 55° only and (d) for four χ_{plate} orientations (5° , 30° , 55° and 80°) and a 5° step in ϕ 113

Figure 36: Defocusing effect in reflection geometry illustrated for a symmetric diffraction line. Two sample orientations are shown, $\chi = 0$ (blue) and $\chi > 0$ (red). 115

Figure 37: a) Peak broadening due to defocusing, illustrated at $\chi = 0$ (left) with typical detecting slits corresponding to a point detector, and at $\chi = 30^\circ$ (right) using integrating slits as available using a 1D detector. b) Typical defocusing curves of a randomly oriented sample obtained theoretically (dark bold), measured using a 0D detector (blue) and measured using integrated intensities and a 1D detector (red). Arrows are located at a χ corresponding to a 50 % correction..... 115

Figure 38: Example of peak defocusing for the (103/013/110) three-components line of an orthorhombic YBCO random powder. 117

Figure 39: Measurable range limitation illustrated for two cases. A) 2θ limitation in reflection geometry and b) ω limitation in transmission. 118

Figure 40: The sample reference frame $\mathbf{K}_A = (\mathbf{x}_A, \mathbf{y}_A, \mathbf{z}_A)$ 119

Figure 41: Crystal and sample reference frames $\mathbf{K}_B = (\mathbf{x}_B, \mathbf{y}_B, \mathbf{z}_B)$ and $\mathbf{K}_A = (\mathbf{x}_A, \mathbf{y}_A, \mathbf{z}_A)$ respectively. Only one crystallite is shown..... 119

Figure 42: a): $P_h(\mathbf{y})$ Diffraction pole figure for one crystallite. The direction \mathbf{y} is associated to the $[hk\ell]^*$ normal. b): Pole figure of a texture component centred on the previous \mathbf{y} , having a Gaussian shape of 10° FWHM, for $\mathbf{h} = \langle 001 \rangle^*$ of an orthorhombic crystal structure. 121

Figure 43: $\{001\}$ pole figure for the two-components texture of..... 122

Figure 44: $\{001\}$ pole figure for the component C_1 of..... 123

Figure 45: Pole figures for the C_1 component for a tetragonal crystal system. a): $\{001\}$ b): $\{100\}$ 123

Figure 46: $\{100\}$, $\{010\}$, $\{001\}$ and $\{110\}$ pole figures of an aragonite (orthorhombic crystal system) layer from the sea shell gastropod *Cypraea testudinaria* 124

Figure 47: Schematic representation of Curie (limit) groups. ∞ left and right (a), ∞m (b), ∞/m (c), $\infty 2$ left and right (d), ∞/mm (e), $\infty\infty$ right and left (f) and $\infty\infty/m$ (g) 125

Figure 48: $\{100\}$, $\{001\}$ and $\{110\}$ pole figures of a random sample. Three degrees of freedom to orient each crystallite..... 126

Figure 49: $\{100\}$, $\{001\}$ and $\{110\}$ pole figures of a planar texture of the orthorhombic crystal system. Rotation axis of the planar texture is with $\langle 100 \rangle^*$ directions perpendicular to X_A 126

Figure 50: $\{100\}$, $\{001\}$ and $\{110\}$ pole figures of a cyclic-planar texture of the orthorhombic crystal system. Rotation axis of the cyclic-planar texture is with $\langle 100 \rangle^*$ directions perpendicular to Z_A 127

Figure 51: $\{100\}$, $\{001\}$ and $\{110\}$ pole figures of a fibre texture of the orthorhombic crystal system. Fibre axis is with $\langle 001 \rangle^*$ directions at ($\theta_y = 45^\circ$; $\phi_y = 45^\circ$)..... 127

Figure 52: $\{100\}$, $\{001\}$ and $\{110\}$ pole figures of a cyclic-fibre texture of the orthorhombic crystal system. Fibre axis is with $\langle 001 \rangle^*$ directions along Z_A 128

Figure 53: $\{100\}$, $\{001\}$ and $\{110\}$ pole figures of a 3D texture of the orthorhombic crystal system, with $\langle 001 \rangle^*$ directions along Z_A and $\langle 100 \rangle^*$ directions along X_A 128

Figure 54: Difference between a perfect single crystal and a polycrystal having perfect 3D crystallite orientations. Normalised pole figures would be identical 129

Figure 55: Definition of the three Euler angles that define the position of the crystallite co-ordinate system $\mathbf{K}_B = (\mathbf{a}, \mathbf{b}, \mathbf{c})$ of an orthogonal crystal cell in the sample co-ordinate system $\mathbf{K}_A = (\mathbf{X}, \mathbf{Y}, \mathbf{Z})$. Note, **100**, **010** and **001** are not Miller indices but vectors referring to an ortho-normal frame aligned with \mathbf{K}_A 131

Figure 56: Definition of the three Euler angles in the a) Roe-Matthies and b) Bunge's conventions 132

Figure 57: $\{001/100/010\}$ multipole figures for an orthorhombic crystal structure for the orientations a): $\{45, 0, 0\}$; b): $\{45, 45, 0\}$; c): $\{45, 55, 45\}$. Roe-Matthies convention..... 133

Figure 58: Used sample reference frames \mathbf{K}_A in texture analysis in, a) metallurgy, b) geology/geophysics, c) molluscan studies, d) thin film growth, e) centrifugation, f) magnetic alignment with $\mathbf{H}_{\text{text}} \perp \mathbf{R}$ for $\mathbf{H}_{\text{meas}} // \mathbf{H}_{\text{text}}$ and g) for $\mathbf{H}_{\text{meas}} \perp \mathbf{H}_{\text{text}}$ (easy-plane samples)..... 135

Figure 59: Pole figure co-ordinates in the sample reference frame \mathbf{K}_A 137

Figure 60: Relationship between the 3D object $f(\mathbf{g})$ and the pole figures $P_h(\mathbf{y})$. To each pole figure cell corresponds several ODF boxes, and each ODF box is linked to several pole figure cells..... 140

Figure 61: Isodensity surfaces representing OD isolated components in a cartesian coordinate system for the \mathcal{H} space..... 142

Figure 62: Several isodensity surfaces representing a cyclic-fibre OD (a) and a cyclic-planar OD (b) in the \mathcal{H} space..... 143

Figure 63: a) Cartesian and b) polar coordinate systems to plot a 2D γ -section. c): OD plot as polar γ -sections using 5° γ steps of a hexagonal crystal system..... 144

Figure 64: a): 3D isometric plot of a sample with several orientation components with no specific symmetry, and a random FON at 0.2 m.r.d.. b): Same OD represented as cartesian γ -sections from $\gamma = 0^\circ$ to 40° (step 10°)..... 145

Figure 65: {100} and {001} pole figures corresponding to the OD of Figure 63c. 146

Figure 66: Evaluation of OD coverage for neutron diffraction measurements of a YBa-Cu-O ceramic containing two main phases, YBa₂Cu₃O₇ (a) and Y₂BaCuO₅ (b) 155

Figure 67: Visual examination of the OD refinement reliability, using experimental and recalculated normalised pole figures (in successive order). WIMV refinements from Beartex. Linear density scale, equal angular projections. a) {111}, {012}, {102} and {221} pole figures of the aragonite outer comarginal crossed lamellar layer of the burgundi snail *Helix pomatia*, maximum density: XXXX m.r.d., minimum density: 0 m.r.d. b) {104}, {110}, {113}, {202}, {116}, {211}, {125} and {300} pole figures of the calcite outer prismatic layer of the deep-ocean mussel *Bathymodiolus thermophilus*, maximum density: 6.3 m.r.d., minimum density: 0 m.r.d. 160

Figure 68: The inverse pole figure sectors in function of the crystal symmetry. The non-redundant sectors are indicated by bold edges. a) triclinic, b) monoclinic, B-setting has been used, c) orthorhombic, d) tetragonal, e) rhombohedral using hexagonal unit-cell, f) hexagonal, g) cubic crystal systems h) inverse pole figure for the drawing axis of an aluminum wire elaborated by cold drawing (linear density scale, cubic sector, equal-area projection). 162

Figure 69: Entropy variation with Texture index. a): for real samples, b): for modelled textures..... 165

Figure 70: Example of an x-ray diffraction diagram for a plasma-treated polypropylene film. 168

Figure 71: Illustration of a case for which a magnetisation measurement operated in two perpendicular directions cannot reveal the magnetic anisotropy. (a) virtual distribution of the magnetic moments, (b) corresponding virtual magnetisation curves..... 169

Figure 72: A specific sample holder for MQTA measurements by difference, mountable in a goniometer head. Cd shields allow insertions of permanent magnets below the sample without visible signals from them in the diagrams 170

Figure 73: One 2D Debye-Scherrer pattern for one sample orientation without field (a) and difference pattern for the corresponding sample orientation (b). 177

Figure 74: {110} pole figures at zero field (a), under 0.3 T (b) and difference (c). Fit of the sum of all diagrams at zero field using the orthorhombic magnetic sub-group in Fullprof (d), and WIMV recalculated-normalised nuclear {110} pole figure (e). Inverse nuclear pole figure for the cylinder sample axis direction (f) and WIMV recalculated-normalised magnetic-scattering contribution for the main orthorhombic axes (g). Recalculated-normalised magnetic-scattering polarisation pole figures for the positive (h) and negative (i) parts of the difference pole figures, and corresponding positive {001} magnetic-scattering pole figure illustrating the magnetic moment reorientation (j). 178

Figure 75: Typical shape of the t(m) function obtained by Fourier transform of a broadened line, provided no truncation effect occurs 187

Figure 76: Various crystallite shapes obtained by variation of the R_i factors in the triclinic crystal system (only non-zero factors are indicated). a): $R_0 = 500$. b): $R_0 = 500, R_1 = -500$. c): $R_0 = 500, R_1 = 500$. d): $R_0 = 500, R_2 = 500$. e): $R_0 = 500, R_3 = 500$. f): $R_0 = 500, R_4 = 500$. g): $R_0 = 500, R_5 = 500$. h): $R_0 = 500, R_6 = 100$. i): $R_0 = 500, R_2 = 500, R_6 = 100$. j): $R_0 = 500, R_6 = -100$ 193

Figure 77: Various crystallite shapes obtained by variation of the R_i factors in the 4/m tetragonal crystal systems (only non-zero factors are indicated). a): $R_0 = 500, R_3 = 100$. b): $R_0 = 500, R_3 = -100$. c): $R_0 = 500, R_4 = 100$. d): $R_0 = 500, R_4 = -100$. e): $R_0 = 500, R_5 = 100$. f): $R_0 = 500, R_5 = -100$ 194

Figure 78: Various crystallite shapes obtained by variation of the R_i factors in the $\bar{3}$ trigonal crystal system (only non-zero factors are indicated). a): $R_0 = 500, R_3 = 100$. b): $R_0 = 500, R_4 = 100$. c): $R_0 = 500, R_5 = 100$ 195

Figure 79: Various crystallite shapes obtained by variation of the R_i factors in the 6/m hexagonal crystal system (only non-zero factors are indicated). a): $R_0 = 500, R_4 = 100$. b): $R_0 = 500, R_5 = 100$. c): $R_0 = 500, R_6 = 100$ 195

Figure 80: Various crystallite shapes obtained by variation of the R_i factors in the m3 cubic crystal system (only non-zero factors are indicated). a): $R_0 = 500, R_1 = 200$. b): $R_0 = 500, R_2 = 200$. c): $R_0 = 500, R_3 = 200$. . 196

Figure 81: Various crystallite shapes obtained by variation of the R_i factors in the cubic m3m Laue group. a): $R_0 = 500, R_1 = 100$. b): $R_0 = 500, R_1 = -100$. c): $R_0 = 500, R_2 = 200$. d): $R_0 = 500, R_2 = -200$ 196

Figure 82: Example of a neutron diffraction diagram (dots) of a biphasic sample, and corresponding fit (line) using QPA as implemented in the MAUD program.	206
Figure 83: QPA refinement example of an x-ray diagram measured on a 85 % amorphous fluorapatite sample. Refinement operated in MAUD, Miro <i>et al.</i> (2005).	208
Figure 84: Phenomenological classification of internal stresses. σ^I , σ^{II} and σ^{III} are respectively macro-, meso- and microscopic stresses. One could have drawn the same diagram with strain types ϵ^I , ϵ^{II} and ϵ^{III} respectively.	209
Figure 85: Schematics of a) specular and b) off-specular reflectivity configurations. The off-specular geometry is illustrated here in the (X_A, Z_A) plane.	215
Figure 86: Calculated specular (line) and specular + off-specular curves of a sample exhibiting strong diffuse signal.	216
Figure 87: Simultaneous acquisition of specular and off-specular scans for a CoSi_2 thin film using a CPS detector. Four scans have been measured at four different counting times to avoid detector saturation at low ω values.	217
Figure 88: Classical wave propagation of a plane wave at an interface.	221
Figure 89: Simulated reflectivity curves for a GaAs layer on a Si substrate, with GaAs thickness at 140 Å (a) , 280 Å (b) and 1400 Å (c) . In (d) a single layer of SiO_2 on Si. Perfect flatness at surface and interface and no background are assumed.	222
Figure 90: Specular reflectivity curves from Si-O-N films deposited on Si(100). An increasing NO content was added during nitridation in the NO/N_2 atmosphere from sample A to E.	223
Figure 91: Evolution of the transmission factor with q_z at an interface.	224
Figure 92: Schematic representation of Yoneda wings on each side of the specular peak	224
Figure 93: 1D schematics of three different characteristic types of interfaces between two layers, with $p(z)$ profiles a): Ideal perfectly flat interface, b) purely rough interface and c) purely diffuse interface [Stearns 1989]	225
Figure 94: Simulation of roughness effect on a bulk silicon substrate for $\sigma = 0, 5, 10, 20$ and 50 Å respectively from the upper to the lower curve.	227
Figure 95: Simulated reflectivity curves for a 140 Å – thick GaAs layer on a Si substrate, with a 10 Å roughness at the surface (a) at interface (b) and at both surface and interface (c) . No background is included in the calculation.	228
Figure 96: Electron Density Profile of the films of Figure 90, and the electron density difference (inset) with respect to Sample A (a) , together with compositional profiles obtained by ToF-SIMS (b)	230
Figure 97: Simulated specular reflectivity of a stack of 12 (Si/GaAs) bilayers on Si(100) substrate. The Si and GaAs layers are 30 Å and 20 Å thick respectively. All interfaces are considered perfectly flat.....	231
Figure 98: Beam imprinting effect occurring at low incidence angle ω . The insert is a schematic view of a specular reflectivity curve showing this effect.	232
Figure 99: Simulated specular reflectivity of a stack of 12 (Si/GaAs) bilayers on Si(100) substrate. The Si and GaAs layers are 30 Å and 20 Å thick respectively. All interfaces are considered perfectly flat, but some energy distribution of the x-ray beam has been included.....	232
Figure 100: Combined algorithm, using least-squares, simulated annealing or genetic refinement procedures.	238
Figure 101: The x-ray diffractometer as set-up at CRISMAT (a) and its schematic showing the angle convention (b)	239
Figure 102: Illustration of defocusing and misadjustment effects on peak shapes and diffractometer resolution function. Measurements on a KCl powder. Diagrams appear on top of each other from $\chi = 0^\circ$ to $\chi = 60^\circ$ by steps of 5° for a) $\omega = 20^\circ$ and b) $\omega = 40^\circ$	240
Figure 103: Illustration of the χ -defocusing effect on peak shapes. Z_S is the spectrometer Z axis. For a given width of incident beam, at larger χ values (blue) the peak broadens.	241
Figure 104: Illustration of the 2θ -defocusing effect on peak shapes. Z_S is the spectrometer Z axis. For a given ω , at larger 2θ values the peak becomes broader.	242
Figure 105: Illustration of the ω -defocusing effect on peak shapes. Z_S is the spectrometer Z axis. At larger ω values, the peak becomes narrower.	243
Figure 106: Origins of the a) 2θ and b) ω broadenings Erreur ! Signet non défini.	
Figure 107: (a) Experimental (\times) and fitted (line) 2θ patterns for selected χ orientations for a nanocrystalline SiC film deposited on a Si single crystal substrate; Bottom pattern: $\chi = 0^\circ$; top pattern: $\chi = 35^\circ$; $\Delta\chi = 5^\circ$. Differences between measured and calculated diagrams are shown for the bottom and top patterns. (b) 2D representation of the experimental (bottom) and simulated (top) datasets for a Co ₃ Al ₄ ceramic. (χ, φ) diagrams are piled up from (0,0) to (0,355°), to (60°, 355°) in a successive manner from bottom to top of the 2D representations.	246

Figure 108: Backscattering SEM image of optimised pure PbO flux PZT powder	248
Figure 109: {001}, {100} and {111} pole figures recalculated from the OD refined by combined analysis, for the a) as-cast and b) cast and sintered PZT samples synthesised by the pure PbO flux route. Linear density scale, equal area projection.	249
Figure 110: 001 inverse pole figure for the as cast PZT sample, recalculated from the OD for the casting axis. Linear density scale, equal area projection.	249
Figure 111: Normalised {111}, {200} and {220} pole figures for typical samples with a) d=40 μm , b) d=120 μm and c) d=220 μm , recalculated from neutron diffraction data. Linear density scales, cut below the 1 m.r.d. level.	252
Figure 112: Typical Stress-strain curves for three specimens: t/d=1, 5 and 14.....	253
Figure 113: (a) evolution of $\sigma d\sigma/d\varepsilon = f(\sigma)$ for 3 Ni polycrystals with t/d = 1, 5 and 14. All the stresses are normalized by the yield stress σ_e with $\varepsilon=0.002$. b) evolution of the strain length of the second hardening stage and c) evolution of the hardening rate $d\sigma/d\varepsilon$ of the second stage versus t/d.....	254
Figure 114: evolution of a) σ_{eff} and b) X components of the flow stress with strain for three t/d values... 255	255
Figure 115: evolution of a) overall flow stress, b) σ_{eff} and c) X components of the flow stress with strain for three $\varepsilon=0.08$. Numbers in parenthesis are the t/d ratio	255
Figure 116: a) SEM image of a kaolinite-muscovite composite sintered at 1250°C without Bi ₂ O ₃ addition, and b) corresponding set of x-ray patterns measured at increasing χ -values (from bottom to top).....	257
Figure 117: a) Recalculated-normalised {020}, {200} and {001} pole figures for the main axes of mullite. b) {001} pole figure represented to show the pole reinforcements linked to the in-plane triangular-like organization of the mullite needles (Figure 116a). Linear density scales.	258
Figure 118: a) Fracture toughness and b) Young modulus of well (lines) and poorly (dashed lines) organised mullite samples in function of the mullite crystal lengths.....	258
Figure 119: Intensity vs. Potential diagram used to adjust the experimental potentials around the frontier between water and oxygen reduction.	260
Figure 120: Experimental x-ray diffraction diagram (dots) of a typical nacre-like film. Note the enhanced (00 ℓ) line compared to a perfect powder, indicating the pronounced (00 ℓ) orientation. Only lines from aragonite are observed. The diagram (line) corresponds to a Rietveld fit without texture correction.	261
Figure 121: SEM backscattering images of aragonite deposits on titanium foils for a) non-optimised deposition conditions showing typically cauliflower-shaped aragonite, b) optimised conditions with nacre-like pseudo-hexagonal-shaped crystals and c) same as b) using a larger magnification showing cross-sectioning cracks	262
Figure 122: X-ray pole figures recalculated from the OD. a) {002} and b) {200} pole figures of an optimised film on Ti foil.....	263
Figure 123: X-ray pole figures recalculated from the OD a) {002} and b) {200} pole figures of the inner columnar nacre layer of the gastropod <i>Haliotis tuberculata</i>	263
Figure 124: X-ray pole figures recalculated from the OD a) {002} and b) {200} pole figures of the inner sheet nacre layer of the bivalve <i>Pinctada maxima</i> . Note the pseudo-hexagonal symmetry of the layer on the {200} pole figure	263
Figure 125: SEM images of the columnar nacre of <i>Haliotis tuberculata</i> (left) and the sheet nacre of <i>Pinctada maxima</i>	265
Figure 126: Neutron diffraction patterns obtained on one Al ₂ O ₃ magnetically aligned slip-casted ceramic (Sample sintered at 1300°C).....	267
Figure 127: {006}, {113} and {110} pole figures recalculated from the OD refined using WIMV. Sample sintered at 1300°C. Linear Density scale, equal area projections. Only a fourth of the axially symmetric pole figures is shown	267
Figure 128: Inverse pole figures calculated for the Z _A cyclic fibre direction for the sintered samples. Linear density scale, equal area projection.....	267
Figure 129: Schematics of a film composed of anisotropically shaped crystallites in a randomly oriented (a) and a textured (b) sample.....	269
Figure 130: Selected fitted χ -scans that shows large peaks and the presence of texture in a Si thin film deposited on amorphous SiO ₂ substrate by magnetron sputtering. The insert shows the net intensity variation of the main peaks, to better visualise the texture.....	270
Figure 131: Inverse pole figure for the normal direction of the Si thin film of Figure 130 calculated from the refined ODF (linear density scale, equal area projection, max = 1.59 m.r.d., min = 0.45 m.r.d.) (a), schematics of the refined mean crystallite shape from Table 8 (b) and (c) high resolution TEM image of the Si crystallites.	270
Figure 132: Experimental and WIMV-recalculated {111} and {202} pole figures for the 15 nm thick gold film. Linear density scale, equal area projection. Max value is 3 m.r.d.....	272

- Figure 133:** Inverse pole figures for the five gold films, as represented in the cubic sector. Linear density scale, equal area projection. Max value are 2.5, 3.8, 33.2, 3.7 and 3.4 m.r.d., min values 0.32, 0.33, 0, 0.29 and 0 m.r.d. respectively 273
- Figure 134:** Representation of the mean crystallite shapes of the gold films, using a harmonic modeling from Popa-refined parameters..... 274
- Figure 135:** Bragg-Brentano diagram of a PCT/Pt/SiO₂/(100)-Si thin structure. Notice the strong overlap between Pt and PCT peaks 275
- Figure 136:** {111}-PCT pole figure recalculated from the OD of a PCT/Pt/SiO₂/(100)-Si thin structure which shows the fibre-type character of the texture. Equal area projection, logarithmic density scale..... 275
- Figure 137:** χ -scans of one film, showing the good agreement between experimental (points) and refined (lines) spectra. Bottom diagram is measured at $\chi = 0^\circ$, top diagram at $\chi = 40^\circ$, by steps of 5° up. 276
- Figure 138:** {111} and {200} recalculated pole figures for the Pt electrode layer (left, max. density is 10 m.r.d., min density is 0 m.r.d.) and {001}, {100}, {101} and {110} for the PCT film (right, max. density is 2.1 m.r.d., min density is 0.15 m.r.d.). Linear density scales, equal area projections. 276
- Figure 139:** Top surface of a Y123 single domain, before perforation with the Sm123 seed in the middle (left) and after perforation (middle). Squares are 1 cm. A seeded Y123 / Y211 ensemble grown on a polyurethane foam. 278
- Figure 140:** The 1368 neutron χ -diagrams measured on the foam sample of Figure 139 **a)** and Rietveld refinement of their sum **b)**, allowing phase, particle size and cell parameters quantitative determinations. Reliability factors: $R_w = 5.43\%$, $R_B = 19.71\%$, used wavelength: 2.53 Å..... 279
- Figure 141:** {003}-Y123 and {010}-Y123 recalculated pole figures of the perforated sample **a)** and of the foam **b)** samples of Figure 139. Linear density scales, equal area projections..... 280
- Figure 142:** $J_c(B)$ curves at 77 K for the plain **a)** and drilled **b)** samples, and corresponding normalised trapped magnetic field maps field cooled in 0.4 T at 77 K **c)** and **d)** respectively..... 280
- Figure 143:** SEM image of a Bi2223 aligned platelet microstructure resulting from the sinter-forging process under uniaxial pressure. Pressure and mean c-axis directions are vertical (**a**). Corresponding {119} pole figure showing the axially symmetric texture. Pressure and mean c-axis directions are perpendicular to the pole figure plane, logarithmic density scale, equal area projection (**b**). 281
- Figure 144:** Neutron χ -scans from the D1B-ILL beamline. Note the strong decrease of 00 l line in the lower χ range, and the strong increase of hk0 lines in the higher χ range (**a**). c-scans fit using the combined approach (**b**). 282
- Figure 145:** Inverse pole figures of the Bi2223 phase calculated for the direction of the applied pressure (fibre axis of the texture). Samples textured during (**a**) 20h, (**b**) 50h, (**c**) 100h and (**d**) 150h. Logarithmic density scale, equal area projection. 283
- Figure 146:** Correlation between FWHM, applied unidirectional stress σ and transport J_c in Bi2223 sinter forged samples. Points for the same σ correspond to identical measurements on various points of the same sample 284
- Figure 147:** TEM micrograph of a fluoroapatite crystal irradiated by 70 MeV Kr ions with a fluence of $9.5 \cdot 10^{10}$ Kr.cm⁻² (**a**) and x-ray diagram of a virgin sample showing the presence of texture (**b**). The diagram has been measured during sample rotation around its normal. 285
- Figure 148:** Same diagram as in Figure 147a with the application of an arbitrary texture correction model (**a**), and 10^{13} Kr.cm⁻² irradiated sample with 85 % of amorphous phase (**b**)..... 286
- Figure 149:** Rietveld refinements of (**a**) the least ($5 \cdot 10^{11}$ I.cm⁻²) and (**b**) most (10^{13} I.cm⁻²) I-irradiated samples, with arbitrary texture correction..... 287
- Figure 150:** Damaged fraction as revealed by x-ray analyses for Kr- (**a**) and I-irradiated samples (**b**). 288
- Figure 151:** XRD diagram showing the experimental (blue points) and fit (line) of the GaN-SiO₂ composite. GaN and silica peak positions are shown, together with the difference curve between simulation and experiment. Note the large bump of silica glass correctly reproduced from the Le Bail model. This fit was obtained with the following reliability factors: $R_w = 3.31\%$, $R_{exp} = 1.11\%$, $GoF = 8.9$. Insert: illustration of the slightly anisotropic mean GaN crystallite shape. 292
- Figure 152:** TEM and HRTEM micrographs of the GaN powder used to dope the SiO₂ matrix. (**a**) grain distributions are multimodal. (**b**) larger magnification of an isolated particle showing several subgrains. (**c**) large magnification of an isolated grain showing the absence of periodicity (scale bar is 50 nm). (**d**) poor crystalline quality at the surface. 293
- Figure 153:** Room temperature PL spectrum of the GaN-SiO₂ composite excited with an energy of **a)** 3.75 eV (325 nm) and **b)** 3.44 eV (360nm). Dots are the experiments and lines the fit with three Gaussian-like bands. The PL spectrum of the free GaN powder is shown for comparison 294
- Figure 154:** PLE spectra of YL in the 2.4-6.0 eV range at room temperature for the GaN-SiO₂ composite and the Free GaN powder 295
- Figure 155:** Used supercell approximant for the Co349 aperiodic structure..... 296

Figure 156: Experimental (dots) and calculated (lines) diagrams for the whole set of χ -scan measurements of a uniaxial stress and magnetically aligned Co349 ceramic 297

Figure 157: $\{003\}$, $\{-183\}$ and $\{-201\}$ experimental (left column) and recalculated (right column) neutron pole figures of the Co349 oriented ceramic. Logarithmic density scale, equal area projection, max density values are 32.5, 2.8 and 2.5 m.r.d. respectively, min density values are 0 m.r.d. 298

Figure 158: Inverse pole figure for the fibre direction of the Co349 oriented ceramic. Logarithmic density scale, equal area projection. 298

Figure 159: X-ray diffraction diagrams of the RTGG Co349 ceramic Sample 3, as a function of tilt χ ... 299

Figure 160: Layered crystal structure of $[\text{Bi}_{0.81}\text{Ca}_2\text{O}_4][\text{CoO}_2]_{1.62}$ misfit phase 300

Figure 161: a: Neutron diffraction pattern (D1B-ILL) of the hot-forged Bi-Ca-Co-O ceramics operated for 19 χ -scans from $\chi = 0$ to 90° (step 5°) using a fixed incidence angle ω of 25.11° ($\{0010\}$ Bragg position). **b:** Experimental (dots) and calculated (lines) neutron diffraction patterns for the corresponding χ orientations (0 to 90°) 301

Figure 162: a: $\{006\}$, $\{024\}$ and $\{100\}$ pole figures recalculated from the refined orientation distribution, assuming an axially symmetric texture. **b:** Inverse pole figures calculated for the fiber direction (**P** direction of the hot-forging process) 302

Figure 163: a): 2D plots of the 936 experimental (lower half) and fitted (upper half) diagrams and **b)** 2D difference diagrams to reveal the errors. 303

Figure 164: Randomly selected diagrams (from bottom to top at increasing χ values and broadening due to defocusing) illustrating the quality of the fit, together with the texture of AlN and Pt. 304

Figure 165: Low-index recalculated pole figures and 00Z inverse pole figures for the three textured phases of the stack. **a):** AlN, **b):** Pt and **c):** Ni-based alloy. Equal-area density projections, linear density scale. 305

Figure 166: Residual stress to texture correlation between the Pt and AlN layers versus the applied electrical bias. 306

Figure 167: a) The *Charonia lampas lampas* shell and **b)** Cross section SEM image of the fractured shell. The (**G,N,M**) reference frame indicated is slightly rotated around **N** compared to the pole figure frame (Figure 58c) 307

Figure 168: SEM images of **(a)** the outer comarginal first order lamellae **(b)** the outer second order lamellae **(c)** intermediate first order radial crossed lamellae and **(d)** second order lamellae **(e)** first and second **(f)** order lamellae of the inner comarginal crossed lamellar layer. 309

Figure 169: Randomly selected diagrams showing the good reproducibility of the experimental (dots) patterns from the combined analysis refinement (lines) for the **(a)** outer **(b)** intermediate and **(c)** inner layers. **(d)** is a 2D plot of experimental (bottom) and recalculated (top) diagrams showing the reproducibility on all the diagrams for the intermediate layer. 311

Figure 170: $\{110\}$, $\{020\}$, $\{002\}$ and $\{200\}$ recalculated normalised pole figures of the **(a)** outer **(b)** intermediate and **(c)** inner layers. Linear density scale, equal area projections 312

Figure 171: SEM images and $\{002\}$ and $\{040\}$ pole figures of aragonite films on Ti-6Al-4V foils, with addition of organic extrata during electrodeposition. **a)** Addition of WSM **b)** Addition of ESM..... 319

Figure 172: Polar **a)** and axial **b)** vectors, and mirror plane effects on axial and polar vectors **c-e)**..... 328

Figure 173: Behaviour of the heat capacity with temperature in monoatomic compounds. **N** stands for the Avogadro number..... 331

Figure 174: Correspondence between tensor χ_{ijkl} (left-hand side) and matrix χ_{IJ} (right-hand side) notations for the Kerr tensor..... 340

Figure 175: Behaviour of the inverse of magnetic susceptibility with temperature for a perfect paramagnetic compound (dashed line) and for a paramagnetic with atomic moments orienting under magnetic field. ... 343

Figure 176: Stress definition relative to the three axes 1, 2 and 3 **(a)**, and projection on the (2,3) plane **(b)**. σ^{ij} : *i* is the force direction, *j* is the surface normal to which the force is applied 345

Figure 177: Correspondence between tensor (left-hand side) and matrix (right-hand side) notations for the compliance **(a)** and stiffness **(b)** constants..... 346

Figure 178: Correspondence between tensor (left-hand side) and matrix (right-hand side) notations for the direct **(a)** and converse **(b)** piezoelectric constants 357

Figure 179: $W_{T1}(y)$, $W_{T2}(y)$ and $W_L(y)$ plots (from left to right) for a single crystal of gold **(a)** and for the 40 nm-thick DC sputtered film **(b)**. Minimum and maximum values can be found for each wave mode in Table 38. Linear velocity scale values, Equal-area plots. 384

Figure 180: Radial distributions of the $\{111\}$ pole figures for the 20 nm RF-sputtered **(a)** and 40 nm DC-sputtered **(b)** gold films. Fits are Gaussians. The two lateral peaks correspond to $\langle 111 \rangle$ equivalents at 70° from the normal to the films. Since the diagrams were measured in a symmetric arrangement, $\chi = \vartheta_y$ 385

Figure 181: Dispersion curves of both longitudinal and shear modes of the gold films. The slopes give the average acoustic speeds in the films. The intercepts are zero within experimental uncertainties 386

Figure 182: Wave velocity pole figures calculated from the single crystal **(a)**, LN/Al₂O₃ **(b)** and LN/Si **(c)** tensors. The left column figures are $W_L(\mathbf{y})$ waves, the central and right columns $W_{T1}(\mathbf{y})$ and $W_{T2}(\mathbf{y})$ waves respectively. Minima and maxima units are km.s⁻¹. 387

Figure 183: Variation of the electrical conductivity and thermoelectric power factor with **P** duration time. Corresponding maxima of the $\{00\ell\}$ pole figures are 13.6, 19.8 and 31.8 m.r.d. for 2h, 6h and 20h of UP time respectively. 389

Figure 184: Variation of the resistivity a) and of the thermoelectric power factor b) with temperature, for a sintered powder, a single crystal and a hot-forged ceramic of the Bi-Ca-Co-O compound. 390

Figure 185: Classical **(a)** and Rotation **(b)** alignment procedures. The diffraction measurement geometry is also shown. 391

Figure 186: Configurations for the magnetisation measurements: $M_{//}$ corresponds to the magnetisation curve of Sample B, with $\mathbf{H}_{\text{meas}} // \mathbf{c}$, and M_{\perp} to the $\mathbf{H}_{\text{meas}} \perp \mathbf{c}$ configuration (Sample A). 391

Figure 187: $\{001\}$ and $\{100\}$ normalised pole figures of Sample B, showing the major $\langle 001 \rangle$ fibre texture. . 392

Figure 188: The two possible configurations for the measurement of the magnetisation curves. We use the left one in this work. 393

Figure 189: $M_{//}$ measured (circles) and simulated (squares) anisotropic magnetisation curves of our magnetically aligned carbide 395

Tables caption

Table 1: Correspondences between the most used Euler angle sets..... 132

Table 2: Definitions of sample configurations in absence of applied magnetic field..... 172

Table 3: Resulting possible sample states after application of a magnetic field 173

Table 4: Typical q_c , ρ_c , δ and β values for few elements and compounds. δ and β are given for $\lambda = 1.5418 \text{ \AA}$ 220

Table 5: model functions to represent typical interface roughness 226

Table 6: Example of six heat treatment conditions and the corresponding mean grain size and t/d ratio. 251

Table 7: Results obtained on the four samples in terms of texture strength and crystallites and grain sizes 268

Table 8: Refined parameters for 8 analysed Si films deposited on various substrates [Morales et al. 2005].
Numbers in parentheses are one standard deviations as refined..... 271

Table 9: Thicknesses as measured by profilometry and refined by the combined analysis, compared to the porosity as determined by x-ray reflectivity [Morales et al. 2005] on two Si nanocrystalline thin films deposited on amorphous SiO₂ substrates..... 271

Table 10: QTA characteristics of the five analysed gold films 272

Table 11: Crystallite anisotropic shape refinement of the analysed gold films..... 273

Table 12: Layer and structural characteristics of the sample of Figure 137. 276

Table 13: Cell parameters and volume fractions of the Y211 and Y123 phases of the foam sample as refined for the summed diagram of Figure 140. Parentheses are one standard deviation. 279

Table 14: Refined parameters extracted from Rietveld/WIMV combined analysis and reliability factors obtained from different sinter-forging time samples. Transport critical current densities, measured on each sample, are also reported. 283

Table 15: Fitted parameters for the different samples irradiated under Kr and I ions with various fluences.
Parentheses are one standard deviations. 287

Table 16: Radiation damage fit results of Figure 150. 290

Table 17: Maximum density of the {003} pole figure, Full Width at Half Density of the {003} pole and Texture Index (F²) values for different uniaxial pressures and duration times..... 299

Table 18: Results obtained from the combined analysis on a AlN/Pt/TiO_x/Al₂O₃/Ni-Co-Cr-Al-Y stack. Standard deviations in parenthesis for the last digit. 303

Table 19: Combined analysis results for the outer, intermediate and inner layers of *Charonia lampas lampas*. We took as reference unit-cell for non-biogenic crystals: a= 4.9623(3) Å, b= 7.968(1)Å, c= 5.7439(3)Å (ICDD Card N° 41-1475)..... 310

Table 20: Refined cell parameters, atomic positions and ΔZ values for *C. lampas* layers, our non-biogenic reference and the *Strombus* species of Pokroy et al. [2007]..... 315

Table 21: Combined analysis results for three mollusc shells, composed of naces and prismatic aragonitic layers. 318

Table 22: Combined analysis results for the electrodeposited aragonite layers on titanium foils..... 318

Table 23: Pure and coupled coefficients of the constitutive thermodynamic relations, with the corresponding tensor rank, units and character..... 326

Table 24: Tensor and polar/axial characters in function of their invariance versus time and/or space inversion, and number of Shubnikov point groups for which the property tensor can be non-zero..... 330

Table 25: Distribution of some tensors versus types and rank 330

Table 26: Nye representation for the κ_{ij} thermal conductivity tensor for all crystal classes 332

Table 27: Some thermal conductivities κ_{ij} (WK⁻¹m⁻¹) and diffusivities K_{ij} (m²s⁻¹) for some crystalline phases at room temperature 332

Table 28: Nye representation for the χ_{ij} dielectric susceptibility tensor for all relevant crystal classes. The twofold axis for the monoclinic case is taken parallel to the x₂ axis. Only above-diagonal terms are shown because of the symmetric character of these tensors..... 333

Table 29: Relative dielectric permittivity of BaTiO₃ at 25°C 333

Table 30: Nye representation for the g_{ij} gyration tensor in the relevant non-centrosymmetric point groups. 336

Table 31: Some electrical resistivities $\rho_{e,ij}$ (10⁻⁸ Ωm) for some crystalline phases at room temperature 337

Table 32: Nye representation for the χ_{ijk} electrooptic tensors for relevant crystal point groups 339

Table 33: Nye representation for the χ_{IJ} electrooptic Kerr tensor for all relevant crystal classes 341

Table 34: Nye representation for the $S_{ijk\ell}$ compliance tensor for all crystal classes..... 346

Table 35: Stiffness tensors (GPa) for some crystalline phases at room temperature..... 348

Table 36: Expressions of the wave velocities for the three main propagation directions of a cubic crystal system. 349

Table 37: Nye representation for the p_i pyroelectric vectors in the relevant non-centrosymmetric crystal classes 352

Table 38: Nye representation for the Se_{ij} and Pe_{ij} Seebeck and Peltier thermoelectric tensors for all crystal classes 354

Table 39: Nye representation for the d_{ijk} piezoelectric moduli for relevant crystal point groups..... 358

Table 40: Piezoelectric coefficients d_{ijk} (10^{-12} m/V) for some compounds at room temperature. Point groups are indicated when necessary. Monoclinic groups are with the "standard" convention, $2 // x_2$, and $m \perp x_2$ 359

Table 41: Nye representation for the b_{ijk} piezomagnetic moduli for relevant magnetic point groups 366

Table 42: Nye representation for the m_{ij} magnetoelectric tensors in the relevant non-centrosymmetric magnetic point groups..... 369

Table 43: Nye representation for the p_{ij} elasto-optic tensor for all relevant crystal classes 372

Table 44: Mean grain size and macroscopic stiffness tensor calculated using the OD and the geometric mean approach, for five rolled Ni samples. 380

Table 45: Elastic properties of the five samples of Table 35. 380

Table 46: Macroscopic elastic stiffness tensors (in GPa) for a single crystal of aragonite (Table 29), and the mineral part of the three layers of *Charonia* as calculated from the OD using the geometric mean..... 382

Table 47: $W_L(\mathbf{y})$, $W_{T1}(\mathbf{y})$ and $W_{T2}(\mathbf{y})$ minimum, maximum and for $\mathbf{y} = (0,0)$ values for a single crystal of gold and for the four DC sputtered gold films analysed. Stiffness values are taken from Table 29. 384

Table 48: Elastic stiffness (GPa) for a $LiNbO_3$ single crystal and calculated from QTA for two films. For this space group, $c_{66} = (c_{11}-c_{12})/2$; $c_{24} = -c_{14}$; $c_{56} = 2c_{14}$ 387